Measurement of Carbon Dioxide Corrosion on Carbon Steel Using Electrochemical Frequency Modulation

A Thesis Submitted to the College of

Graduate Studies and Research

in Partial Fulfillment of the Requirements

for the Degree of Master of Science

in the Department of Chemical Engineering

University of Saskatchewan

Saskatoon

By

Venkatasubramaniyan Sridharan

© Copyright Venkatasubramaniyan Sridharan, June 2009. All rights reserved.

Permission to Use

In presenting this thesis in partial fulfillment of the requirements for a Postgraduate degree from the University of Saskatchewan, I agree that the Libraries of this University may make it freely available for inspection. I further agree that permission for copying of this thesis in any manner, in whole or in part, for scholarly purposes may be granted by Dr. Richard Evitts who supervised my thesis work or, in his absence, by the Head of the Department or the Dean of the College in which my thesis work was done. It is understood that any copying or publication or use of this thesis or parts thereof for financial gain shall not be allowed without my written permission. It is also understood that due recognition shall be given to me and to the University of Saskatchewan in any scholarly use which may be made of any material in my thesis.

Requests for permission to copy or to make other uses of materials in this thesis in whole or part should be addressed to:

Head of the Department of Chemical Engineering
University of Saskatchewan
Saskatoon, Saskatchewan S7N 5A9
Canada
OR

Dean
College of Graduate Studies and Research
University of Saskatchewan
107 Administration Place
Saskatoon, Saskatchewan S7N 5A2
Canada

Abstract

Electrochemical frequency modulation (EFM), which has been widely used in the research field of semiconductors, was used to study CO_2 corrosion on carbon steel under film forming and non-film forming conditions. In the EFM technique two sinusoidal voltage signals of different frequencies are applied to the system and the response current is measured at zero, harmonic and intermodulation frequencies from which the corrosion rate is calculated. The corrosion rate calculation depends upon whether the system is under activation, diffusion or passivation control. In this research rotating cylindrical electrodes made of AISI carbon steel 1018 were immersed in 3% (w/w) NaCl solution saturated with carbon dioxide. The experiment was done at 5 rpm, 24 rpm and 100 rpm simulating laminar, transient and turbulent flow regions respectively. The exposure time was varied from 1 hour to 24 hours and the results were compared with other electrochemical methods such as linear polarization (LP) and electrochemical impedance spectroscopy (EIS). It was found that it was crucial to select the correct EFM model to ensure accurate corrosion rate measurement. A very good agreement in the polarization resistance was obtained between EIS and EFM indicating that EFM can be used as an effective tool in corrosion studies providing that the corrosion mechanism is known.

Acknowledgements

I am very grateful to my supervisor Dr. Richard W. Evitts for giving me a great opportunity to be a part of his research group. This thesis would not have been made possible without his excellent guidance and valuable suggestions. Since the time I have worked with him (January 2007), he has provided immense supervision and steered me in the proper direction. Among all the people whom I have/will come across in life, he will always stand out for his kindness, support, understanding, character and dedication.

I would like to extend my sincere appreciation to my committee members Prof. Aaron Phoenix and Prof. Ikechukwuka N. Oguocha, for making this research more effective with their invaluable knowledge and guidance. I also extend my thanks to all staff members of Department of Chemical Engineering, University of Saskatchewan for their great assistance.

I would also like to thank University of Saskatchewan for the Graduate Scholarship and Natural Sciences and Engineering Research Council of Canada (NSERC) for their financial support throughout my stay here.

I would like to thank Venu, Raj, Napa, Nagaraj and Samy for making this place a home away from home. Thanks to Sailu, Rohith and Jagan for their help and support at all times.

Finally, above all, to my family and friends without whom this work wouldn't have been made possible. Their unwavering love, support, and encouragement has been my biggest companion and asset. I am indebted to all of you.

Dedication

To My Parents

Sridharan and Thenmozhi Sridharan

And

My brother Mageshkumar Sridharan

And

My Grandmother Poomani

With deep gratitude!

Table of Contents

Permission to Use i

Abstract ii

Acknowledgements iii

Dedication iv

Table of Contents v

List of Tables ix

List of Figures x

List of Abbreviations and Symbols xiv

1. Introduction 1

1.1. Carbon Dioxide Corrosion Mechanism 2

1.2. Knowledge Gap and Objectives 3

1.3. Thesis Outline 5

2. Literature Review 6

2.1. Factors Affecting CO_2 corrosion 6

2.1.1. Effect of pH 6

2.1.2. Effect of temperature 8

2.1.3. Effect of hydrodynamics 10

2.1.4. Effect of CO_2 partial pressure 12

2.1.5. Effect of Fe^{2+} concentration 13

2.2. Electrochemical Techniques 13
2.2.1. Linear polarization method 14
2.2.2. Electrochemical impedance spectroscopy 16
2.2.2.1. Principle of the EIS technique 16
2.2.2.2. Equivalent electric circuit models 19
2.2.2.3. Diffusion control model 21
2.2.2.4. Constant phase element model 23
2.2.3. Electrochemical frequency modulation 25
2.2.3.1. Principle and theory of EFM 26
2.2.3.2. Activation controlled system 28
2.2.3.3. Diffusion controlled system 30
2.2.3.4. Passivation controlled system 32
2.2.3.5. Data validation 33
2.3. Summary 34
3. MATERIALS AND METHODS 36
3.1. Sample Preparation Procedures 36
3.2. Electrolyte Preparation 37
3.3. Equipment 37
3.4. Corrosion Rate Measurement Methods 38
3.5. Summary 39

4. RESULTS AND DISCUSSION 41

4.1. Analysis of Dummy Cell Using EFM 41

4.2. Effect of Baseline Frequency and Corrosion Model 42

4.3. Reproducibility and Uncertainty Analysis 46

4.3.1. Reproducibility of corrosion rate and polarization resistance using EFM 46

4.4. Analysis of CO_2 Corrosion at Non-Film Forming Conditions Using EFM 48

4.4.1. EFM measurements carried out at various exposure times in laminar flow and comparison with EIS and LP 49

4.4.2. EFM measurements carried out at various exposure times in transient hydrodynamic region and its comparison with EIS and LP 57

4.4.3. EFM measurements carried out at various exposure times in turbulent flow region and its comparison with EIS and LP 61

4.5. Analysis of CO_2 Corrosion at Film Forming Conditions Using EFM 65

4.5.1. EFM measurements in the stagnant region and its comparison with LP and EIS methods 66

4.5.2. EFM measurements in the transition region and its comparison with LP and EIS methods 69

4.5.3. EFM measurements in the turbulent region and its comparison with LP and EIS methods 72

4.6. Summary 76

5. CONCLUSIONS AND RECOMMENDATIONS 77

REFERENCES 80

APPENDIX A 85

Rotation Rate Calibration for MSR Style Rotators 85

APPENDIX B 87

Mathematical Derivation for Activation Control System in EFM 87

Mathematical Derivation for Diffusion Control System in EFM 90

Mathematical Derivation for Passivation Control System in EFM 92

APPENDIX C 95

Corrosion Rate Calculation by LP Method Using Tafel Slopes from EFM 95

Activation Control System: 95

Diffusion Control System: 96

List of Tables

Table 3.1. Chemical composition of AISI 1018 carbon steel[55] 37

Table 4.1. EFM analysis of 100 ohm resistor in a dummy cell analyzed with a frequency of 2 and 5 Hz. 42

Table 4.2. EFM analysis of AISI 1018 carbon steel at various base frequencies in CO_2 saturated NaCl solution at room temperature, 3.7 pH and stagnant condition (5 rpm) after 1 hour of exposure. 43

Table 4.3. CPE model parameters obtained by fitting the model to experimental data at 5 rpm, pH = 3.7, 1 atm partial pressure and at room temperature. 56

Table 4.4. CPE model parameters obtained by fitting model to experimental data in turbulent flow regime at 100 rpm, pH = 3.7, 1 atm partial pressure and at room temperature. 64

Table B.1. Summary of response current components of activation, diffusion and passivation control models in EFM 94

List of Figures

Figure 2.1. Current-potential curve using LPR technique after 5 hours of exposure in 3% (w/w) NaCl solution at a pH of 6.50, 5 rpm and at room temperature..... 15

Figure 2.2. Equivalent circuit of simplified Randles cell. 21

Figure 2.3. Nyquist plot for a simplified Randles cell circuit in Figure 2.2. 21

Figure 2.4. Bode plot for a simplified Randles cell in Figure 2.2..... 23

Figure 2.5. Nyquist plot for an electrochemical process under diffusion control..... 24

Figure 2.6. Electrical circuit for a constant phase element model. 25

Figure 3.1. Photograph of the experimental setup used for the study..... 39

Figure 4.1. Bode plot from EIS performed on AISI 1018 carbon steel after 1 hour of exposure at 3.7 pH, 5 rpm and room temperature. 45

Figure 4.2. Average corrosion rate of AISI 1018 carbon steel at different exposure time obtained using EFM at 5 rpm, pH =3.7 and room temperature. 47

Figure 4.3. Average polarization resistance of AISI 1018 carbon steel at different exposure time obtained using EFM at 5 rpm, pH =3.7 and room temperature. 48

Figure 4.4. Change in linear polarization curves with time at pH =3.7, 5 rpm, 1 atm CO_2 partial pressure and at room temperature. 50

Figure 4.5. Comparison of corrosion rate between EFM and LP at 5 rpm, pH = 3.7, 1 atm partial pressure and at room temperature. 51

Figure 4.6. Nyquist plot from EIS performed at 5 rpm, pH = 3.7, 1 atm partial pressure and at room temperature over a period of time. 53

Figure 4.7. Plot of modulus of impedance verses frequency from EIS performed at 5 rpm, pH = 3.7, 1 atm partial pressure and at room temperature over 24 hour period. 54

Figure 4.8. Plot of phase angle verses frequency from EIS performed at 5 rpm, pH = 3.7, 1 atm partial pressure and at room temperature over 24 hour period. 54

Figure 4.9. Bode plot fitted with CPE model in EIS method carried out at 5 rpm, pH = 3.7, 1 atm partial pressure and at room temperature after 1 hr of exposure. 55

Figure 4.10. Nyquist plot fitted with CPE model in EIS method done at 5 rpm, pH = 3.7, and at room temperature after 1 hr of exposure in 3% (w/w) NaCl solution saturated with CO_2. 55

Figure 4.11. Equivalent circuit of constant phase element model used to fit the experimental data. 56

Figure 4.12. Comparison of polarization resistance value between EFM, EIS and LP at 5 rpm, pH = 3.7, 1 atm partial pressure and at room temperature. 57

Figure 4.13. Comparison of corrosion rate between EFM at 0.01 Hz and LP with default Tafel slopes at 24 rpm, pH = 3.7. 58

Figure 4.14. Comparison of corrosion rate between EFM at 0.01 Hz and LP with both default Tafel slopes and Tafel slopes from EFM at 24 rpm, pH = 3.7. 59

Figure 4.15. Comparison of polarization resistance between EFM, LP and EIS at 24 rpm, pH = 3.7 and at room temperature. 59

Figure 4.16. Variation of polarization resistance curves with exposure time at 24 rpm, pH = 3.7, 1 atm CO_2 partial pressure and at room temperature. 60

Figure 4.17. AC impedance measurements of AISI carbon steel 1018 in 3% (w/w) NaCl solution done at 24 rpm, pH = 3.7, 1 atm CO_2 partial pressure and at room temperature. 60

Figure 4.18. Potentiostatic EIS Bode plot at different exposure time of AISI 1018 carbon steel in 3% (w/w) NaCl solution at 100 rpm, pH = 3.7. 62

Figure 4.19. Comparison of corrosion rate between EFM (0.005 Hz) and LP method with error bars at 100 rpm, pH = 3.7 and at room temperature. 63
Figure 4.20. Comparison of polarization resistance values between EFM, EIS and LP method at 100 rpm, pH = 3.7 and at room temperature. 63
Figure 4.21. Comparison of corrosion rate from EFM of AISI 1018 carbon steel in different flow regime at pH = 3.7, 1 atm CO_2 partial pressure and at room temperature. 65
Figure 4.22. Variation of corrosion rate with exposure time for different electrochemical methods at 5 rpm, pH = 6.5 and at room temperature. 67
Figure 4.23. Comparison of polarization resistance values between EFM, EIS and LP method at 5 rpm in non-film forming condition. 68
Figure 4.24. Nyquist plots of AISI 1018 carbon steel sample in CO_2 solution at various exposure times in film forming conditions at 5 rpm. 69
Figure 4.25. Variation of corrosion rates with exposure time for different electrochemical methods at 24 rpm and film forming conditions. 70
Figure 4.26. Comparison of polarization resistance values between EFM, EIS and LP method at 24 rpm and film forming conditions. 71
Figure 4.27. Variation of corrosion rates with exposure time for different electrochemical methods at 100 rpm and at film forming conditions. 73
Figure 4.28. Surface morphology of AISI 1018 carbon steels exposed at film forming (a) and non-film forming conditions (b) at 100 rpm and room temperature. 74
Figure 4.29. Comparison of polarization resistance values between EFM, EIS and LP method at 100 rpm and film forming conditions. 75

Figure 4.30. Effect of velocity on corrosion rate analyzed using EFM at a pH of 6.5, 1 atm CO_2 partial pressure and at room temperature. 76

Figure A.0.1. Rotation rate calibration chart of MSR style rotators. 86

List of Abbreviations and Symbols

[ ]	Concentration of species, mol/L
A/V	Surface area to volume ratio, cm^{-1}
b_a, b_c	Tafel slope (anodic and cathodic), mV/decade
C	Capacitance, F
C^O, C^R	Concentration of oxidant, reductant, mol/L
CPE	Constant phase element
CR	Corrosion rate, mpy
D	Average diffusion coefficient, cm^2/s
D_O, D_R	Diffusion coefficient of oxidant, reductant, cm^2/s
E	Potential, mV
E_0	Amplitude of potential signal, mV
E_{corr}	Corrosion potential, mV
E^o	Equilibrium potential, mV
E_{rev}	Reversible potential, mV
F	Faraday constant (96485), coulomb/mol
I	Current, μA

i	Net current density, $\mu A/cm^2$
i_{corr}	Corrosion current density, $\mu A/cm^2$
i_{fr}	Faraday rectification current density, $\mu A/cm^2$
i_{lim}	Limiting current density, $\mu A/cm^2$
i_o	Exchange current density, $\mu A/cm^2$
k_{gr}	Growth rate constant, s^{-1}
K_{sp}	Solubility product
M	Molecular weight, g/mol
n	Exponent factor
R	Resistance, ohms
R_{ct}, R_p, R_s	Charge transfer, polarization and solution resistance, ohms
Re	Reynolds number
R_{FeCO3}	Rate of precipitation of iron carbonate, $kmol/m^3$ s
R_{gr}	Crystal growth rate
S	Supersaturation
T	Temperature, °C
t	Time, h

U_0	Amplitude of signal, mV
Y_o	Magnitude of admittance, $s^{1/2}.ohm^{-1}$
Z	Impedance, ohms
z	Moles of electrons/mole of metal
Z_w	Warburg impedance, ohms

Greek Symbols

α	Exponent factor
β_a, β_c	Tafel constants ($\beta_a = b_a/2.303$, $\beta_c = b_c/2.303$)
δ	Thickness of diffusion layer, cm
η	Overpotential, mV
ρ	Density, kg/m^3
σ	Warburg coefficient, $ohm.s^{-1/2}$
ϕ	Phase change, degrees
ω	Radial frequency, Hz

1. Introduction

A wide range of liquids is extracted from oil and gas fields to meet the energy demands of the world. In addition to these liquids, compounds such as carbon dioxide, water and hydrogen sulphide are present naturally in gas wells. Carbon dioxide which is present naturally is also injected purposely into gas wells to enhance oil recovery. These compounds combine to form a corrosive environment under different environmental conditions such as temperature, pressure, pH and concentration. Carbon dioxide (CO_2) corrosion, also known as "sweet corrosion" is one of the major problems in oil and gas industry, costing billions of dollars every year[1]. In CO_2 corrosion, CO_2 dissolves and hydrates to form carbonic acid (H_2CO_3), which then dissociates into bicarbonate, carbonate and hydrogen ions[2-8]. Due to its low cost and availability, carbon steel is used as the primary construction material for pipelines in oil and gas industries, but it is very susceptible to corrosion in CO_2 environments. Aqueous carbon dioxide (carbonic acid) is corrosive and corrodes the carbon steel pipelines. Carbon dioxide corrosion has been of interest to researchers in oil industries for many years and there exists many theories about the mechanism of CO_2 corrosion[9, 10].

The mechanisms of CO_2 corrosion and the formation and removal of protective iron carbonate films are not fully understood due to the complex reaction mechanisms and the presence of many critical environmental factors such as pH, temperature, dissolved species

concentration and hydrodynamics that can appreciably change the corrosion rate. In addition, CO_2 corrosion products can also form protective iron carbonate ($FeCO_3$) films on the surface under certain conditions and can prevent the metal from further corrosion by acting as a diffusion barrier[11-15]. The protective nature of these iron carbonate films depends on the environmental factors as well. Understanding the properties of surface films and the rate at which they form on the pipelines due to the presence of carbon dioxide will help in achieving better protection of oil tube steels. It will also help to increase the efficacy of corrosion mitigation techniques.

1.1. Carbon Dioxide Corrosion Mechanism

Although a lot of reaction mechanisms exist for CO_2 corrosion, the most widely accepted mechanism is given as follows.

CO_2 hydration:

$$CO_2\,(g) \leftrightarrow CO_2\,(aq) \tag{1.1}$$

$$CO_2(aq) + H_2O\,(l) \rightarrow H_2CO_3(aq) \tag{1.2}$$

The carbonic acid dissociates into bicarbonate and carbonate ions in two cathodic steps. The cathodic reaction also includes reduction of hydrogen ions.

$$2H_2CO_3 + 2e^- \rightarrow H_2 + 2HCO_3^- \tag{1.3}$$

$$2HCO_3^- + 2e^- \rightarrow H_2 + 2CO_3^{2-} \tag{1.4}$$

$$2H^+ + 2e^- \rightarrow H_2 \tag{1.5}$$

The CO_2 corrosion reaction includes the anodic dissolution of iron at the metal surface and given by,

$$Fe \rightarrow Fe^{2+} + 2e^{-} \quad (1.6)$$

The overall electrochemical reaction of CO_2 corrosion is given by,

$$Fe + CO_2 + H_2O \rightarrow FeCO_3 + H_2 \quad (1.7)$$

Thus, the overall reaction of CO_2 corrosion leads to the formation of $FeCO_3$ with the liberation of hydrogen gas. $FeCO_3$, if precipitated, could form a protective film on the metal surface and prevent the metal from further corrosive attack. The properties of the $FeCO_3$ layer are greatly influenced by the corrosion rate and environmental conditions.

In spite of extensive research on CO_2 corrosion over decades, it is still unclear which of the three cathodic reactions dominates the corrosion reaction in different environmental conditions. The net cathodic reaction current is assumed to be the sum of all the three cathodic reaction currents and according to mixed potential theory this sum must equal the total anodic dissolution current. From this complex corrosion mechanism it can be expected that the corrosion rate of carbon steel can be greatly affected by the environmental factors like fluid hydrodynamics which might affect the rate of the reaction[16, 17]. The formation of corrosion product scales and their protective properties which are affected by these environmental factors could greatly influence the corrosion rate. The effects of some of these environmental factors are discussed in detail in Chapter 2.

1.2. Knowledge Gap and Objectives

Corrosion rate data are frequently determined using gravimetric or weight-loss methods which are time consuming and overall corrosion rates obtained this way are time-averaged. Electrochemical methods like Tafel extrapolation, linear polarization resistance (LPR) and

electrochemical impedance spectroscopy (EIS) have the advantage over gravimetric methods because the instantaneous corrosion rate and many other kinetic and thermodynamic parameters are obtained relatively more quickly than from gravimetric methods. Each of these electrochemical methods has their own merits and demerits. For example, Tafel extrapolation has the advantage of determining the kinetic parameters of a metal in a particular environment but on the other hand, the sample surface may be damaged due to large degrees of surface overpotential and also incorrect interpretation of the graphical result may result in error in the estimation of the Tafel slopes. In the LPR method Tafel slopes have to be known prior, either from other experiments or from the open literature available.

Most experimental studies conducted to date on CO_2 corrosion have been performed using electrochemical methods like Tafel extrapolation[18-20], LPR and EIS[21-26]. No studies have been performed using a non destructive electrochemical technique called electrochemical frequency modulation (EFM). EFM is a relatively new technique that is simple and non destructive, but it has been used only on few corrosion systems [27-29]. The EFM technique has internal checking parameters called causality factors, by which the experimental data can be verified.

The main objective of this research work is to evaluate the effectiveness of EFM for determining the kinetic parameters of carbon steel corrosion on Fe-H_2O-CO_2 system under various film and non-film forming conditions, including variation in hydrodynamic intensity. Experiments were performed using rotating cylinder electrode system at different hydrodynamic situations simulating laminar, transition and turbulent regions. Also the pH of the bulk solution was changed to achieve film and non-film forming conditions. The results of EFM were compared with LP and EIS methods.

1.3. Thesis Outline

The following paragraph gives a brief outline of the chapters in this thesis

Chapter 2 presents the literature review providing details about present knowledge on CO_2 corrosion mechanism and how the mechanism is affected by the environmental factors which have been found from various research works so far. Also the conditions for film and non-film forming situations on carbon steel are discussed followed by the description of electrochemical methods used for analyzing CO_2 corrosion giving some importance to the new technique EFM.

In Chapter 3, the materials used for the experiments, methods of sample preparation and the conditions used for the experiments are discussed. Also, the electrolyte preparation procedure and the equipment used for analysis are described. The electrochemical methods and their systematic procedure for analyzing CO_2 corrosion are also explained.

Chapter 4 presents and discusses the results obtained from this research. An uncertainty analysis was performed for EFM and the results were compared with LPR and EIS methods to assess the effectiveness of this new technique. The experimental results of CO_2 corrosion under film and non-film forming conditions at different hydrodynamic situation using EFM, LPR and EIS methods are also compared.

The conclusions and recommendations section summarizes the prospective use of EFM as a non-destructive method for analyzing CO_2 corrosion found from experiments, followed by some recommendations and directions for future research work.

2. Literature Review

This chapter presents a detailed literature review of CO_2 corrosion on carbon steels used in oil and gas industry. The mechanism and the environmental factors affecting CO_2 corrosion on carbon steel at various film and non-film forming conditions are discussed. Also the electrochemical methods that have been used to date for analyzing CO_2 corrosion are discussed and explained in detail emphasizing EFM method.

2.1. Factors Affecting CO_2 corrosion

There are several environmental factors which affect the formation of corrosion product scales on the surface of the metal, which in turn affect the corrosion rate of the metal[17]. The factors include pH, hydrodynamics, partial pressure of CO_2, temperature and concentration of Fe^{2+} ions[30].

2.1.1. Effect of pH

One of the important cathodic reactions in the CO_2 corrosion process is the reduction of H^+ ions[19], thus pH plays an important role in the cathodic reaction. In 1989, Tebbal and Hackerman showed that there is change in the pH immediately adjacent to the electrode surface in the electrolyte and it has a major effect on the physical properties of precipitates such as iron carbonate and iron sulphide[31]. The corrosion rate of carbon steel at room temperature changes considerably, with change in solution pH. With change in electrolyte pH, the

concentration of dissolved species such as HCO_3^-, CO_3^{2-} and H_2CO_3 changes, which in turn affects the rate of cathodic reaction[32]. This has been proven experimentally and theoretically[32, 33]. In 1996, Nesic *et al.,* found that the anodic dissolution reaction rate of iron in CO_2 environments is not strongly dependent on pH and the effect was found to be below than the dissolution of iron in HCl solutions[5].

In CO_2 corrosion systems, when the solution pH is less than 4, the available H^+ ions makes H^+ reduction the dominating cathodic reaction. Also the corrosion rate is found to be flow sensitive at this low pH[20]. The fact that reduction of H^+ ions is much more flow sensitive than H_2CO_3 reduction, causes the corrosion rate to be more sensitive to flow at low pH values (pH<4) than at high pH values (pH >6)[34]. Between pH 4 and pH 6, the corrosion rate decreases due to the depletion of H^+ in the electrolyte which is required for one of the cathodic reactions in CO_2 corrosion. In addition, another significant cathodic reaction takes place: the direct reduction of H_2CO_3. The reduction of H_2CO_3 can be either under charger transfer control or under chemical reaction control which comes from the chemical step: hydration of CO_2 into H_2CO_3 [20]. At this intermediate pH (4<pH<6), the cathodic limiting current (i_{lim}) in CO_2 solutions decreases threefold since the limiting current is a combination of chemical reaction and a H^+- limiting current. The chemical reaction limiting current does not vary with pH, whereas the limiting current for H^+ reduction changes with pH and is proportional to $[H^+]$. At pH=6.5, the bulk solution contains about 30% H_2CO_3 and 70% HCO_3^- ions, which leads the cathodic process to occur in several pathways simultaneously[32].

At room temperature either the pH or the Fe^{2+} ion concentration has to be high (pH> 6) in the bulk solution to attain a protective iron carbonate film on the metal surface in a short time period[14]. The pH has to exceed a critical value above which the concentration of Fe^{2+} and CO_3^{2-}

exceeds the solubility limit and precipitates as iron carbonate. This critical value depends on temperature, Fe^{2+} concentration, etc. Above the critical value, the concentration of Fe^{2+} and CO_3^{2-} ions exceeds the solubility limit and precipitate as iron carbonate on the metal surface. Nesic *et al*., found that the precipitation of iron carbonate film initiates at a pH equal to 6, but no protective dense film formation occurs until the pH reaches 6.8 which is the critical pH for the experimental conditions opted by them. Once this critical pH of 6.8 is attained, supersaturation of Fe^{2+} and CO_3^{2-} ions exceeded and precipitation of iron carbonate starts[30]. In general the increase in pH of the bulk solution decreases the solubility of iron carbonate and increases the precipitation rate, thereby increasing the rate of formation of the protective iron carbonate layer. The increase in concentration of H_2CO_3 and HCO_3^- ions with increasing pH increases the overall rate of cathodic process until the iron carbonate layer formed as a result of anodic process reaches its critical thickness[32]. The kinetics of film removal by chemical reaction i.e., dissolution, also depends strongly on pH[35]. The concentration of Fe^{2+} and CO_3^{2-} in the bulk solution increases as the dissolution of $FeCO_3$ takes place leading to an increase in pH value.

2.1.2. Effect of temperature

Temperature plays a significant role in the formation of protective iron carbonate films in CO_2 corrosion as it increases the rate of chemical reaction, transport of chemical species to and from the bulk solution and the electrochemical reaction rate at the metal-solution interface. It has been reported in the literature that to form protective iron carbonate in a short time period, either the temperature or the pH has to be high. Increasing the temperature initially increases the rate of corrosion until a critical temperature is reached[30]. Beyond the critical temperature, the precipitation of an iron carbonate film starts which reduces the corrosion rate of the metal by

acting as a diffusion barrier. The critical temperature also varies with pH and Fe^{2+} ion concentration in the bulk solution as shown in Eqn 2.1.

The rate of precipitation of iron carbonate (R_{FeCO3}) can be expressed as a function of temperature (T), supersaturation (S), the solubility limit (K_{sp}) and surface area to volume ratio (A/V)[36, 37].

$$R_{FeCO_3} = (A/V) * f(T) * K_{sp} * f(S) \quad (2.1)$$

Temperature can also change the molecular form of surface films by increasing the nucleation rate and a subsequent enhanced growth rate[38]. When the precipitation rate is controlled by the crystal growth rate, the crystal growth rate can be expressed in terms of supersaturation as

$$R_{gr} = k_{gr}(S-1)^2 \quad (2.2)$$

where, R_{gr} is the growth rate and k_{gr} is the growth rate constant. To get a considerable precipitation rate, supersaturation (defined as the ratio of the product of concentration of Fe^{2+} and CO_3^{2-} ions to the solubility product (K_{sp}) has to be larger than unity and the kinetic growth rate constant has to be large. Increasing the temperature helps in attaining the supersaturation state by increasing this kinetic constant (k_{gr}) factor. Hunnik *et al*., developed a mechanistic model that predicts the kinetic constant (k_{gr}) to increase by several orders when the temperature is increased from room temperature to 50°C[37]. Nesic *et al*., proved experimentally that the precipitation rate constant increases with increasing temperature.

Increasing the temperature can either increase or decrease the corrosion rate depending on whether the solubility product of iron carbonate is exceeded[36]. At low pH when the protective film does not form, the corrosion rate increases with increasing temperature; however at high pH,

when the concentration of Fe^{2+} and CO_3^{2-} exceeds the solubility limit, increasing the temperature will increase the rate of precipitation and enables the formation of protective iron carbonate films and decreases the corrosion rate. Surface films formed at high temperatures are continuous, compact and more stable than those formed at low temperature[24]. The protective nature of iron carbonate films can be increased at elevated temperature.

2.1.3. Effect of hydrodynamics

Hydrodynamics affects corrosion rate by changing the rate of mass transfer involved in CO_2 corrosion. Due to the flow sensitive nature of the cathodic reactions, at higher velocities H^+ reduction is mass transfer controlled (when the overall reaction rate is controlled by the rate of diffusion of H^+ to the electrode surface) and H_2CO_3 reduction is controlled by both mass transfer and chemical reaction, while the latter part comes from the hydration of CO_2 to H_2CO_3[8]. For a corrosion form that involves fluid flow, the effects due to mass transfer and momentum transfer has to be considered. The shear stress at the interface between the solid wall and fluid represents the momentum transfer rate, whereas the mass transfer rate constant represents the mass transfer rate. The effect of wall shear stress on mass transfer was explained by Silverman[39]. It was found from experiments that the magnitude of the wall shear stress is too low for hydrodynamic scale destruction[40, 41]. On the other hand, it was found that above a critical wall shear stress flow induced localized corrosion is initiated[42].

When there is no protective film formed on the surface, increasing the velocity of the fluid increases the corrosion rate by increasing the mass transfer of species between the electrode surface and the bulk solution. The effect of turbulent flow on corrosion rate when there is no protective film present can be given by the following equation[34]

$$\text{Corrosion Rate} = x * (\text{flow rate})^n \quad (2.3)$$

where, x is a constant and n is the exponent factor which depends on the corrosion mechanism involved. The exponent factor has a value of 0.8 for a diffusion controlled reaction in a smooth pipe and varies between 0.4 – 0.7 for those reactions which are partially controlled by chemical reaction and diffusion reaction[8]. The exponent factor gives an indication of flow sensitive nature of the cathodic reaction, and the higher the value the more flow sensitive is the corrosion rate. When the corrosion reaction is dominated by charge transfer, the increase in velocity has less effect on the corrosion rate. Increase in velocity decreases the precipitation rate and surface saturation of Fe^{2+} and CO_3^{2-} because of near wall turbulence, which prevents Fe^{2+} ions from precipitating[30]. On the other hand, at low velocity, the rate of precipitation is higher than the corrosion rate thus enabling protective film formation.

The surface films formed on carbon steels at higher velocity are less protective than those formed at low velocity. The surface supersaturation is less than one when the velocity is greater than 3 m/s. After film formation, hydrodynamics can affect the corrosion rate by mechanically removing the film[14]. Based on experimental results, Ruzic *et al*., assumed that the mechanical removal of film in single phase flow takes place in the following sequential steps[14].

i. Separation from substrate
ii. Vertical cracking
iii. Crack opening and widening
iv. Film detachment.

After the film gets damaged, it creates a potential difference between the protected and unprotected region on the carbon steel, which increases the corrosion rate by localized corrosion

called galvanic corrosion[43]. A galvanic corrosion cell is formed when two similar or dissimilar metals are electrically connected where the metal with more electronegative potential will preferentially corrode.

2.1.4. Effect of CO_2 partial pressure

The formation of protective iron carbonate film on the surface of carbon steel depends on conditions such as temperature, partial pressure, pH and Fe^{2+} concentration which are interrelated to each other. In the absence of film forming conditions such as high temperature and pH greater than 6[30], increasing the partial pressure of CO_2 increases the H_2CO_3 concentration following Henry's law, which increases the corrosion rate by direct reduction of carbonic acid[19, 20]. An increase in partial pressure of CO_2 increases the corrosion rate of carbon steel by increasing the concentration of H_2CO_3 in solution, while at favourable film forming conditions such as high pH; it gives an opposite effect of increasing the rate of iron carbonate precipitation and helps in reducing the corrosion rate. At atmospheric pressure, an increase in temperature gives rise to the contrasting effect of increasing the kinetics of precipitation and reducing the supersaturation. Lin *et al*., found that the thickness of iron carbonate scale formed with increasing partial pressure reaches maximum at 6.89 MPa. Above 6.89 MPa the thickness of the scale decreases possibly due to the maximum corrosion rate reached at a particular environmental condition or due to the inhibiting property of the CO_2 corrosion process[44]. Laboratory experiments are usually carried out at low partial pressures of CO_2, which are unusual in gas fields; only a few high pressure experimental results are available in open literature. Wu *et al*., conducted experiments at supercritical partial pressures (> 7.382 MPa) and found that a protective film is formed at supercritical partial pressure and provides an inhibiting function on the CO_2 corrosion process[25].

2.1.5. Effect of Fe^{2+} concentration

The rate of formation of iron carbonate on the metal surface depends on the precipitation rate of Fe^{2+} and CO_3^{2-}, which is governed by precipitation kinetics. When an iron carbonate layer forms on the surface it acts as a diffusion barrier and prevents the metal from further corrosion. Precipitation of iron carbonate occurs when the concentrations of Fe^{2+} and CO_3^{2-} exceeds the solubility limit[15, 30], or in other words the degree of supersaturation has to exceed unity to achieve precipitation. For iron carbonate, it is given as

$$\text{Supersaturation} = C_{Fe}^{2+} C_{CO3}^{2-} / K_{sp} \quad (2.4)$$

where, K_{sp} is the solubility limit which allows for the determination of the activity of ions in solution using the equilibrium reaction equation. Therefore, increasing the concentration of Fe^{2+} ions in solution either from external source or from anodic reaction helps to achieve a protective film by increasing supersaturation. The rate of precipitation can be varied by changing the temperature of the bulk solution as explained earlier and also by changing the degree of supersaturation.

2.2. Electrochemical Techniques

Corrosion of metal occurs through electrochemical reactions at the metal-solution interface. Understanding the electrochemical phenomenon of a corrosion process will help to monitor and mitigate corrosion reaction. By using electrochemical methods, it is possible to monitor as well as understand the actual electrochemical process taking place on the metal surface. Unlike weight loss or gravimetric methods, electrochemical methods are fast in determining and analyzing the electrochemical properties. The electrochemical methods used for this study are described in the following sub-sections.

2.2.1. Linear polarization method

In a corroding electrode, a region of linear dependence exists between current and the potential applied over a small range close to the free corrosion potential. Free corrosion potential is the potential measured when no current flows through the electrode. This linear current-potential response is due to the exponential relation of anodic and cathodic currents of a corroding electrode to potential, derived from Butler-Volmer equation[45]. Over a small potential range (<20 mV), the difference between cathodic and anodic exponential curves is almost linear. This linear dependence was first noted by Stern and Geary in 1957 and they derived an equation known as Stern-Geary equation, relating the slope of the linear region to the Tafel slopes and corrosion current.

$$\text{Stern} - \text{Geary Equation}: \; R_p = \frac{b_a.b_c}{2.303(b_a+b_c)*i_{corr}} = \frac{\Delta E}{\Delta I} \qquad (2.5)$$

where, R_p is the polarization resistance, i_{corr} is the corrosion current and b_a , b_c are anodic and cathodic Tafel slopes respectively.

Eqn 2.5 served as an important tool for a new experimental approach to study the electrochemistry of corrosion reactions. The Linear polarization resistance (LPR) technique is based on the above mentioned theoretical fact. It is a non destructive method used for calculating polarization resistance which in turn used for calculating corrosion rate.

LPR technique generates a plot of current verses potential over a small potential range. In this method the metal sample is polarized step-wise, starting below the corrosion potential (usually -20 mV) and ending above the corrosion potential (usually +20 mV). The plot of current versus potential is linear, the slope of which gives the polarization resistance (R_p)[46]. The polarization resistance is inversely proportional to the uniform corrosion rate and can be used in

the Stern-Geary equation to determine the corrosion current and corrosion rate[47]. A plot of current verses potential using LPR technique is shown below in Figure 2.1.

The grey line on the graph is the sample plot of experimental data obtained using LPR technique. The linear fit of experimental data was performed using "Gamry- Echem analyst" software and shown as a black line. From the experimental fit line the corrosion rate and polarization resistance are calculated. The calculation of corrosion rate using LPR technique is based on few fundamental assumptions such as the corrosion rate is uniform, both anodic and cathodic reactions are under activation control (kinetic control), a negligible solution resistance and most importantly known values of Tafel slopes.

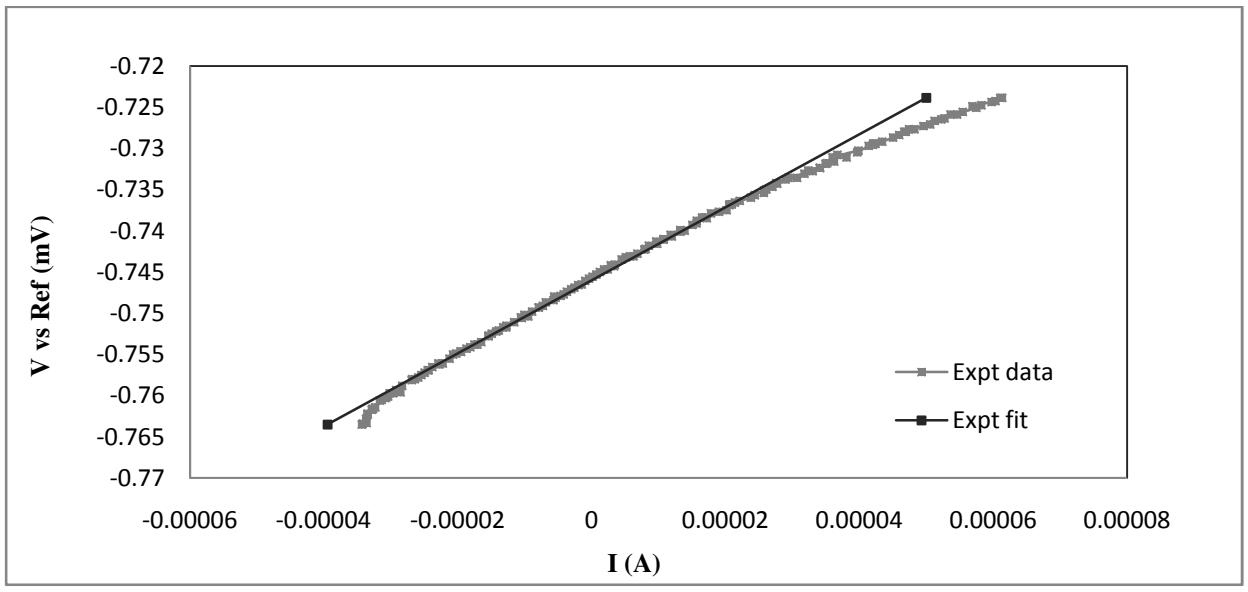

Figure 2.1. Current-potential curve using LPR technique after 5 hours of exposure in 3% (w/w) NaCl solution at a pH of 6.50, 5 rpm and at room temperature

The advantage of LPR technique is that data acquisition can be done quicker compared to other electrochemical methods. This method is non destructive since the potential applied to

the sample is very small. The main demerit of this technique is that it needs Tafel data to calculate corrosion rate, which must be obtained either from literature or from other experiments.

2.2.2. Electrochemical impedance spectroscopy

Electrochemical Impedance Spectroscopy (EIS) also known as AC impedance spectroscopy is a non destructive electrochemical method that is used to evaluate the electrochemical properties of electrode and electrode/electrolyte interface. EIS has found its application in the field of electrochemistry due to the vital information that is extracted about the electrode surface and the interfacial properties with an electrically conducting electrode. Corrosion is one such field where EIS plays a major role in analyzing the kinetic properties and the mechanism. More than determining the surface electrical properties of an electrode system, EIS is mainly used for determining the interfacial properties where a number of basic microscopic processes take place. Knowing and understanding the basic electrochemical reactions at the electrode surface and electrode/electrolyte interface is the key factor in understanding the corrosion mechanisms and its properties.

2.2.2.1. Principle of the EIS technique

EIS is based on Ohm's law on electrical circuits which defines resistance as the ratio of voltage over current.

$$R = E/I \tag{2.6}$$

where, R is the resistance, I is the current through the resistor and E is the voltage across the resistor

The ability of a conducting material to resist the flow of current in an electrical circuit is called resistance and the material is called a resistor. For ideal resistors, the resistance value is independent of frequency at all current and voltage values. Impedance is the general term similar to resistance and is used where complex behaviour of one or more electrical circuit elements exists. In EIS a small AC voltage (1-10 mV) is applied to the electrochemical system over a wide range of frequencies and the response to the input signal i.e., current, is measured. The response current signal usually has a phase difference with the applied potential signal. The change in output potential with phase difference when an AC current is applied to a system is called overvoltage. When an electrochemical system is stimulated by a potential signal it causes various fundamental processes such as electron transfer within the electrode and at the electrode/electrolyte interface to and from, from a charged species. Each electrode/electrolyte interface will behave uniquely when the system in disturbed by an electrical signal. By measuring this unique transient response it is possible to extract various properties of that electrochemical system with a single measurement.

The rate of transfer of charged particles within the electrolyte, electrode and at electrode/electrolyte interface depends on the resistance of the electrolyte, electrode and on the rate of reaction at the interface. Surface structural defects, crystallographic orientation, inclusion of foreign species can also influence the local electric field[45, 48]. EIS always applies a small potential disturbance in order to maintain the pseudo linearity in the cell's response. For small electrical signals the response is always pseudo linear with a small change in phase between the applied and response signal.

Consider an AC sinusoidal potential signal as shown below as the input to the electrochemical system:

$$E = E_0 \sin(\omega t) \quad (2.7)$$

where, E is the potential at time t, E_0 is the amplitude of the signal, ω and t are radial frequency and time respectively.

The response to the above sinusoidal potential signal will be a sinusoidal current signal which has the same frequency with different amplitude and a phase shift. It is given as

$$I = I_0 \sin(\omega t + \phi) \quad (2.8)$$

where, I_0 is the amplitude and I is the current response at time t with a phase change ϕ.

By applying Ohm's law on electrical circuits to the above input and response signal we can calculate the impedance as below.

$$Z = E/I \quad (2.9)$$

$$Z = \frac{E_0 \sin(\omega t)}{I_0 \sin(\omega t + \phi)} \quad (2.10)$$

$$Z = Z_0 \frac{\sin(\omega t)}{\sin(\omega t + \phi)} \quad (2.11)$$

Where $Z_0 = E_0/I_0$ is the amplitude of the impedance.

By applying Euler's rule of complex functions for the above relation, it is possible to express impedance in the form of complex function with both real and imaginary parts as given below

$$Z = Z_0 (\cos\phi + j\sin\phi) \quad (2.12)$$

The complex function is expressed in one or both of the two graphical representations called Bode and Nyquist plots. If the real part of the impedance is plotted against the imaginary part of the impedance on abscissa and ordinate axes respectively, we get a Nyquist plot. From the

Nyquist plot it is possible to extract few electrochemical parameters such as solution resistance, polarization resistance and total resistance. Also it is possible to determine the number of time constants involved in the electrochemical reaction by looking at the shape of the Nyquist plot. Each semicircle in the Nyquist plot is characteristic of a time constant involved in the electrochemical process.

A Nyquist plot does not show any frequency value although some definite frequency was used to get the impedance at each data point. To overcome this shortcoming, a Bode plot was developed to indicate exactly what frequency was used to create a data point. Thus a Bode plot is plotted with frequency on the abscissa axis and the absolute value of impedance and the phase angle on the ordinate axes. From the Bode plot it is possible to read impedance with respect to frequency and also the involvement of capacitance and resistance in the electrochemical reaction from the phase angle and frequency.

2.2.2.2. Equivalent electric circuit models

The analysis of Nyquist and Bode plots from experimental data is done by fitting the experimental curves to an equivalent electrical circuit consisting of common electrical circuit elements such as resistors, capacitors, and inductors. These circuit elements should have some physical relationship to the electrochemical parameters of the reaction. For example a resistor can be used in places where there are possible conductive paths in the electrochemical reaction. Therefore electrochemical parameters such as solution resistance (between the reference electrode and the working electrode) and polarization resistance are represented by an equivalent resistor in the model circuit. Capacitors and inductors are used where there are possible space charge polarization region in the electrochemical process. The impedance of a capacitor has

inverse relationship with frequency and the current through a capacitor leads the voltage across the capacitor by 90 degrees.

These electric circuit elements are connected in a fashion that represents the actual electrochemical process taking place. Since electrical circuit models can be made in different configurations with different elements to give the same output, there could be more than one possible circuit model for a particular electrochemical reaction. The most common circuit model is the simplified Randles cell (Figure 2.2) which consists of a capacitor and resistors. The Randles cell takes into consideration a simple electrochemical reaction with solution resistance (R_s), a double layer capacitance (C_{dl}) and charge transfer resistance (R_{ct}). The double layer capacitance is replaced by a capacitor, and the solution resistance and charge transfer resistance are replaced by resistors R_s and R_{ct} respectively. In a three electrode system, the double layer capacitance lies parallel to the charge transfer resistance.

It can be seen from the equivalent circuit model that Randles cell has only one time constant, therefore a Nyquist plot for a simplified Randles cell is always a semicircle (Figure 2.3). The point where the impedance curve meets the real axis in the high frequency region i.e., close to the origin, gives the solution resistance. The sum of charge transfer resistance and solution resistance is calculated by reading the point where the impedance curve meets the real axis in low frequency region. Therefore the diameter of the impedance curve in a Nyquist plot gives the charge transfer resistance.

The Bode plot for the electric circuit in Figure 2.2 is shown in Figure 2.4. From the Bode plot in Figure 2.4 other information such as frequency verses phase angle and impedance can be

read allowing us to make a good judgement on resistor, capacitor and inductor and design the equivalent electric circuit accordingly.

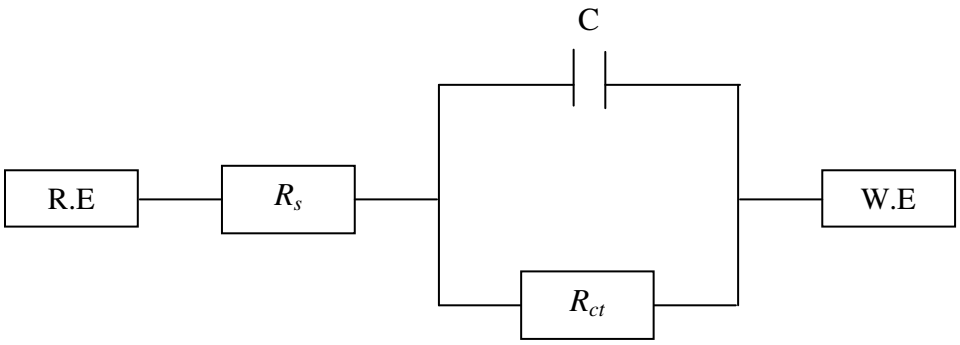

Figure 2.2. Equivalent circuit of simplified Randles cell.

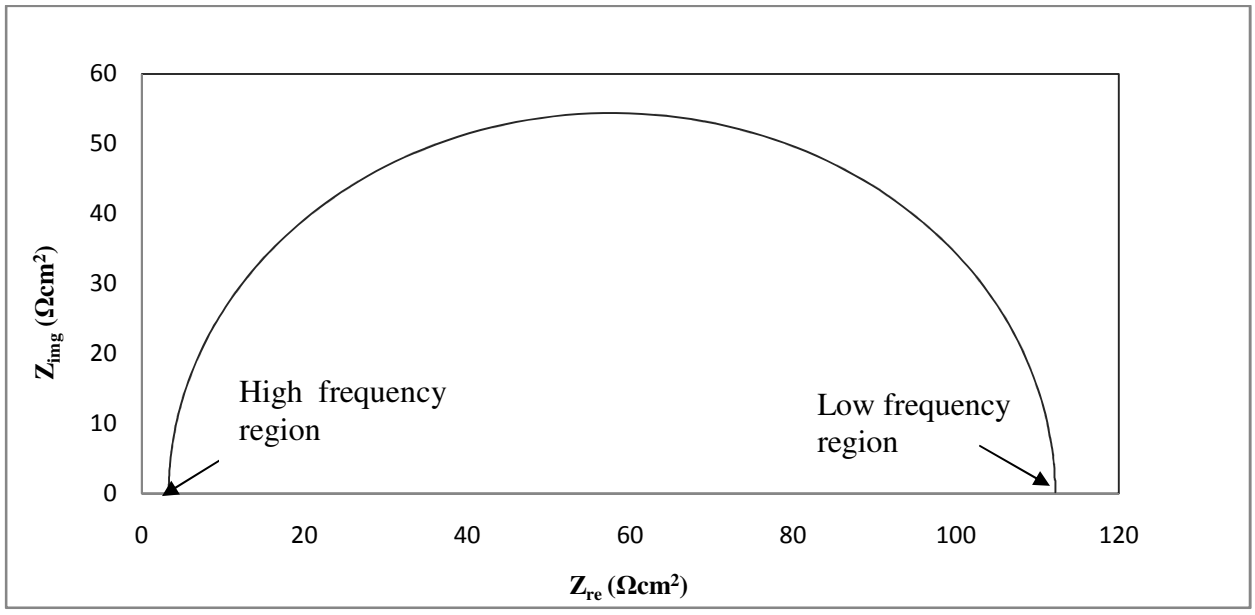

Figure 2.3. Nyquist plot for a simplified Randles cell circuit in Figure 2.2.

2.2.2.3. Diffusion control model

The corrosion process is said to be in diffusion control when the movement of reactants and products is the rate determining step, that is when the diffusion rate is slower than the reaction rate. The impedance created by a diffusion process is usually represented by Warburg

impedance. The diffusion controlled process can take place either in a finite boundary layer or in an infinite boundary layer. The impedance is different for both situations and depends on the frequency of the potential disturbance. The Warburg impedance assumes the diffusion process to take place in an infinite boundary layer since it is very difficult to predict the shape and path of a diffusion process. In such situations the Warburg impedance is inversely proportional to the frequency and represented as in Eqn 2.13

$$Z_w = \sigma\,(\omega)^{-1/2}\,(1 - \mathrm{j}) \tag{2.13}$$

In which $\sigma = \frac{RT}{z^2F^2A\sqrt{2}}\left(\frac{1}{C^O\sqrt{D_O}} + \frac{1}{C^R\sqrt{D_R}}\right)$

where, Z_w is the Warburg impedance, σ is the Warburg coefficient, R is the Universal Gas Constant, F is the Faraday constant, T is the temperature, A is the area of working electrode, z is the charge number, ω is the frequency, C^O is the concentration of the oxidant, D_O is the diffusion coefficient of the oxidant, C^R is the concentration of the reductant and D_R is the diffusion coefficient of the reductant.

With the above equation, if the real part of Z_w is plotted against the imaginary part a straight line is obtained with a slope of one and it is shown in Figure 2.5. In a Bode plot it will have a phase shift of 45 degrees. In situations such as turbulent and transient flow conditions where the diffusion process takes place through a finite boundary layer, the impedance equation seen above will no longer be valid. In such situations, the impedance through a finite boundary layer is represented by the equation below.

$$Z_O = \sigma\omega^{-1/2}(1 - \mathrm{j})\tanh\left[\delta(\mathrm{j}\omega/D)^{1/2}\right] \tag{2.14}$$

where, δ is the thickness of diffusion layer and D is the average diffusion coefficient

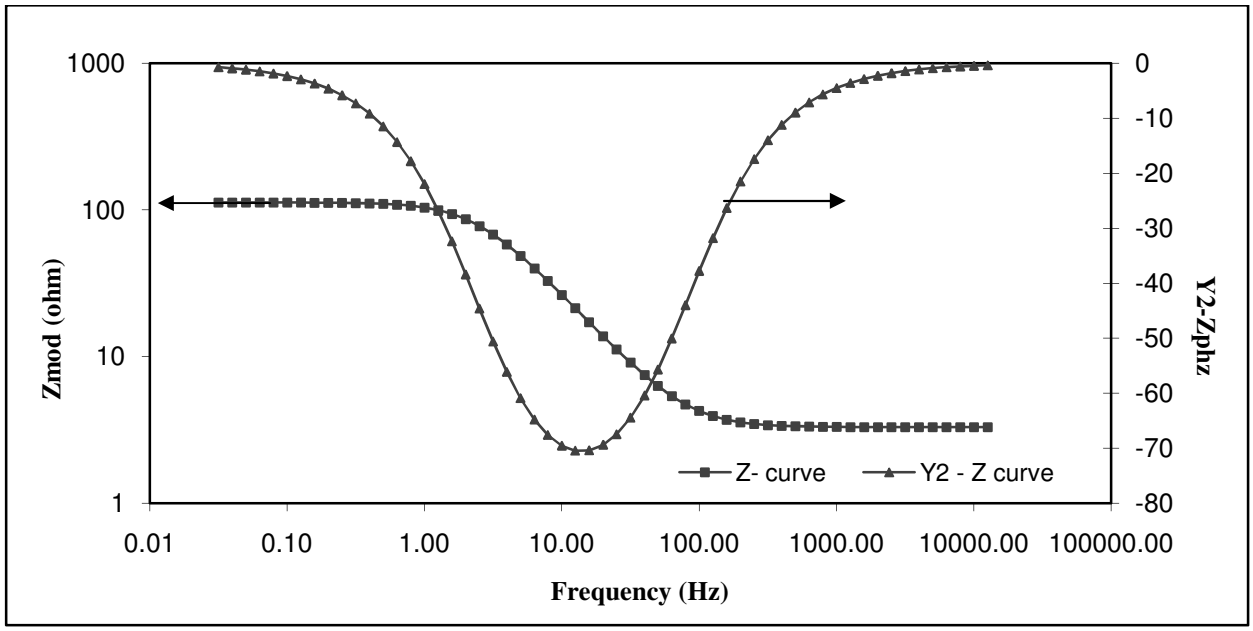

Figure 2.4. Bode plot for a simplified Randles cell in Figure 2.2.

Thus by looking at the shape of a Nyquist plot it is possible to say whether the reaction is under diffusion or charge transfer control. An increase in the thickness of the boundary layer increases the diameter of the semicircle in the Nyquist plot in the low frequency region, which ultimately turns into a straight line when the thickness of the boundary layer becomes infinite.

2.2.2.4. Constant phase element model

When an electrode is immersed in an electrolyte, due to the separation of charges on the electrode/electrolyte interface a region is formed called the electrochemical double layer. This is also called the Helmholtz double layer. It consists of two layers of charge separated by a small region with a potential drop and is similar to electrical capacitors. Although the electrochemical double layer looks similar to an electrical capacitor, they do not behave exactly the same. Therefore in impedance experiments an electrochemical double layer cannot be modelled using ideal capacitors, instead a constant phase element (CPE) is used. The impedance of an ideal

capacitor and a constant phase element differs only by the exponent factor used in the impedance expression. The impedance of capacitor is given as below

$$Z = \left(\frac{1}{C}\right)(j\omega)^{-\alpha} \qquad (2.15)$$

where, C is the capacitance, ω is the angular frequency, α is an exponent factor and j =√-1

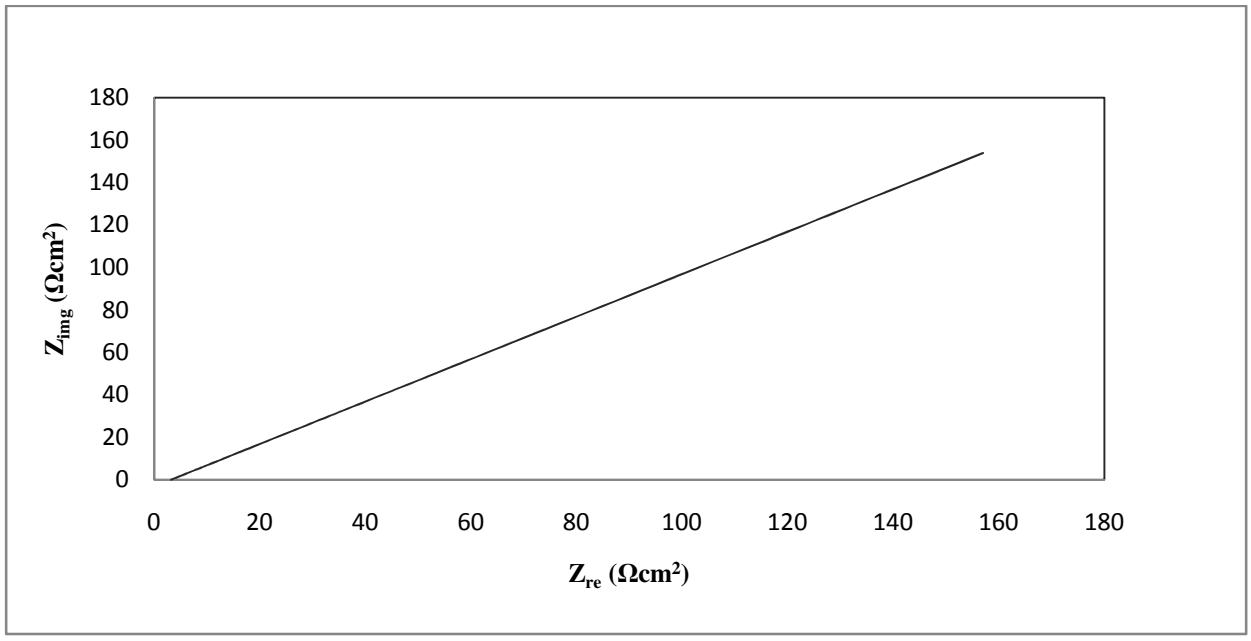

Figure 2.5. Nyquist plot for an electrochemical process under diffusion control

Ideal capacitors have an 'α' value of one, where as for constant phase element it is always less than one. A constant phase element is used instead of a capacitor because the curves in the Nyquist and Bode plots are affected by various local factors such as non-uniform distribution of charges, surface roughness of the electrode, impurities in electrolyte and so on. The constant phase element is assumed to be in parallel with a polarization resistance and the equivalent circuit is shown in Figure 2.6. This constant phase element model is used to analyze the

experimental data on CO_2 corrosion to extract valuable information about the processes occurring.

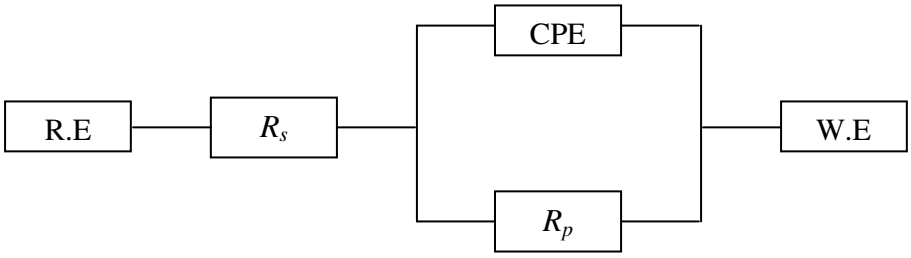

Figure 2.6. Electrical circuit for a constant phase element model.

2.2.3. Electrochemical frequency modulation

Various electrochemical techniques are available for determining the corrosion behaviour of metals. Of the electrochemical methods, there are destructive as well as non-destructive methods which have their own merits and demerits. LP and EIS are non-destructive methods, as mentioned previously in which only a small potential (± 20 mV for LP and 10 mV for EIS) is applied to the corrosion system. The basic disadvantage of these methods is that, they need Tafel coefficients (anodic b_a and cathodic b_c) to determine the corrosion currents and corrosion rates from the polarization resistance value (R_p) using the Stern-Geary equation. These two methods are based on linear measurements.

There are also electrochemical methods based on non-linear measurements, in which a slightly higher potential around 30 mV is applied and such methods include Faradaic rectification (FR), nonlinear EIS, harmonic analysis (HA), harmonic impedance spectroscopy (HIS) and Harmonic synthesis (HS). These methods use a harmonic signal to disturb the corrosion system and this disturbance signal can be AC or DC depending upon the type of signal

applied. Of these electrochemical techniques, the Faradaic rectification method needs at least one Tafel coefficient for determining corrosion current and corrosion rate[49] where as all other experiments determine the kinetics of corrosion process and simultaneously measure the Tafel coefficients. These electrochemical methods based on nonlinear response current measurements are restricted to activation-controlled corrosion processes. This restriction has been overcome by a new method called electrochemical frequency modulation (EFM) which is also based on non-linear measurements.

In EFM, a small potential signal (20 mV) is applied to perturb the corrosion system and the nonlinear current response is measured. One of the advantages of EFM is that it does not apply a large potential signal to the sample thereby avoiding sample degradation. Also EFM measures the corrosion rate instantaneously without the knowledge of Tafel coefficients. EFM also has a factor called the causality factor which can be used as an internal check to validate the experimental data obtained.

2.2.3.1. Principle and theory of EFM

Electrochemical methods based on analyzing the harmonics of response current to a potential perturbation have gained much advantage over other electrochemical methods in recent times. All these methods based on harmonics rely on the fact that a potential perturbation of a corrosion system by one or more input signals leads to a nonlinear current response due to the nonlinear nature of corrosion processes. These methods have the advantage of determining the kinetics of a corrosion process and Tafel parameters in a short period of time. In case of corrosion reaction where the anodic and cathodic reactions are under charge transfer or mass transfer control, separate equations were derived for analyzing the harmonics. In 1996 Bosch and Bogaerts proposed a model for determining the corrosion rate and Tafel parameters of a

corrosion system, in which the total corrosion reaction rate depends on both activation and diffusion control i.e., the anodic reaction was under activation control and the cathodic reaction was under diffusion control[50]. The model was based on analyzing the first three harmonics of the AC current response to a 20 mV potential perturbation without looking at the intermodulation response. In the same year they proposed a technique based on intermodulation current responses of a corrosion system to determine the corrosion rate and Tafel parameters[51]. This intermodulation technique applies a potential perturbation at two different frequencies to the corrosion system so that the nonlinear current response contains intermodulation frequencies in addition to the harmonic frequencies. The primary advantage of the intermodulation technique over the harmonic technique is that the current response at the intermodulation frequencies is not affected by the harmonics of the applied frequency signal. The intermodulation technique model was derived using a simple Taylor series expansion for the current-voltage relationship of a corrosion process.

In 2001 Bosch *et al*., proposed a novel technique based on intermodulation frequency called Electrochemical Frequency Modulation (EFM)[52]. The advantage of EFM over the earlier proposed intermodulation technique is that it allowed for the validation of experimental data using causality factors [10] and the selection of different corrosion models. EFM could be used in different environments with different corrosion kinetics such as activation controlled, diffusion controlled and passivation controlled. Each model has separate equations derived from different current-voltage relationship of the corrosion process. This new method was tested for only a few corrosion systems and proved to work well for some corrosion systems[27, 29].

In EFM two different voltage excitation sine waves of frequency ω_1 and ω_2 are applied to a corrosion system and the AC nonlinear current response to the perturbation signal is

measured at the zero, harmonic ($2\omega_1$, $2\omega_2$, $3\omega_1$, $3\omega_2$...,) and intermodulation frequencies ($\omega_1 \pm \omega_2$, $2\omega_1 \pm \omega_2$, $\omega_1 \pm 2\omega_2$...,) the latter of which are frequencies at zero Hertz, multiples of the base frequencies, and sum and difference of the base frequencies respectively. Analyzing the peaks of current at harmonic and intermodulation frequencies gives the corrosion rate and Tafel parameters. The input signal in the form of a sine wave with two different frequencies (ω_1 and ω_2) is represented as below.

$$\eta = U_0 \sin \omega_1 t + U_0 \sin \omega_2 t \tag{2.16}$$

where, η is the overpotential, U_0 is the amplitude of the applied signal; ω_1 and ω_2 are two different frequencies. The mathematical derivation using the above input signal for different corrosion kinetics was first derived by Bosch *et al*., in 2001 and it is derived in the following sub-sections.

2.2.3.2. Activation controlled system

The rate of any electrochemical reaction depends on the rate of two individual processes, the anodic and cathodic processes, taking place in the electrochemical cell. These two processes can take place through different mechanisms. If an electrochemical reaction (corrosion) is controlled by the kinetics of the reaction at the metal surface then the reaction is said to be under kinetic control, charge transfer control or activation control. The corrosion system under activation control obeys the Tafel equation which can be written for both anodic and cathodic processes as below.

$$i = i_o \exp\left[\frac{2.303(E-E^o)}{b}\right] \tag{2.17}$$

where, i is the net current density from the individual cell reaction, i_o is exchange current density, E is the potential of the electrode, E^o is the equilibrium potential for a given reaction and b is the Tafel constant.

The above equation for both anodic and cathodic processes can be combined together to derive a generalized equation for a kinetic controlled process called the Butler-Volmer equation[53] and given as

$$i = i_{corr}\left[\exp\left\{\frac{2.303(E-E_{corr})}{b_a}\right\} - \exp\left\{-\frac{2.303(E-E_{corr})}{b_c}\right\}\right] \quad (2.18)$$

where, i is the net current from both anodic and cathodic reaction, i_{corr} is the corrosion current, E is the electrode potential, E_{corr} is the corrosion potential, b_a is the anodic Tafel constant and b_c is the cathodic Tafel constant.

From Eqn 2.18 it can be seen that the difference between the resultant electrode potential (E) and the corrosion potential (E_{corr}) of each individual reaction is the overpotential (η). So the equation reduces to the following form

$$i = i_{corr}\left[\exp\left\{\frac{2.303(\eta)}{b_a}\right\} - \exp\left\{-\frac{2.303(\eta)}{b_c}\right\}\right] \quad (2.19)$$

For mathematical simplicity in the following derivations the constant term 2.303 or $\ln_{10}$ in the above equation is modified with Tafel constants as $\beta_a = b_a/2.303$ and $\beta_c = b_c/2.303$ and Eqn 2.19 reduces to

$$i = i_{corr}\left[\exp\left(\frac{\eta}{\beta_a}\right) - \exp\left(-\frac{\eta}{\beta_c}\right)\right] \quad (2.20)$$

Now the input perturbation potential signal in the form of sine waves with two different frequencies as described in Eqn 2.16 can be substituted in the above equation. The detailed

derivation is given in Appendix B and the final equation is given as Eqn 2.21.

$$i = i_{fr} + i_{\omega_1}\sin\omega_1 t + i_{\omega_2}\sin\omega_2 t - i_{2\omega_1}\cos 2\omega_1 t - i_{2\omega_2}\cos 2\omega_2 t - i_{3\omega_1}\sin 3\omega_1 t - i_{3\omega_2}\sin 3\omega_2 t + i_{\omega_2\pm\omega_1}\cos(\omega_2 t - \omega_1 t) - i_{\omega_2\pm\omega_1}\cos(\omega_2 t + \omega_1 t) + i_{2\omega_2\pm\omega_1}\sin(2\omega_2 t - \omega_1 t) - i_{2\omega_2\pm\omega_1}\sin(2\omega_2 t + \omega_1 t) + i_{2\omega_1\pm\omega_2}\sin(2\omega_1 t - \omega_2 t) - i_{2\omega_1\pm\omega_2}\sin(2\omega_1 t + \omega_2 t) \quad (2.21)$$

where, i_{fr} is the current due to Faraday rectification. $i_{2\omega_1}$, $i_{2\omega_2}$are the currents measured at harmonic frequency $2\omega_1$ and $2\omega_2$ respectively, similarly $i_{\omega_{2+\omega_1}}$ and $i_{\omega_{2-\omega_1}}$are the currents measured at intermodulation frequencies $\omega_2+\omega_1$ and $\omega_2-\omega_1$ respectively. From the harmonic and intermodulation current relations which are explained detail in Appendix B, the following expressions for corrosion rate parameters are obtained for activation controlled system[52].

$$i_{corr} = \frac{{i_{\omega_1,\omega_2}}^2}{2\sqrt{8 i_{\omega_1,\omega_2} i_{2\omega_2\pm\omega_1} - 3{i_{2\omega_2\pm\omega_1}}^2}} \quad (2.22)$$

$$\beta_a = \frac{i_{\omega_1,\omega_2} U_0}{i_{\omega_2\pm\omega_1} + \sqrt{8 i_{\omega_1,\omega_2} i_{2\omega_2\pm\omega_1} - 3{i_{\omega_2\pm\omega_1}}^2}} \quad (2.23)$$

$$\beta_c = \frac{i_{\omega_1,\omega_2} U_0}{-i_{\omega_2\pm\omega_1} + \sqrt{8 i_{\omega_1,\omega_2} i_{2\omega_2\pm\omega_1} - 3{i_{\omega_2\pm\omega_1}}^2}} \quad (2.24)$$

2.2.3.3. Diffusion controlled system

When the diffusion of reactants or the products from the surface of the metal or from the electrolyte limits the rate of reaction, then the process is said to be mass transfer controlled or diffusion controlled. If the cathodic reaction alone is limited by mass transfer then the Tafel coefficient b_c becomes infinite. In this case the current-potential relationship can be written as shown in Eqn 2.25.

$$i = i_{corr}\left[\exp\left(\frac{\eta}{\beta_a}\right) - 1\right] \tag{2.25}$$

The input potential signal in the form of sine waves is used here to derive an expression for diffusion controlled system. The detailed derivation of the expression is given in Appendix B. The final expression consisting of harmonic and intermodulation current components from which the corrosion current and anodic Tafel coefficient b_a are calculated is given below

$$i = i_{fr} + i_{\omega_1}\sin\omega_1 t + i_{\omega_2}\sin\omega_2 t - i_{2\omega_1}\cos 2\omega_1 t - i_{2\omega_2}\cos 2\omega_2 t - i_{3\omega_1}\sin 3\omega_1 t - i_{3\omega_2}\sin 3\omega_2 t + i_{\omega_2\pm\omega_1}\cos(\omega_2 t - \omega_1 t) - i_{\omega_2\pm\omega_1}\cos(\omega_2 t + \omega_1 t) + i_{2\omega_2\pm\omega_1}\sin(2\omega_2 t - \omega_1 t) - i_{2\omega_2\pm\omega_1}\sin(2\omega_2 t + \omega_1 t) + i_{2\omega_1\pm\omega_2}\sin(2\omega_1 t - \omega_2 t) - i_{2\omega_1\pm\omega_2}\sin(2\omega_1 t + \omega_2 t) \tag{2.26}$$

where, $i_{\omega_1} = i_{\omega_2} = i_{corr}\frac{U_0}{\beta_a}$

$$i_{2\omega_1} = i_{2\omega_2} = i_{corr}\frac{1}{4}\left(\frac{U_0}{\beta_a}\right)^2$$

$$i_{3\omega_1} = i_{3\omega_2} = i_{corr}\frac{1}{24}\left(\frac{U_0}{\beta_a}\right)^3$$

$$i_{\omega_2\pm\omega_1} = i_{corr}\frac{1}{2}\left(\frac{U_0}{\beta_a}\right)^2$$

$$i_{2\omega_2\pm\omega_1} = i_{2\omega_1\pm\omega_2} = i_{corr}\frac{1}{8}\left(\frac{U_0}{\beta_a}\right)^3$$

The harmonic and intermodulation current relationships shown above are solved to derive equations for calculating corrosion current and anodic Tafel coefficient when the cathodic process under diffusion control.

$$i_{corr} = \frac{{i_{\omega_1,\omega_2}}^2}{2i_{\omega_{2\pm\omega_1}}} \quad (2.27)$$

$$\beta_a = \frac{{i_{\omega_1,\omega_2}}^2}{2i_{\omega_{2\pm\omega_1}}} U_0 \quad (2.28)$$

2.2.3.4. Passivation controlled system

When the potential of a metal is moved in a more positive direction starting from the corrosion potential (E_{corr}), the dissolution current of the metal increases, i.e. the metal will start corroding more quickly. This increasing trend in dissolution current or corrosion current with increasing potential occurs up to a certain critical potential. When the critical potential is reached, the current-potential curve will change its direction and the dissolution current will start decreasing with potential due to the formation of a passive film on the surface that prevents the metal from further corrosion. This critical potential corresponding to the maximum in the current-potential curve, is called as the passivation potential and the phenomenon is called as passivation[53]. The corrosion system is said to be under passivation control at potentials higher than this passivation potential. The passivation potential differs from metal to metal and environmental conditions. EFM can be used at these conditions for measuring the corrosion rate and Tafel coefficients[52].

The anodic Tafel parameter goes to infinity ($\beta_a \rightarrow \infty$) under passivation control and the current-potential relationship can be written as

$$i = i_{corr}\left[1 - \exp\left(-\frac{\eta}{\beta_c}\right)\right] \quad (2.29)$$

The input signal applied in the form of sine wave with two different frequencies is substituted in the equation above (see Appendix B). After mathematical manipulation the final output response current consisting of harmonic and intermodulation current components is given below.

$$i = i_{fr} + i_{\omega_1} \sin \omega_1 t + i_{\omega_2} \sin \omega_2 t + i_{2\omega_1} \cos 2\omega_1 t + i_{2\omega_2} \cos 2\omega_2 t - i_{3\omega_1} \sin 3\omega_1 t - i_{3\omega_2} \sin 3\omega_2 t - i_{\omega_2 \pm \omega_1} \cos(\omega_2 t - \omega_1 t) + i_{\omega_2 \pm \omega_1} \cos(\omega_2 t + \omega_1 t) + i_{2\omega_2 \pm \omega_1} \sin(2\omega_2 t - \omega_1 t) - i_{2\omega_2 \pm \omega_1} \sin(2\omega_2 t + \omega_1 t) + i_{2\omega_1 \pm \omega_2} \sin(2\omega_1 t - \omega_2 t) - i_{2\omega_1 \pm \omega_2} \sin(2\omega_1 t + \omega_2 t) \quad (2.30)$$

From Eqn 2.30 the corrosion current and cathodic Tafel coefficient for a system under passivation control can be calculated using the relation

$$i_{corr} = \frac{{i_{\omega_1,\omega_2}}^2}{2 i_{\omega_2 \pm \omega_1}} \quad (2.31)$$

$$\beta_c = \frac{{i_{\omega_1,\omega_2}}^2}{2 i_{\omega_2 \pm \omega_1}} U_0 \quad (2.32)$$

2.2.3.5. Data validation

One of the primary advantages of EFM is that the experimental data can be verified using internal check factors called causality factors. The nonlinear current response of the electrochemical systems contains components of the zero, harmonic and intermodulation frequency. The harmonic current components $i_{2\omega_1}, i_{2\omega_2}, i_{3\omega_1}, i_{3\omega_2}$ which are measured at harmonic frequencies $2\omega_1$, $2\omega_2$, $3\omega_1$, $3\omega_2$ respectively have a unique relation with the intermodulation current components ($i_{\omega_2 \pm \omega_1}, i_{2\omega_1 \pm \omega_2}, i_{2\omega_2 \pm \omega_1}$) measured at intermodulation frequencies ($\omega_2 \pm \omega_1$, $2\omega_1 \pm \omega_2$, $2\omega_2 \pm \omega_1$). This relationship can be used to check the validity of

the response data obtained due to the perturbation signal. The relationship between harmonic and intermodulation current components is given below[52]

$$i_{\omega_2 \pm \omega_1} = 2i_{2\omega_1} = 2i_{2\omega_2} \tag{2.33}$$

$$\Rightarrow \frac{i_{\omega_2 \pm \omega_1}}{i_{2\omega_1}} = 2$$

$$i_{2\omega_1 \pm \omega_2} = i_{2\omega_2 \pm \omega_1} = 3i_{3\omega_1} = 3i_{3\omega_2} \tag{2.34}$$

$$\Rightarrow \frac{i_{2\omega_1 \pm \omega_2}}{i_{3\omega_1}} = 3$$

These two relations are called causality factor (2) and causality factor (3) respectively. These theoretical factors indicate that harmonic and intermodulation components in the response current signal always follow the same relationship, which in turn can be used to validate the data obtained. A small deviation from these theoretical values of 2 and 3 can be due to the influence of external factors such as noise and the data obtained can be assumed to be invalid if the causality factors deviate significantly from theoretical value of 2 and 3.

2.3. Summary

In the preceding sections, the basics of the CO_2 corrosion mechanism and the influence of environmental factors on their mechanism and reaction rate are discussed. It is evident that there is a lack of knowledge in using electrochemical methods, especially EFM, to understand CO_2 corrosion of carbon steel. Performing preliminary experimental work using EFM will determine the feasibility of using this technique for CO_2 corrosion measurement, the main objective of this research work. It will also help in addressing many unanswered questions about the CO_2

corrosion mechanism under different environmental conditions. The forthcoming chapter discusses the materials and methodology used for this research work in detail.

3. MATERIALS AND METHODS

This chapter describes the methodology used for carrying out the experiments under film and non-film forming conditions. The methodology includes sample preparation, electrolyte preparation, equipment used and the electrochemical methods used for analysis.

3.1. Sample Preparation Procedures

AISI 1018 carbon steel cylindrical samples with the chemical composition shown in Table 3.1 were used for this study. A three electrode assembly was used with a saturated calomel electrode as the reference electrode and a platinum electrode as the counter electrode. The rotating cylinder electrode (RCE) samples of AISI 1018 steel were made with an outer diameter of 11.99 mm, inner diameter of 6.35 mm and a height of 7.98 mm. The RCE samples had a surface area of 3 cm^2 and were made according to the drawing specifications of Pine Instrument Inc[54]. The density of the metal was 7.87 gm/cm^3 with an equivalent weight of 27.92 g/mol. The test coupons were then polished successively with 240, 320, 400 and 600 grit size silicon carbide papers on a slow running lathe. The samples were cleaned ultrasonically with ethanol for 5 minutes followed by rinsing with deionized water and then with acetone, and the dried in hot air. The samples were then kept in a desiccator until they were ready to be tested. After testing, samples were again cleaned with acetone, dried in hot air and kept in a desiccator for further analysis.

Table 3.1. Chemical composition of AISI 1018 carbon steel[55]

Chemical constituent	C	Mn	P	S	Si	V	Fe
Composition (wt. %)	0.16	0.67	0.007	0.015	0.23	-	Bal

3.2. Electrolyte Preparation

The test solution used for the experiments was 3% (w/w) sodium chloride (NaCl), which was prepared using ACS grade sodium chloride (100% assay) and reverse osmosis water. The test solution was deaerated by bubbling CO_2 for at least 1 hour before exposing the sample into the solution. Beverage grade CO_2 with a quality assay of 99.99% was used for this purpose. The concentration of O_2 and H_2O in the CO_2 gas was less than 10 and 15 ppm respectively. For non-film forming conditions, the pH of the solution was maintained at 3.7, which is the saturation pH of CO_2 in the NaCl solution at room temperature (≈ 23°C). The CO_2 gas was continuously bubbled into the solution throughout the experiment. For film forming conditions the pH of the solution was adjusted to 6.5 using a saturated sodium bicarbonate ($NaHCO_3$) solution which was bubbled with beverage grade CO_2 before making the addition. All experiments were done at room temperature and at atmospheric pressure.

3.3. Equipment

Experiments were done using a rotating cylinder electrode system[56] at room temperature, atmospheric pressure and using a GAMRY PC4 potentiostat. A Modulated Speed Rotator (MSR) was used for rotating the working electrode to simulate laminar, transient and turbulent flow situations which are characterized using Reynolds number. The MSR style rotator was calibrated using stroboscope and the calibration results are shown in Appendix A. The PC4 potentiostat was calibrated periodically with a dummy cell. A Pyrex™ glass vessel of 1 litre capacity with

openings for a three electrode assembly was set up. A saturated calomel electrode was used as the reference electrode and a platinum electrode as the counter electrode. The pH of the solution was monitored using an Oakton pH 5 acorn series pH meter. The pH meter was calibrated every week with Fisher buffer solutions of 4, 7 and 10. A photograph of the experimental setup is shown in Figure 3.1.

3.4. Corrosion Rate Measurement Methods

EFM was used to analyse CO_2 corrosion at various conditions and the results of EFM were compared with LPR and EIS. For simulating laminar, transient and turbulent flow situations, the cylindrical electrodes were rotated at 5, 24 and 100 rpm corresponding to a Reynolds number of 42, 202 and 844 respectively[39]. For the RCE electrode, the transition from laminar to turbulent flow occurs when the Reynolds number exceeds 200. The EFM method was used with a multiplexer frequency of 2 and 5 Hz with 4 cycles. The amplitude of the excitation signal was 10 mV. The calculations of polarization resistance (R_p) value from the Tafel slopes obtained from EFM are shown in Appendix C. The electrochemical methods were used in sequence of EFM, LPR and EIS.

In the LPR method the metal sample was polarized ±20 mV around the open circuit potential (E_{corr}) with a scan rate of 0.125 mV/sec. E_{corr} is the potential at which no net electric current flows through the electrode. The sample was polarized with a sample period of 2 seconds to measure the total resistance of the solution. The polarization resistance was calculated using default Tafel slopes of 120 mV/decade. The EIS method was used to verify the R_p value obtained from EFM. In EIS the sample was polarized with an AC potential signal of amplitude 10 mV over a wide range of frequencies (10^3 kHz to 0.005 Hz).

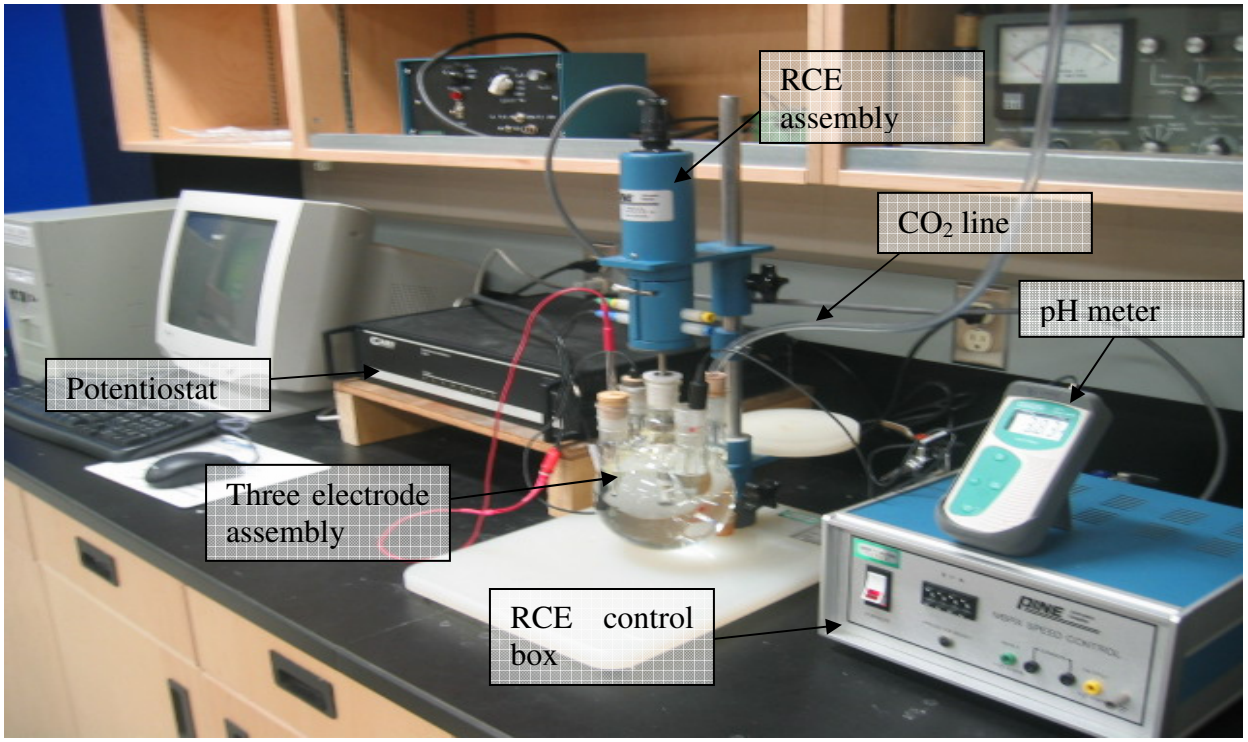

Figure 3.1. Photograph of the experimental setup used for the study.

The response to the AC potential signal in EIS was an AC current signal with phase lag, from which the total impedance of the system was calculated through two graphical representations (Bode and Nyquist plots). The results were then fitted with standard models to obtain the R_p values. In order to confirm the consistency of results obtained from various electrochemical methods an experimental uncertainty analysis was done for all the electrochemical methods used in this study.

3.5. Summary

The materials and the methodology used for analyzing CO_2 corrosion of carbon steel under film forming and non-film forming conditions are discussed in this chapter. Also the sequence of using electrochemical methods and their default hardware settings was discussed. In

the upcoming chapter, the results of CO_2 corrosion kinetics obtained using EFM and its comparison with other electrochemical methods are discussed and analyzed.

4. RESULTS AND DISCUSSION

This chapter presents the experimental results obtained using various electrochemical methods under film forming and non-film forming conditions at RCE speeds of 5 rpm, 24 rpm and 100 rpm simulating laminar, transient and turbulent flow regions respectively. Several reproducibility studies and a comparison of EFM results with other electrochemical methods are presented in this chapter.

4.1. Analysis of Dummy Cell Using EFM

EFM was used to find the resistance value of a resistor in a dummy cell. A dummy cell is one which has known value of electrical components, fabricated on a printed circuit board to test the electrochemical methods of the GAMRY system. A 100 ohm resistor was connected to a dummy cell and EFM data was obtained for the resistor with a baseline frequency of 1 Hz. Since an ideal resistor is independent of frequency at all current and voltage values, the baseline frequency of 1 Hz gave reasonable results. The results of EFM analysis are shown in Table 4.1.

It can be seen from Table 4.1 that the R_p value calculated from EFM approximately matches the resistance value of the resistor in the dummy cell. Although the anodic and cathodic Tafel slopes calculated from EFM were close to each other, they have no physical meaning for an ideal resistor. It can also be seen that the causality factors CF (2) and CF (3) have deviated from the theoretical value of 2 and 3 respectively.

Table 4.1. EFM analysis of 100 ohm resistor in a dummy cell analyzed with a frequency of 2 and 5 Hz.

Parameters	Value
I_{corr} (μA)	3792
b_a (mV/decade)	1716
b_c (mV/decade)	1764
B (mV/decade)	378.1
R_p (ohms)	99.73
CF(2)	3.922
CF(3)	0.7125

4.2. Effect of Baseline Frequency and Corrosion Model

As mentioned in section 2.2.3, the EFM method applies a potential perturbation in the form of a sine wave at two different frequencies (ω_1 and ω_2) to the metal sample. The current response to the potential excitation consists of harmonics of the base frequencies due to the non-linear nature of corrosion processes. The current response was read at zero, harmonic and intermodulation frequencies to obtain corrosion current, corrosion rate and the Tafel constants. Since frequency plays a key role in obtaining the results precisely from EFM [29, 52] a study was carried out to see the effect of frequency and also to choose a proper corrosion model and frequency. Different baseline frequencies of 1 Hz, 0.1 Hz, 0.01 Hz 0.005 Hz with multiplexer frequencies of 2 and 5 Hz were chosen to study this effect. As explained by Bosch *et al*., the frequency should be low to avoid any influence from the capacitive behaviour of the electrochemical double layer on the corroding metal[52].

The experimental results of AISI carbon steel 1018 after 1 hour of exposure in CO_2 saturated NaCl solution at room temperature is shown in Table 4.2. The experiment was carried out assuming that the reaction is under either diffusion control or activation control and not using the passivation model since AISI carbon steel 1018 does not form passive films at these

conditions. It can be seen from Table 4.2 that as the frequency decreases by an order of magnitude the corrosion rate decreases considerably and the values of I_{corr} and Tafel slopes differ significantly paralleling the observations of Kus and Mansfled[29] for other corrosion systems. The EFM method was able to analyse the system using the activation and diffusion control models at 1 Hz and 0.1 Hz base frequencies, but only succeeded with the diffusion model at 0.01 and 0.005 Hz. Even though the causality factors CF(2) and CF(3) are close to their theoretical values of 2 and 3 respectively, the EFM technique measured different corrosion rates at different frequencies irrespective of the corrosion model chosen, thus showing the necessity of using proper base frequency to obtain correct corrosion rate.

Table 4.2. EFM analysis of AISI 1018 carbon steel at various base frequencies in CO_2 saturated NaCl solution at room temperature, 3.7 pH and stagnant condition (5 rpm) after 1 hour of exposure.

	2 and 5 Hz		0.2 and 0.5 Hz		0.02 and 0.05 Hz		0.01 and 0.025 Hz	
Parameters	Active	Diffusion	Active	Diffusion	Active	Diffusion	Active	Diffusion
I_{corr} (μA)	464.9	1356	344.4	391.3	-	354.4	-	287.8
b_a (mV)	95.99	187.6	69.13	73.15	-	57.49	-	66.3
b_c (mV)	197.66	∞	1173.62	∞	-	∞	-	∞
B (mV)	28.06	81.55	28.35	31.76	-	24.96	-	28.79
R_p (ohms)	60.35	60.14	82.31	81.17	-	70.44 ± 1.62	-	100.03
Corrosion rate (mpy)	70.81	206.5	52.46	59.6	-	53.98 ± 4.6	-	58.35
CF (2)	1.9824	1.9798	1.9778	1.962	-	1.988	-	2.012
CF (3)	2.9474	3.0064	3.011	2.963	-	3.35	-	3.368

From Table 4.2, it can be seen that at each frequency the R_p value remains the same irrespective of the corrosion model. This is due to the fact that the R_p depends only on the response current peak at a particular intermodulation frequency[28], i.e.,

$$R_p = \frac{U_0}{i_{\omega k}}; \qquad k = 1, 2 \tag{4.1}$$

where, R_p is the polarization resistance, U_o is the amplitude of potential perturbation and $i_{\omega k}$, is the current responses at angular frequency ω_k where k =1,2..

Therefore it is clear that the Tafel slopes and the corrosion current values are calculated to validate the relation, $B/i_{corr} = R_p$ = constant and it has no correlation with the calculations based on Stern-Geary equation which are given as

$$\text{Activation Control}: \; i_{corr} = \frac{b_a.b_c}{2.303(b_a+b_c)*R_p} \tag{4.2}$$

$$\text{Diffusion control}: \; i_{corr} = \frac{b_a}{2.303R_p} \tag{4.3}$$

The variation in corrosion rate and polarization resistance at different frequencies could be due to the influence of capacitive behaviour of the electrochemical double layer which is more pronounced at higher frequency than at lower frequency. As previously stated, one of the important criteria for EFM to work well is that the frequency should be free from capacitive behaviour. To elucidate more information on the selection of proper base frequency and the influence of capacitive behaviour, EIS was used. The EIS method was carried out over a wide frequency, ranging from 10 kHz to 10^{-3} Hz, to see the effect of double layer capacitance and the interfacial impedance.

The high-frequency limiting value in EIS corresponds to the electrolyte resistance, whereas the low-frequency limiting value corresponds to the slope of the polarization curve[57]. EIS analysis was carried out on AISI 1018 carbon steel sample under same set of conditions as before and the results are shown in Figure 4.1. It can be seen from Figure 4.1 that the frequency range (0.1 – 1.5 Hz) used in the EFM method fall into the capacitive region of the cell. The variation in corrosion rate and polarization resistance at higher frequencies could be attributed to this frequency region. Therefore the results calculated by EFM with a baseline frequency of 1 Hz and 0.1 Hz were meaningless irrespective of the corrosion model chosen and the causality factors obtained. Since the only meaningful data was obtained at 0.01 Hz and the fact that the diffusion model is the only valid model at this frequency, the system must be dominated by diffusion control.

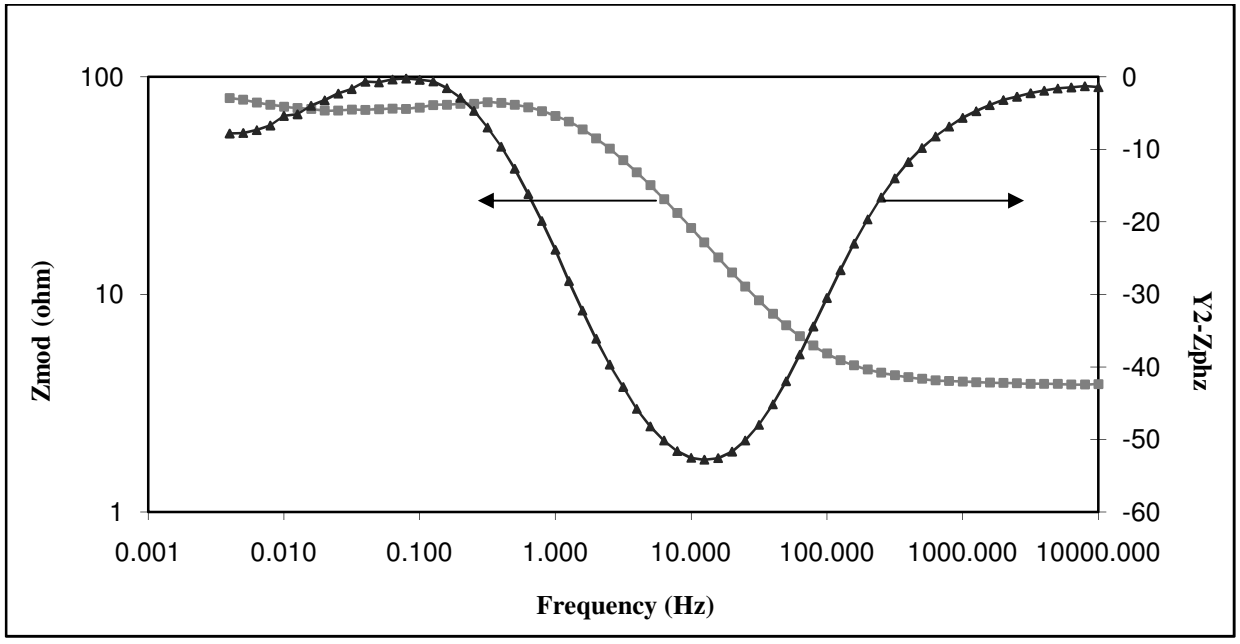

Figure 4.1. Bode plot from EIS performed on AISI 1018 carbon steel after 1 hour of exposure at 3.7 pH, 5 rpm and room temperature.

4.3. Reproducibility and Uncertainty Analysis

In order to check the consistency of results obtained from various electrochemical methods, an uncertainty analysis was performed for each electrochemical method used.

4.3.1. Reproducibility of corrosion rate and polarization resistance using EFM

As EFM has never been used before to analyze a CO_2 corrosion system, an uncertainty analysis on the data was performed. The RCE sample made of AISI 1018 carbon steel was prepared as explained in Chapter 3. The sample was mounted in a rotating cylindrical electrode assembly and immersed in a 3% (w/w) NaCl solution saturated with CO_2 at a pH of 3.7 and at room temperature. The speed of the RCE was set at 5 rpm to keep the sample in a near stagnant condition. The sample was exposed for various times ranging from one to 24 hours. The experiment was repeated several times and a student's-t test was done on the corrosion rate and polarization values obtained using EFM at different exposure times. If the corrosion rate and polarization values are distributed as Student's-t distribution with a *v* degrees of freedom, then there is a probability (1-*a*) that the next value will lie in the range of $\bar{X} \pm P_{\bar{T}}$.

$$P_{\bar{T}} = t\frac{SD}{\sqrt{N}} \tag{4.4}$$

where $\bar{X}$ is the mean of the sample, *SD* is the sample's standard deviation of the mean, *N* is the number of samples.

In the initial phase the experiment was done at different base frequencies and with different corrosion models to find the exact baseline frequency suitable for analyzing CO_2 corrosion at the above mentioned environmental conditions. Finally the base frequency was chosen to be 0.01 Hz with a multiplexer frequency of 2 Hz and 5 Hz and a diffusion model was

chosen. The frequency and corrosion model selection was justified using the EIS method (Figure 4.1). The results of Student's t- test with error bars for corrosion rate and polarization resistance obtained using EFM at various exposure times are shown in Figure 4.2 and 4.3 respectively.

It can be seen from Figure 4.2 that the corrosion rate of AISI 1018 carbon steel increased gradually with time reaching a maximum of 73 mpy after 24 hours of exposure in the CO_2 saturated NaCl solution. Within the 95% confidence interval limits, the uncertainty in the data was found to be 7.8 mpy was observed for the experiment carried out after 24 hours of exposure, and 7.4 and 6.9 mpy was observed for those experiments performed after 5 and 15 hours of exposure respectively. It can be concluded that within experimental uncertainty the corrosion rate increased only slightly over the 24 hour exposure period. There was no protective film formed on the metal surface after 24 hours of exposure, which is in agreement with findings of Nesic *et al*., that to form iron carbonate film at room temperature, the pH has to be high and a long exposure time is required[30].

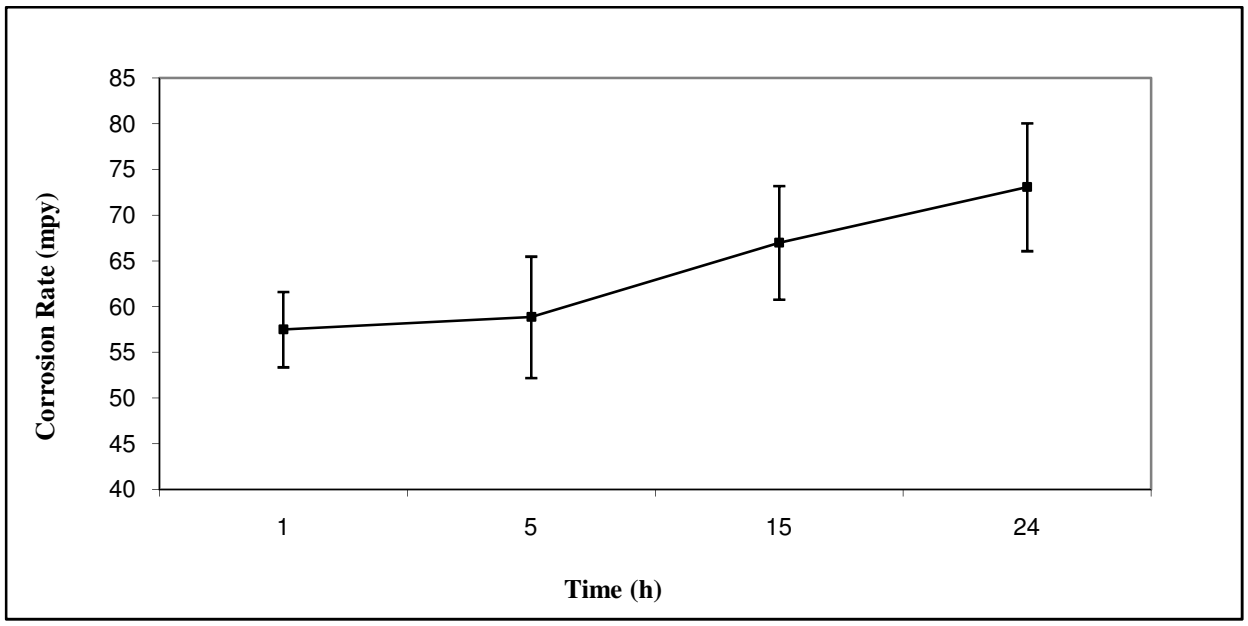

Figure 4.2. Average corrosion rate of AISI 1018 carbon steel at different exposure time obtained using EFM at 5 rpm, pH =3.7 and room temperature.

The variation of polarization resistance with time is shown in Figure 4.3. It was observed that the polarization resistance decreased slightly with time after 24 hours of exposure. From the Tafel slopes and i_{corr} values obtained from EFM, the polarization resistance was calculated using the Stern-Geary equation. The polarization resistance value measurements using the EFM method was always within the experimental uncertainty limit, with an uncertainty of 6.5 ohms at the 95% confidence interval. It can be inferred that the EFM technique can produce reproducible corrosion rate and polarization resistance data.

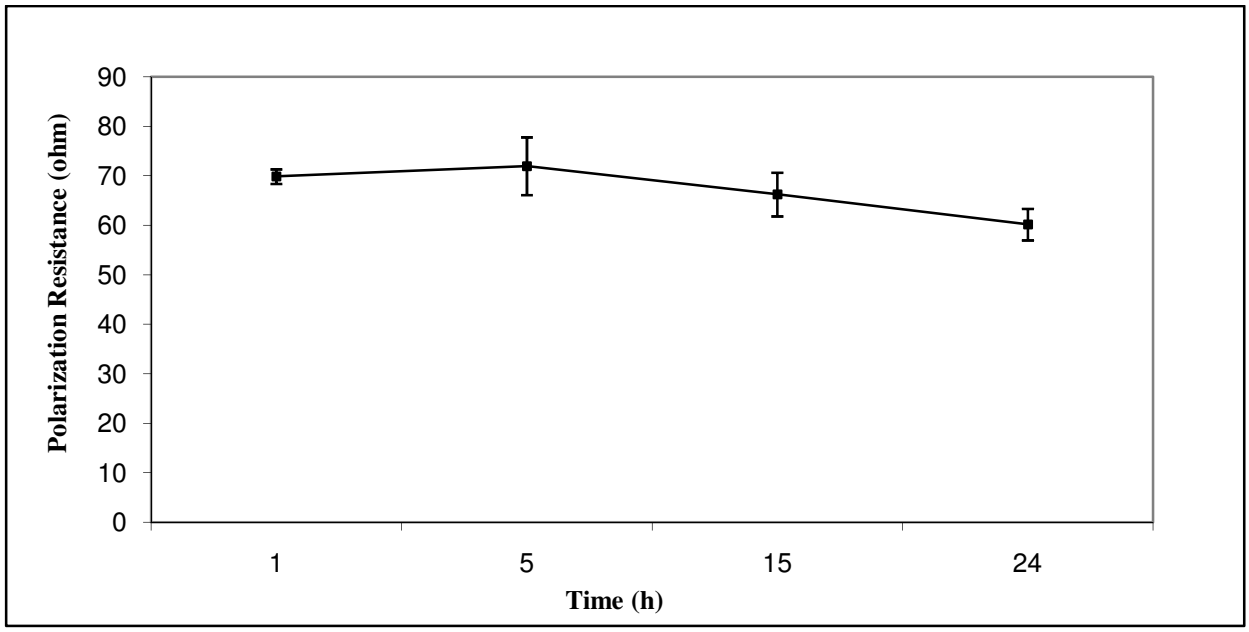

Figure 4.3. Average polarization resistance of AISI 1018 carbon steel at different exposure time obtained using EFM at 5 rpm, pH =3.7 and room temperature.

4.4. Analysis of CO_2 Corrosion at Non-Film Forming Conditions Using EFM

Iron carbonate which is the primary corrosion product of CO_2 corrosion, forms on the surface of the metal if the concentration of Fe^{2+} and CO_3^{2-} exceeds the solubility limit. The corrosion product scale can be protective, which forms a barrier and prevents the metal from further corrosion. Iron carbonate film formation and growth depends on the kinetics of the

precipitation reaction which is a function of temperature, pH, fluid flow and various other factors [11, 37]. At room temperature and a low pH, the kinetics of the precipitation reaction is slow and does not initiate film formation[13]. To analyse CO_2 corrosion under non-film forming conditions, the experiments were performed using 3 % (w/w) NaCl solution at room temperature, a pH of 3.7, at atmospheric pressure and at different hydrodynamic conditions. The salt solution was saturated with CO_2 by bubbling CO_2 gas for at least one hour before exposing the metal sample. The saturated solution was maintained at a pH of 3.7 by continuously bubbling CO_2 gas into the solution throughout the experiment and the results are discussed in the following sections.

4.4.1. EFM measurements carried out at various exposure times in laminar flow and comparison with EIS and LP

The RCE sample was exposed to laminar flow conditions for different exposure times ranging from 1 hour to 24 hours. Fresh samples were prepared for each exposure times. The carbon steel sample was exposed to the same environment as in section 4.3 and was analyzed using LPR, EIS and EFM. EFM analysis was performed with a baseline frequency of 0.01 Hz and by using diffusion control model and it was assumed that the metal surface is not affected to a great extent during the course of the electrochemical analysis. A frequency of 0.01 Hz was chosen to be the idle base frequency as it gave comparable results with LPR and EIS without having to use a very low frequency (0.005 Hz) that would have caused protracted experiments, while the base frequencies 1 Hz and 0.1 Hz were influenced by the capacitive behaviour of the electrochemical double layer.

The variation of LPR curves with time is shown in Figure 4.4. It can be seen from Figure 4.4 that as the exposure time increased the corrosion potential and corrosion current increased

without affecting the slope of the curve. Since the slopes of the curves are nearly the same, it can be assumed that the reaction mechanism (activation control or diffusion control) remains same over the period of exposure time (1 to 24 hours). The increase in corrosion current is directly proportional to the corrosion rate and inversely proportional to the polarization resistance as given by Stern-Geary equation.

The corrosion rate calculated from EFM technique was compared to the LPR results and shown in Figure 4.5. Error bars were calculated for each data points in Figure 4.5 using the Student's-t test at the 95% confidence interval multiplied by the standard error of the estimate.

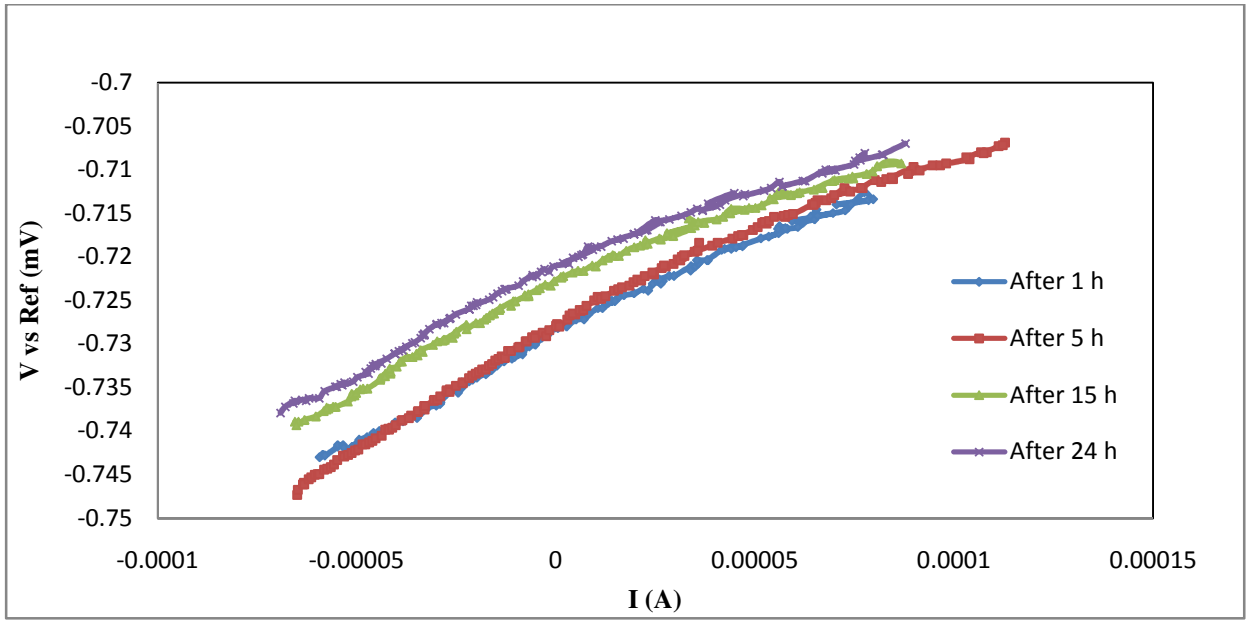

Figure 4.4. Change in linear polarization curves with time at pH =3.7, 5 rpm, 1 atm CO_2 partial pressure and at room temperature.

Since the error bars at each data point overlap, it can be concluded that the corrosion rate did not change significantly over the 24 hour period. It can be seen from Figure 4.5 that there is significant variation in the corrosion rates as determined by EFM and LPR. This deviation can be

attributed to the choice of the default Tafel slopes used in the LP analysis (120 mV/decade); also it assumes that the system is under activation control by default. However,

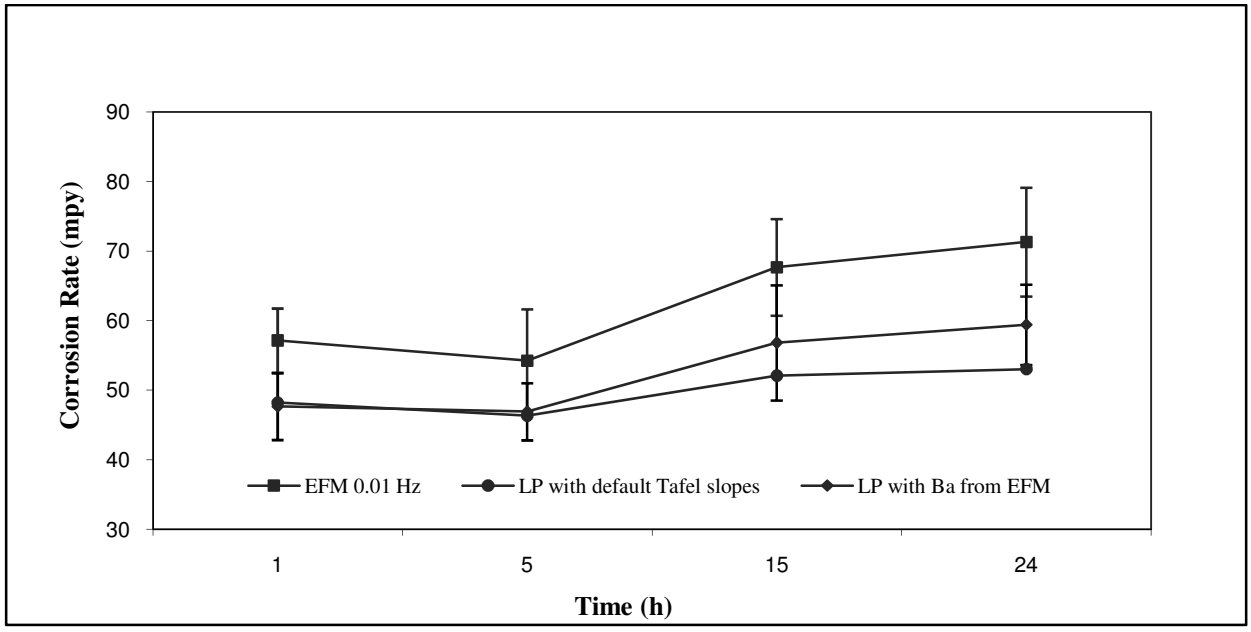

Figure 4.5. Comparison of corrosion rate between EFM and LP at 5 rpm, pH = 3.7, 1 atm partial pressure and at room temperature.

only the diffusion control model worked with EFM at this condition and the corrosion rate was once again calculated by LP method using the anodic Tafel slope obtained from EFM in Stern-Geary equation given by

$$\text{Diffusion control}: \; i_{corr} = \frac{b_a}{2.303 R_p} \tag{4.5}$$

The corrosion rate calculation using Eqn 4.5 is shown in Appendix C. It can be seen from Figure 4.5 that the agreement in corrosion rate between EFM and LP increased when the Tafel slopes used in LP was changed from its default value. Although the error bars at each data point overlaps each other the gap between EFM and LP is of concern. To elucidate more on the results

obtained from this new technique (EFM), EIS was chosen to compare the polarization resistance (R_p).

The basics of the EIS method are explained in chapter 2. EIS analysis was carried out at various exposure times with same set of environmental conditions used for the EFM and LPR methods. Each EIS analysis was carried out over a broad frequency range (10 kHz – 10^{-3} Hz) to see the effect of any double layer capacitance which might vary the polarization resistance. The results of EIS analysis over a 24 hour period, consisting of Nyquist and Bode plots are shown in Figures 4.6 to 4.8. At each exposure time, the Nyquist plot (Z_{img} verses Z_{real}) had one semicircle similar to the response of a Randles cell without Warburg impedance. The shape of the Nyquist plot looks comparable to the experiments done by Zavala and Hernandez[26] at a pH of 3.8. As observed by Zavala and Hernandez, the diameter of the semicircle slightly increased with time from one hour to 5 hours. However, the diameter of the semicircle decreased over time between 15 and 24 hours (Figure 4.6). The shape of the Nyquist plot remained the same with one depressed semicircle in all the experiments.

The point where the semicircle of the Nyquist plot intersects the real axis at high frequency (close to the origin) yields solution resistance (R_s). The intercept on real axis at the other end of the semicircle (low frequency) gives the sum of solution resistance and the polarization resistance. Hence the polarization resistance value is simply the diameter of the semicircle. The two horizontal regions in Figure 4.7, one at high frequency and another at low frequency correspond to the solution resistance (R_s) and polarization resistance (R_p) respectively. The diagonal region in between the high frequency and low frequency region has a negative slope due to the capacitive behaviour of the electrochemical double layer. It can be seen from the Bode plot (phase angle verses frequency Figure 4.8), that there is only one peak observed at an

angle of -52 degrees due to single time constant. As the exposure time increased the peak slightly moved towards the low frequency region with the phase angle remaining close to -52 degrees.

The depressed semicircles observed in Nyquist plot suggest us to use a constant phase element in place of a capacitor due to the non ideal behaviour of electrochemical double layer. For capacitors the impedance is expressed by the following relation.

$$Z = (1/C)(j\omega)^{-\alpha} \qquad (4.6)$$

where, C is the capacitance, α is an exponent factor, ω is the angular frequency, $j = \sqrt{-1}$. Since the electrochemical double layer deviates from ideal capacitors and resembles a constant phase element, the CPE model was used to fit the experimental data and the results are shown in Figures 4.9 and 4.10.

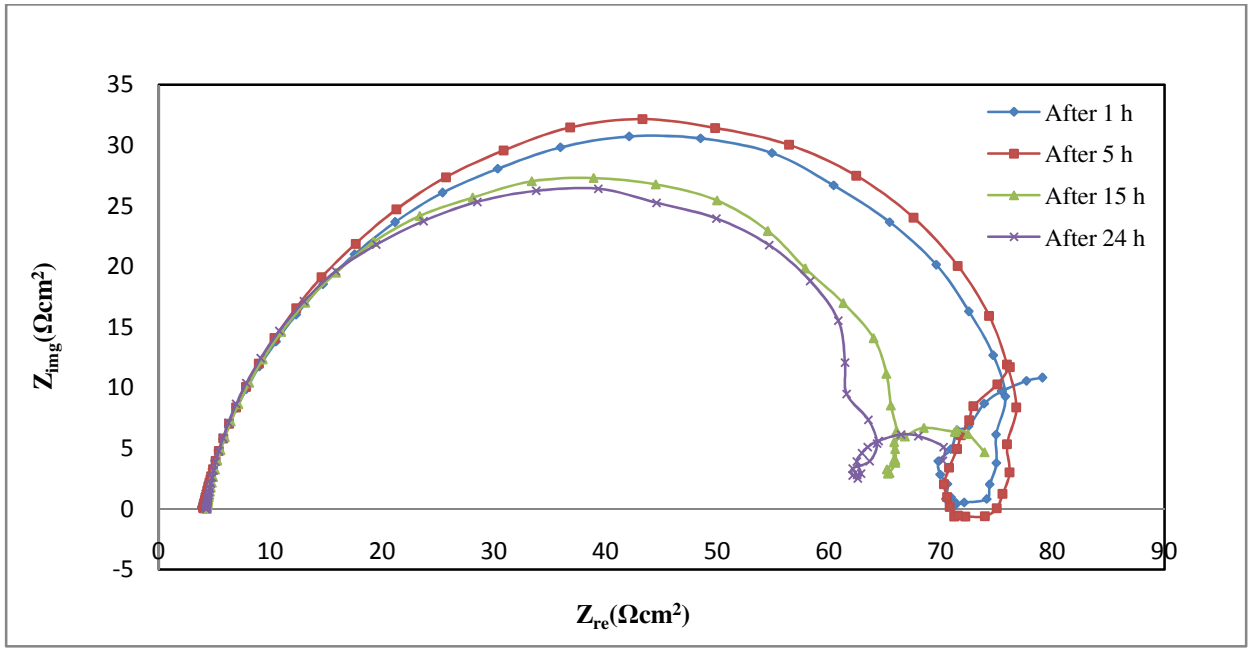

Figure 4.6. Nyquist plot from EIS performed at 5 rpm, pH = 3.7, 1 atm partial pressure and at room temperature over a period of time.

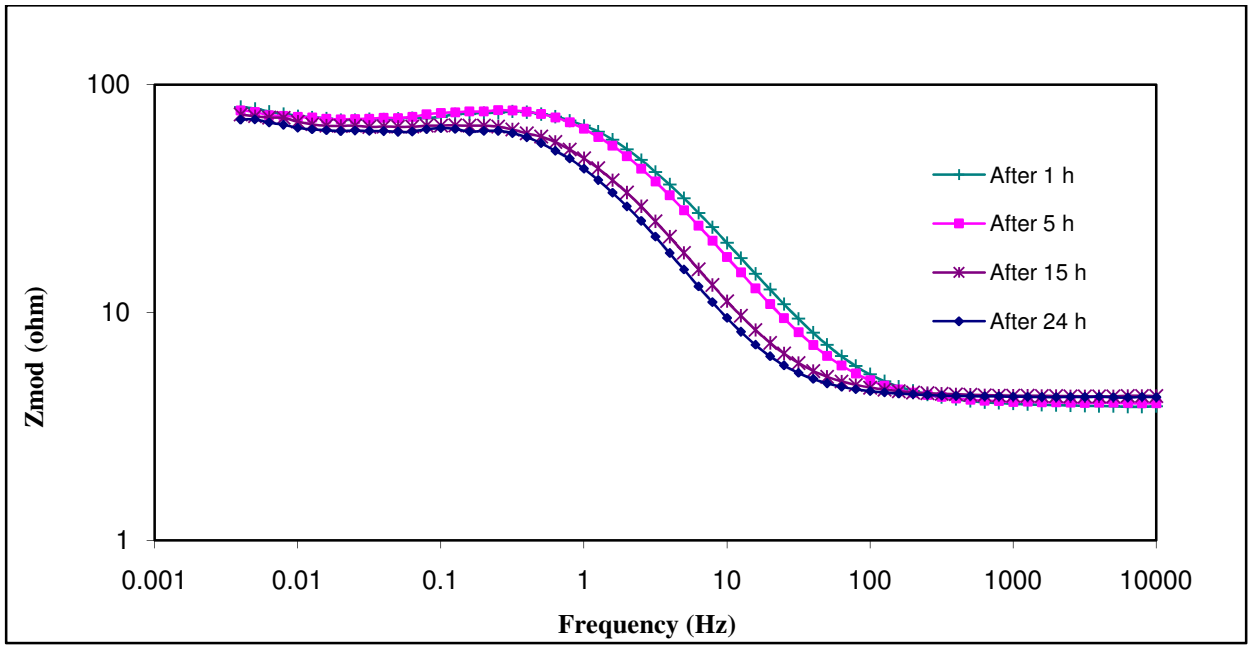

Figure 4.7. Plot of modulus of impedance verses frequency from EIS performed at 5 rpm, pH = 3.7, 1 atm partial pressure and at room temperature over 24 hour period.

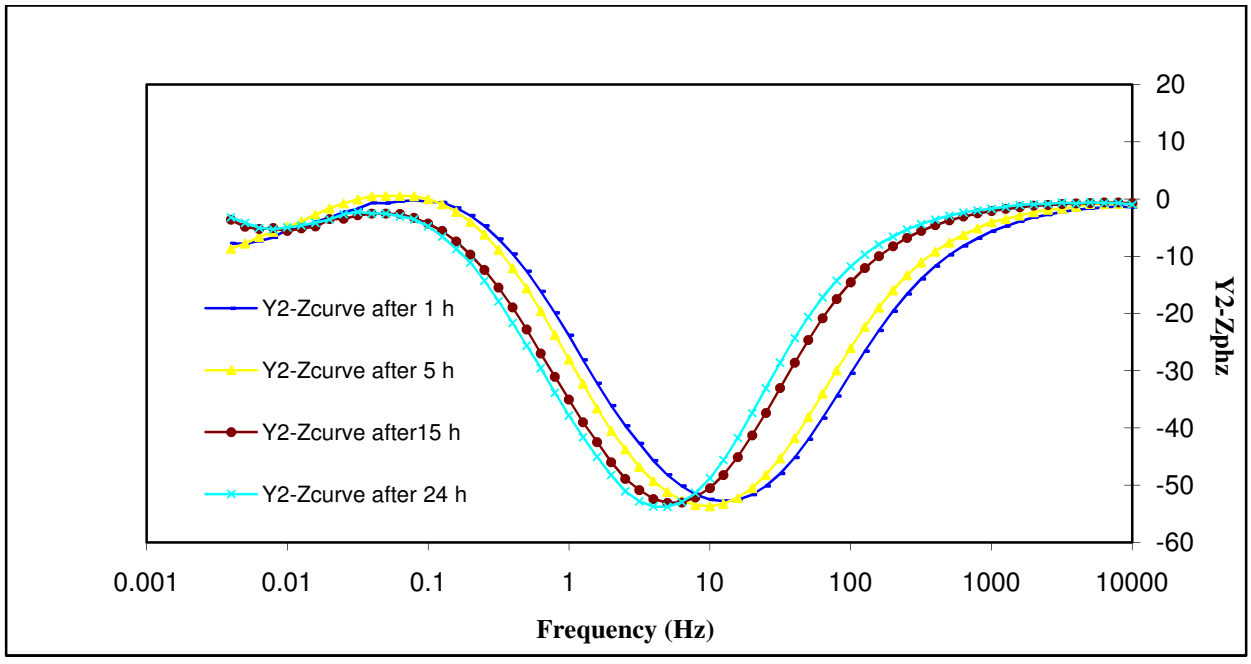

Figure 4.8. Plot of phase angle verses frequency from EIS performed at 5 rpm, pH = 3.7, 1 atm partial pressure and at room temperature over 24 hour period.

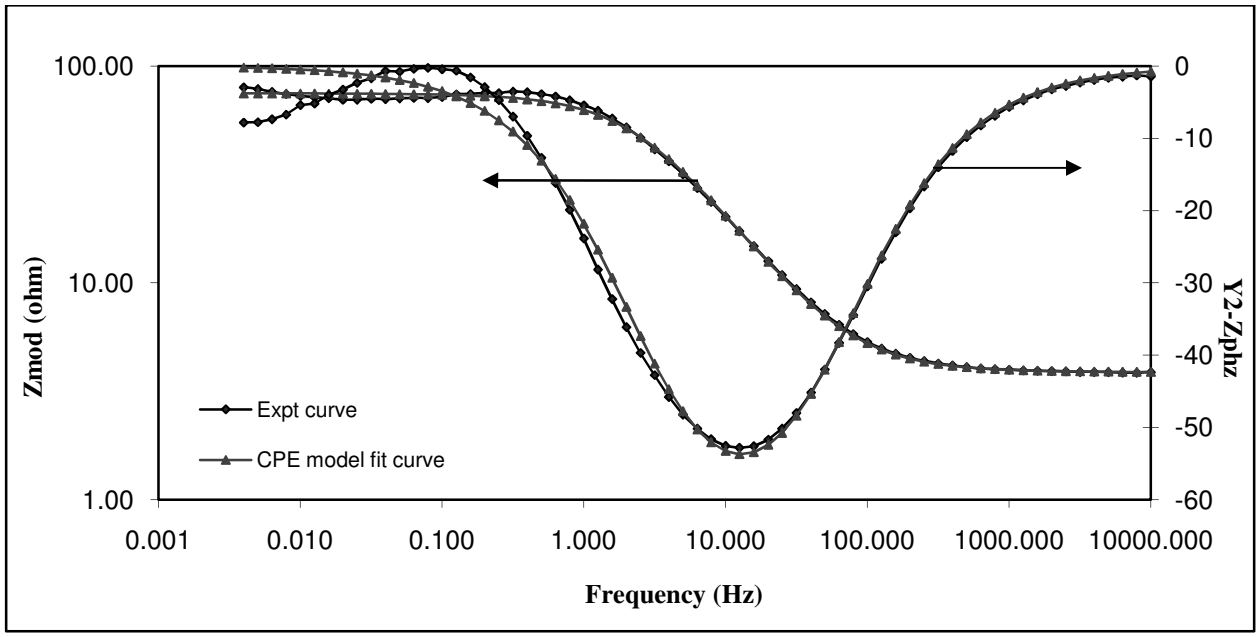

Figure 4.9. Bode plot fitted with CPE model in EIS method carried out at 5 rpm, pH = 3.7, 1 atm partial pressure and at room temperature after 1 hr of exposure.

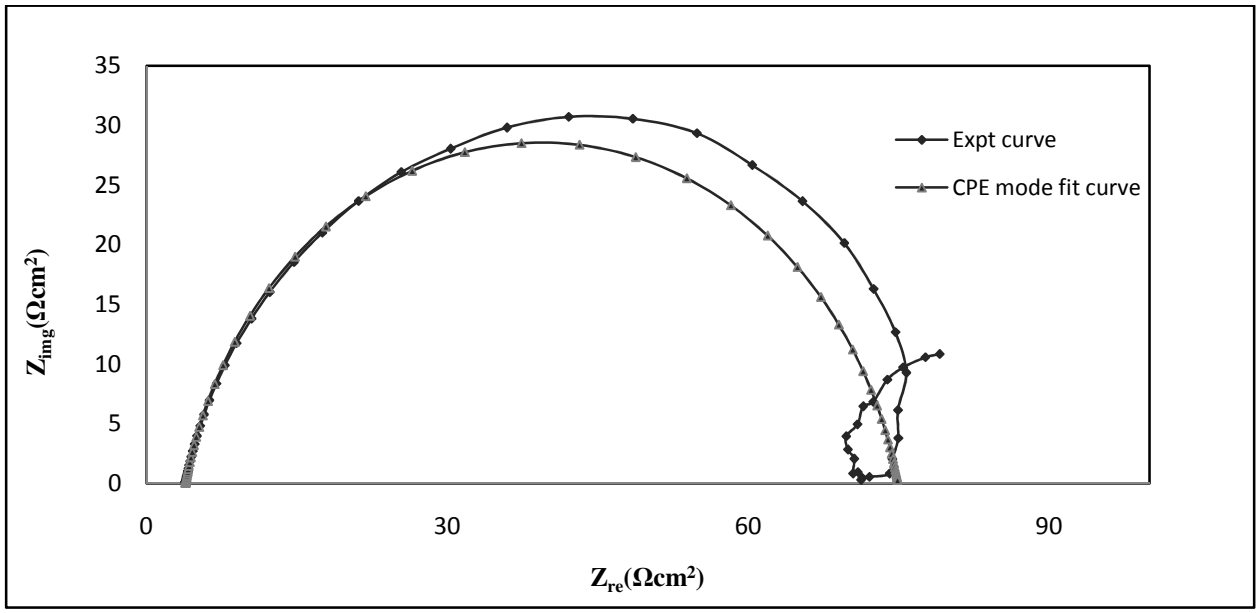

Figure 4.10. Nyquist plot fitted with CPE model in EIS method done at 5 rpm, pH = 3.7, and at room temperature after 1 hr of exposure in 3% (w/w) NaCl solution saturated with CO_2.

The equivalent circuit of CPE model that was used to fit the experimental data is given in Figure 4.11. For all the exposure times, the CPE model fits the experimental data very well.

From the fitted model, the R_p value and other kinetic parameters belonging to CPE model were obtained and shown in Table 4.3. The polarization resistance and solution resistance values are in good agreement with literature[26]. From the Tafel slopes and i_{corr} value obtained from EFM, the polarization resistance was calculated using the relation

$$\text{Diffusion control}: \; i_{corr} = \frac{b_a}{2.303 R_p} \tag{4.7}$$

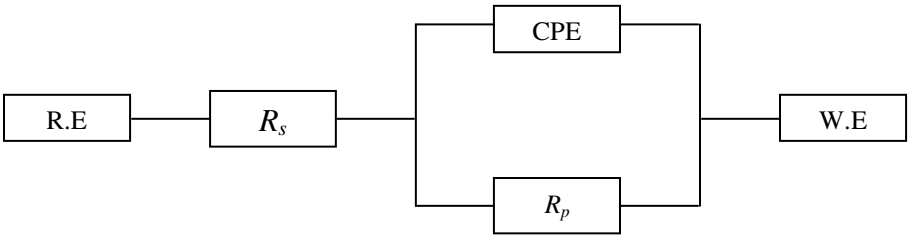

Figure 4.11. Equivalent circuit of constant phase element model used to fit the experimental data.

The polarization resistance value obtained using EFM, EIS and LP at various exposure times is compared in Figure 4.12. Although the polarization resistance determined by EFM and EIS agree within the experimental uncertainty bounds and the polarization resistance determined by the LP method is higher than the other two methods. All three methods show same trend in polarization resistance over the period of exposure time from one hour to 24 hours.

Table 4.3. CPE model parameters obtained by fitting the model to experimental data at 5 rpm, pH = 3.7, 1 atm partial pressure and at room temperature.

Exposure Time	R_p (ohms)	R_s (ohms)	Y_o x 10^{-3}	α x 10^{-3}	Goodness of fit
After 1 h	77.56	4.060	1.126	871.1	3.507
After 5 h	73.53	5.481	1.934	843.3	9.043
After 15 h	67.99	4.277	2.353	886.6	1.586
After 24 h	63.26	3.768	3.031	882.9	2.612

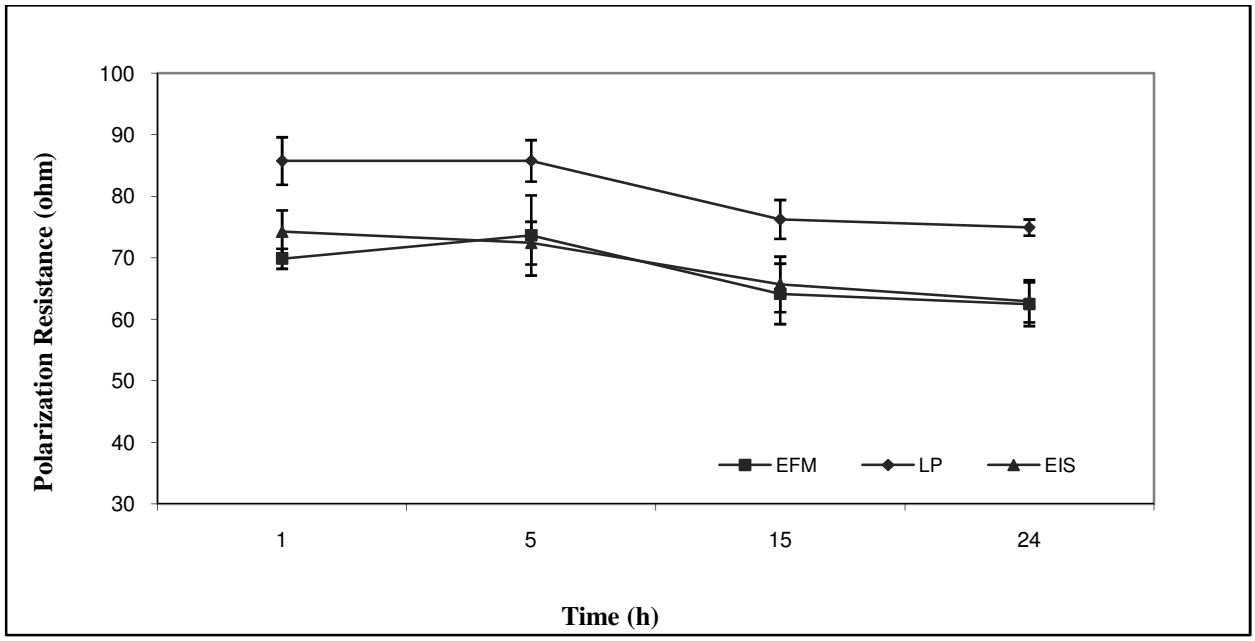

Figure 4.12. Comparison of polarization resistance value between EFM, EIS and LP at 5 rpm, pH = 3.7, 1 atm partial pressure and at room temperature.

4.4.2. EFM measurements carried out at various exposure times in transient hydrodynamic region and its comparison with EIS and LP

Experiments were performed using RCE samples and rotated at 24 rpm simulating transient hydrodynamic region (a region in between laminar and turbulent regime). The EFM method was used with a baseline frequency of 0.01 Hz in order to negate the influence of capacitive behaviour of the electrochemical double layer. At a concentration of 3% (w/w) NaCl, 24 rpm, pH of 3.7, 1 atm partial pressure of CO_2 and room temperature, the corrosion rate increased slightly over time suggesting that there was no protective film formed at these conditions confirming the findings of Nesic *et al*., who stated protective iron carbonate films would form when the temperature, pH and partial pressure were high. At this frequency (0.01 Hz) the EFM technique was not able to calculate the corrosion parameters using the activation model, but was able to with the diffusion model similar to laminar hydrodynamic condition at a

pH of 3.7. When the corrosion rate determined from EFM using the diffusion model was compared with the LP method, it was again higher. The results are shown below in Figure 4.13. The difference in corrosion rate between EFM and LP is due to the Gamry system's default Tafel slopes used for the corrosion rate calculation in the LPR method. To prove the above fact, the Tafel slopes from EFM were used in LP method to recalculate the corrosion rate, and shown in Figure 4.14.

If the reproducibility data and error bars on corrosion rate and polarization resistance that were calculated for EFM and LP at 5 rpm and a pH of 3.7 were employed in illustrating this data, assuming the error to be the same for both experimental methods at different environmental conditions, the results would be in good agreement uncertainty limits overlapping. The polarization resistance values that were calculated from the EFM method using the Stern-Geary equation were compared with EIS and LP to support the results of the EFM measurements and shown in Figure 4.15.

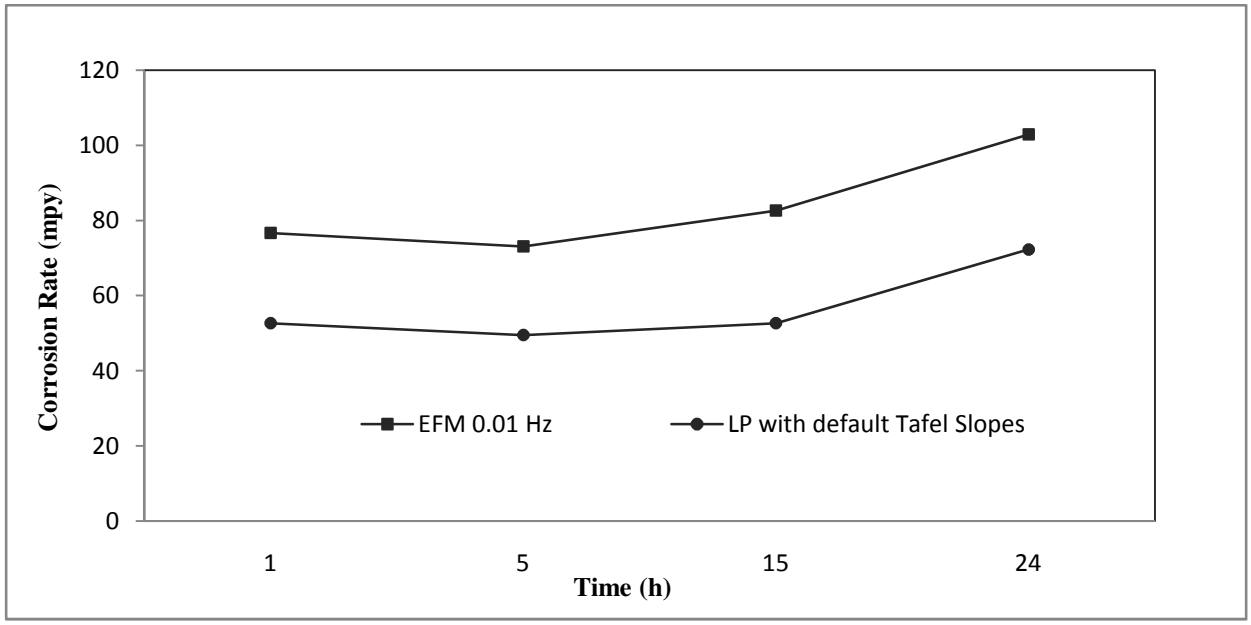

Figure 4.13. Comparison of corrosion rate between EFM at 0.01 Hz and LP with default Tafel slopes at 24 rpm, pH = 3.7.

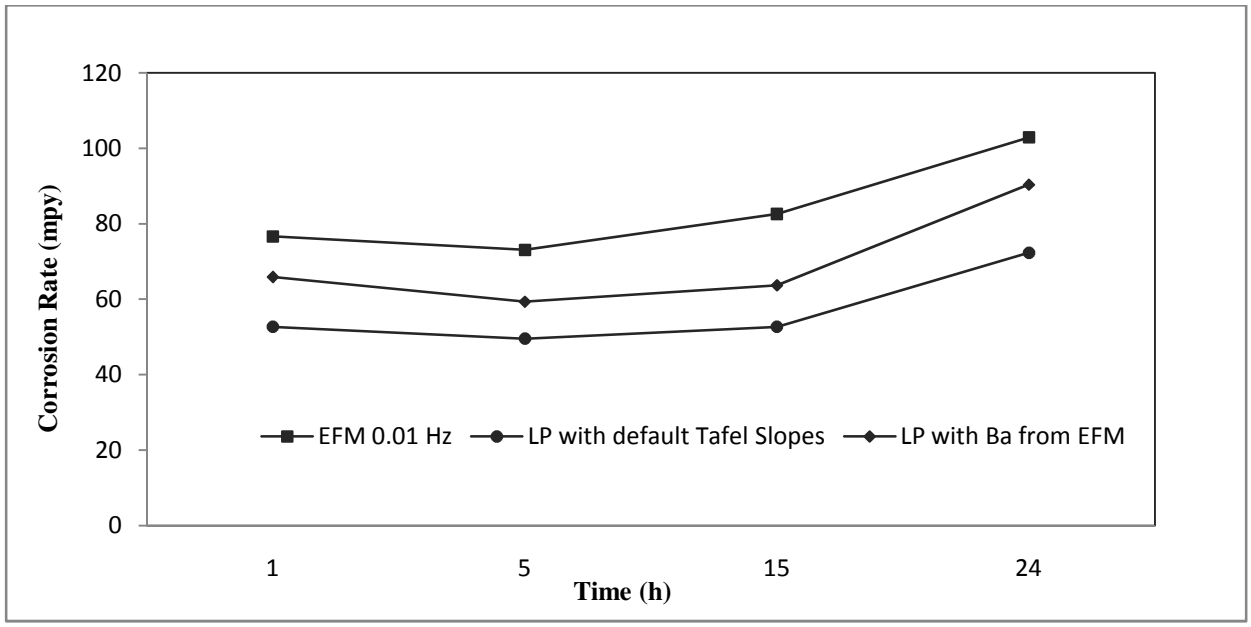

Figure 4.14. Comparison of corrosion rate between EFM at 0.01 Hz and LP with both default Tafel slopes and Tafel slopes from EFM at 24 rpm, pH = 3.7.

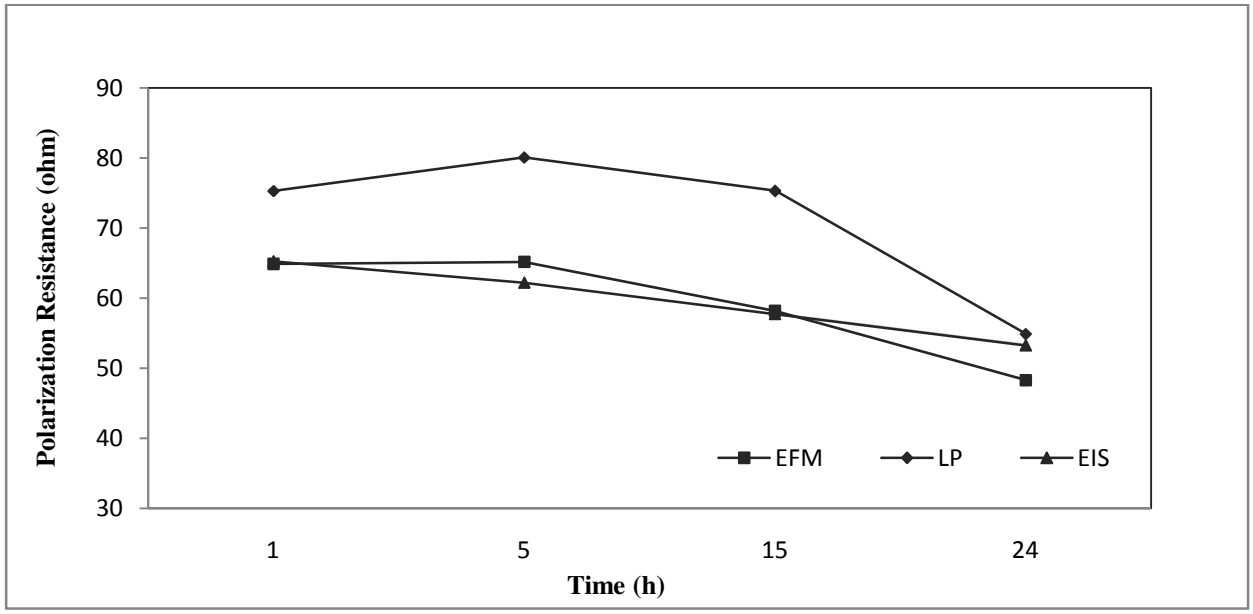

Figure 4.15. Comparison of polarization resistance between EFM, LP and EIS at 24 rpm, pH = 3.7 and at room temperature.

The variation of LPR curves and EIS curves over the period of time from one hour to 24 hours is shown in Figures 4.16 and 4.17. It was observed from Figure 4.17 that the solution

resistance remains almost the same over the period of 24 hours exposure with difference in the polarization resistance.

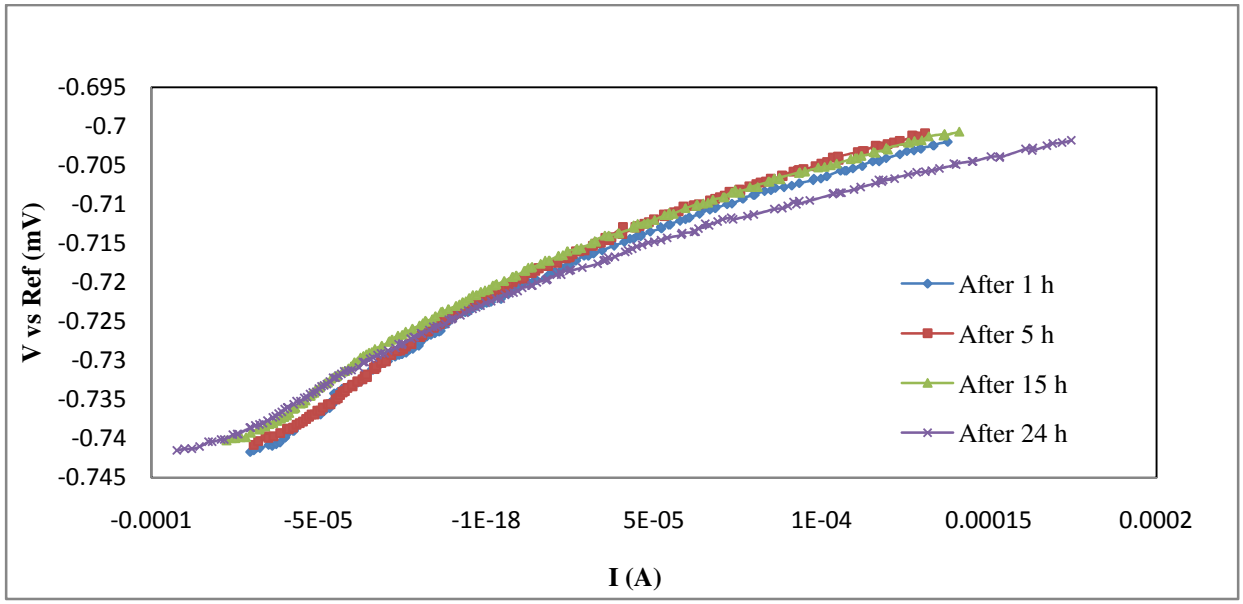

Figure 4.16. Variation of polarization resistance curves with exposure time at 24 rpm, pH = 3.7, 1 atm CO_2 partial pressure and at room temperature.

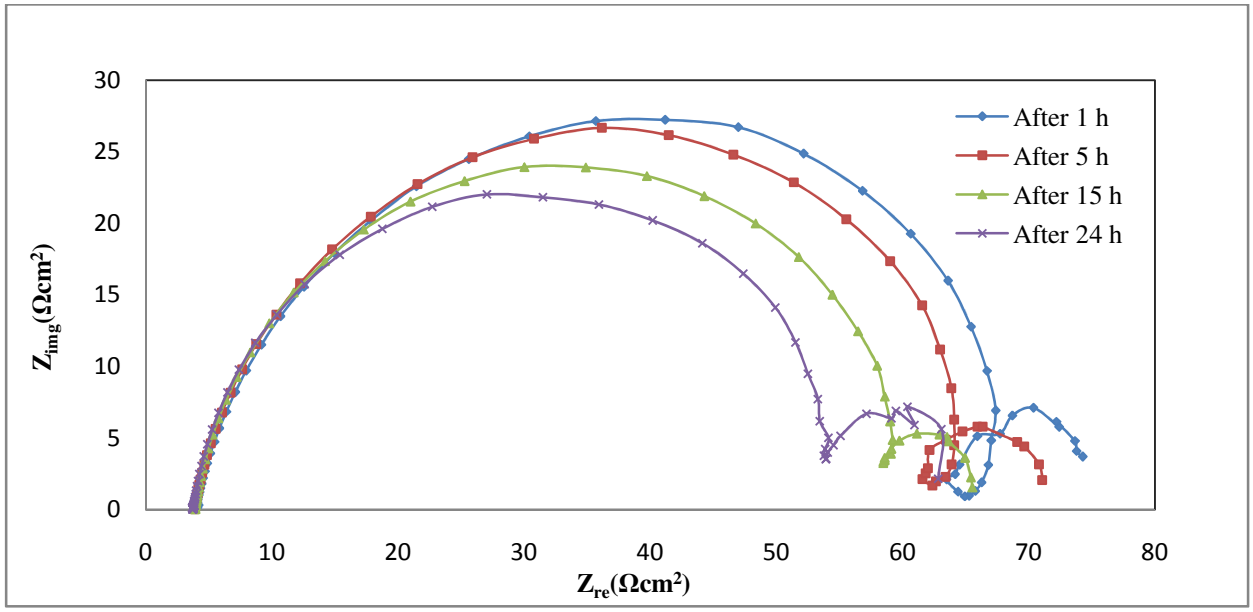

Figure 4.17. AC impedance measurements of AISI carbon steel 1018 in 3% (w/w) NaCl solution done at 24 rpm, pH = 3.7, 1 atm CO_2 partial pressure and at room temperature.

4.4.3. EFM measurements carried out at various exposure times in turbulent flow region and its comparison with EIS and LP

To analyze CO_2 corrosion under turbulent flow conditions, the RCE sample was rotated at 100 rpm in the same environmental conditions as for the previous experiments. At this rotational speed, both activation and diffusion models could be implemented by the EFM system at all base line frequencies (1 Hz, 0.1 Hz, 0.01 Hz, and 0.005 Hz). A base line frequency of 0.005 Hz was used to avoid the influence of an electrochemical double layer present at higher frequencies. It can be seen from the Bode plot on Figure 4.18 that the frequency range 0.01 to 0.15 Hz falls in the capacitive region.

The corrosion rate determined by EFM using the activation control model differed from the one obtained using diffusion model. Although the corrosion rate determined by each model was slightly different, the polarization resistance was the same. This is because the EFM algorithm calculates Tafel slopes and i_{corr} values to keep the relation $B/i_{corr} = R_p$ = constant, irrespective of the model. Also in CO_2 corrosion, the cathodic reaction can take place through different reaction mechanisms [2, 10, 19, 58], although a large contribution to the cathodic reaction current at this low pH comes from H^+ reduction. It was assumed that both activation and diffusion controlled reactions take place at these conditions and the corrosion rate was taken as average obtained using both the models.

The average corrosion rate from the activation and diffusion models is compared with the LP method in Figure 4.19. A small variation in anodic Tafel slope was found between activation and diffusion control models in the EFM method. Therefore the Tafel slope from each model was used in the LP method to obtain two different corrosion rates from which an average

corrosion rate was calculated. Compared to the corrosion rate from the LP method using default Tafel slopes, the average corrosion rate from the LP method using Tafel slopes from the EFM method are in very good agreement with EFM and can be seen in Figure 4.19.

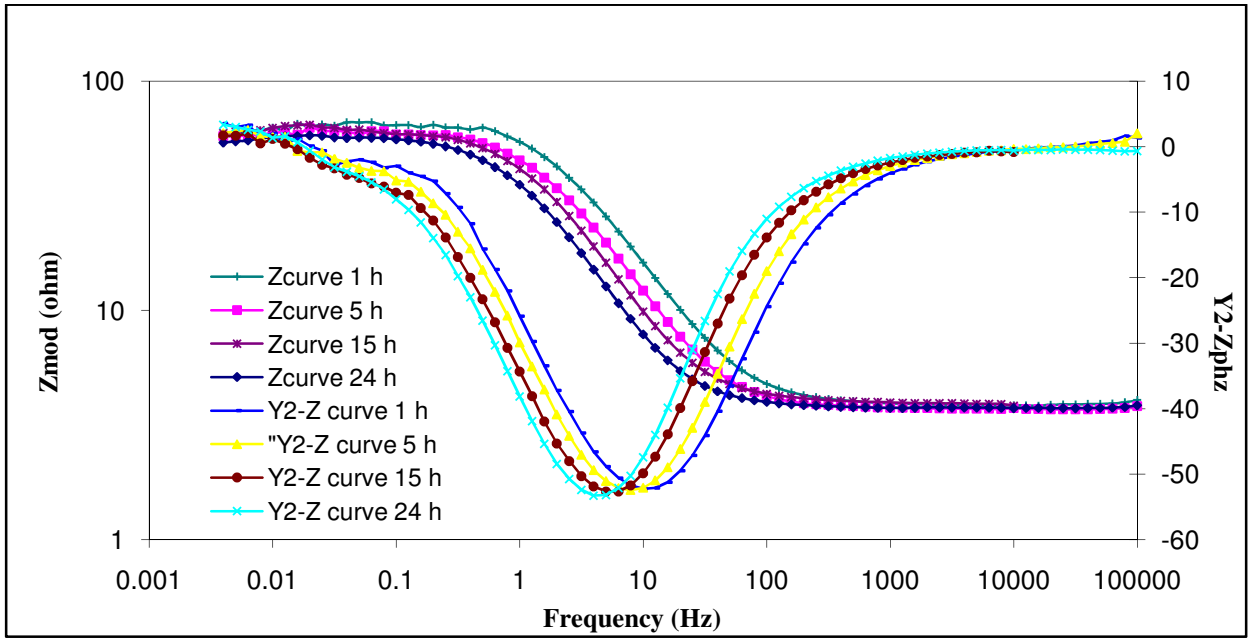

Figure 4.18. Potentiostatic EIS Bode plot at different exposure time of AISI 1018 carbon steel in 3% (w/w) NaCl solution at 100 rpm, pH = 3.7.

Although the corrosion rate and Tafel slopes change with the model, the polarization resistance value remains almost the same with a difference of less than one ohm. Therefore an average polarization resistance value from the activation and diffusion model was used and compared with the EIS and LP methods and shown in Figure 4.20. A good agreement in polarization resistance was obtained between EFM and EIS, with a maximum difference of 18 ohms. Also it can be seen from Table 4.4 that the polarization resistance value did not change significantly during over the 24 hour exposure period.

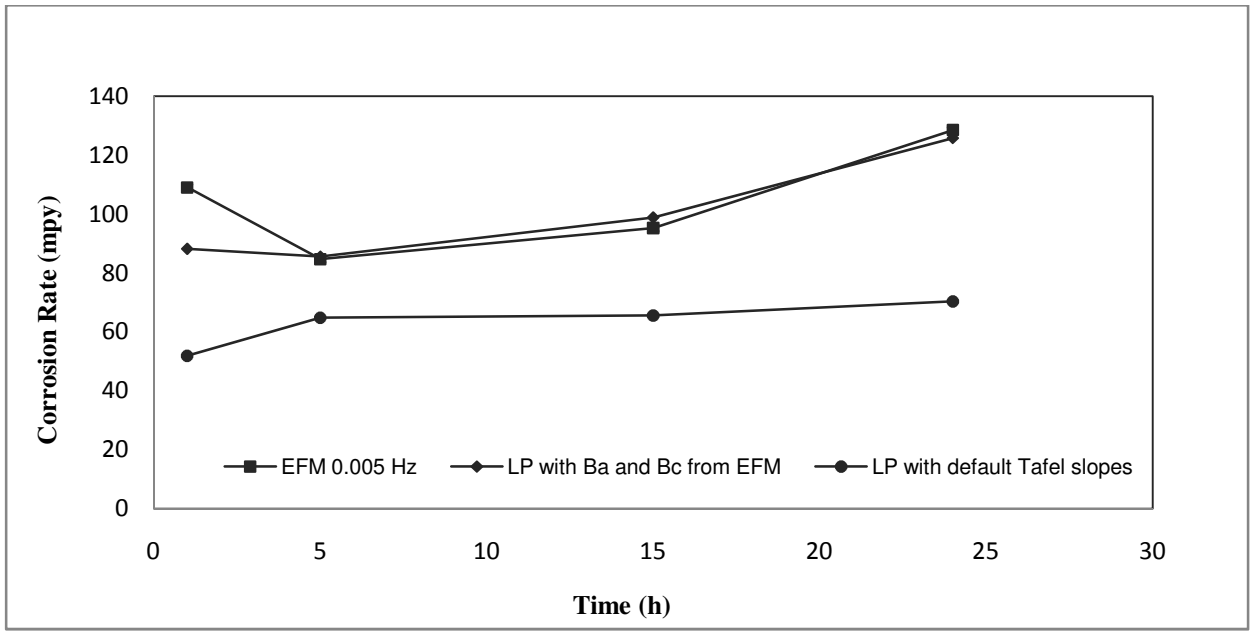

Figure 4.19. Comparison of corrosion rate between EFM (0.005 Hz) and LP method with error bars at 100 rpm, pH = 3.7 and at room temperature.

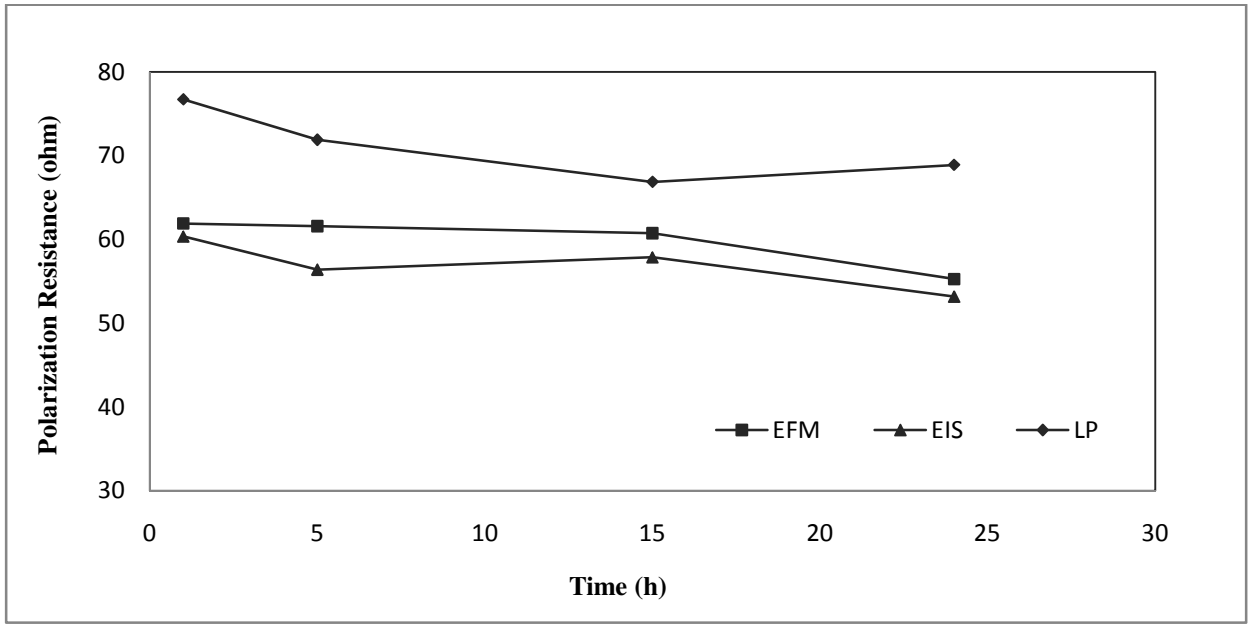

Figure 4.20. Comparison of polarization resistance values between EFM, EIS and LP method at 100 rpm, pH = 3.7 and at room temperature.

Table 4.4. CPE model parameters obtained by fitting model to experimental data in turbulent flow regime at 100 rpm, pH = 3.7, 1 atm partial pressure and at room temperature.

Exposure Time	R_p (ohms)	R_u (ohms)	Y_o x 10^{-3}	α x 10^{-3}	Goodness of fit
After 1 h	60.39	3.889	1.764	874.6	1.222
After 5 h	56.40	3.718	2.472	876.3	0.412
After 15 h	57.88	3.932	3.242	876.4	0.3975
After 24 h	53.17	3.755	4.052	892.6	0.4772

The variation of corrosion rate with time under different flow regimes at non-film forming conditions is shown in Figure 4.21. It can be seen from Figure 4.21 that the corrosion rate increases with time and flow regimes. The increase in corrosion rate in different flow regimes is attributed to the flow sensitive nature of the cathodic reactions in CO_2 corrosion. This flow dependent corrosion rate obtained using EFM is in very good agreement with the findings of Wang[34]. With a RCE under a turbulent flow situation, the reduction of carbonic acid in CO_2 corrosion is under mixed chemical reaction and mass transport control reaction. When the flow rate increases, the limiting current of the cathodic reaction increase; this increases the overall corrosion rate. The increase in corrosion rate with flow velocity is more evident at this low pH which is similar to the results of Nesic *et al*., at a pH of 4[20]. Thus flow dependent corrosion rates obtained using the EFM method with different corrosion models are in good agreement with literature and giving insight into the CO_2 corrosion mechanism under non-film forming conditions.

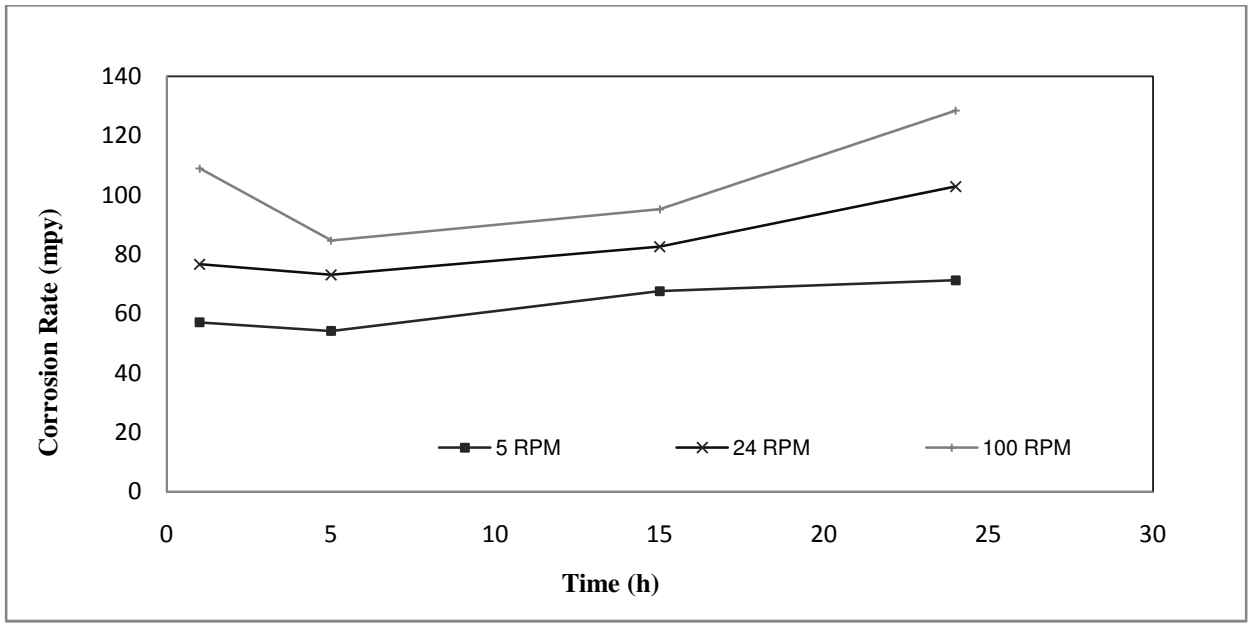

Figure 4.21. Comparison of corrosion rate from EFM of AISI 1018 carbon steel in different flow regime at pH = 3.7, 1 atm CO_2 partial pressure and at room temperature.

4.5. Analysis of CO_2 Corrosion at Film Forming Conditions Using EFM

The formation of iron carbonate films from CO_2 corrosion depends on various environmental factors such as temperature, pH of the bulk solution, partial pressure of CO_2, Fe^{2+} ion concentration and velocity of the fluid. At room temperature, either pH or the Fe^{2+} ion concentration has to be high in the bulk solution to attain a protective film on the metal surface in a short period of time. In this study, the pH of the solution was increased to attain the film forming conditions in CO_2 corrosion. The pH of the solution has to exceed a critical pH above which the saturation limit of Fe^{2+} and CO_3^{2-} are surpassed and precipitation begins. Nesic *et al*., found that above pH 6, the cathodic reaction in CO_2 corrosion is dominated by the direct reduction of carbonic acid[30]. Although the formation of a dense protective film is not likely below a pH of 6.8, the initiation for protective film starts at a pH of 6 and the precipitation begins at pH 6.6 at a temperature of 20℃.

Therefore, for experiments under film forming conditions, a pH of 6.5 was chosen at room temperature (≈23℃) to compensate for the slightly elevated in temperature. The 3% (w/w) NaCl solution was first saturated with CO_2 by bubbling CO_2 gas through it for one hour. After the solution was saturated, the pH was adjusted to 6.5 by adding sodium bicarbonate solution ($NaHCO_3$). The metal sample, prepared as explained in Section 3.1, was then immersed in solution for various exposure times at specific rotational speeds to simulate different hydrodynamic conditions.

4.5.1. EFM measurements in the stagnant region and its comparison with LP and EIS methods

To perform CO_2 corrosion experiments at film forming conditions and in stagnant regions, the pH of the solution was increased to 6.5 and maintained throughout the experiment at room temperature. The working electrode was mounted to a RCE assembly and rotated at 5 rpm creating stagnant flow situation. After exposing the sample for a certain period of time, the sample was analysed using EFM and other electrochemical methods to determine the electrochemical properties. Under these conditions, the EFM method was able to analyze the CO_2 corrosion system using both activation and diffusion control models at a base frequency of 0.01 Hz. The baseline frequency selection was also supported by the EIS Bode plot which shows the baseline frequency is free from electrochemical double layer influence. Each model gave different values of corrosion rate and corrosion current with almost identical polarization resistance values.

In a model proposed by Nesic *et al*., at pH 6 the dominant cathodic reaction was direct H_2CO_3 reduction and at higher negative overpotentials, the dominant cathodic reaction was H_2O

reduction. Due to the involvement of three different cathodic reactions, it is really difficult to say which one is the rate determining step at this set of environmental conditions. Since EFM does not have an option of analyzing a corrosion system which is under mixed control, the corrosion rate obtained from both corrosion models were averaged and compared with other electrochemical methods such as LP and EIS. Figure 4.22 shows the comparison of the corrosion rate obtained using the EFM and LP methods at various exposure times.

It can be seen from Figure 4.22 that the corrosion rate dropped after 5 hours of exposure lasting the same thereafter. This reduction in corrosion rate can be attributed to the formation of iron carbonate films on the surface[12]. The corrosion rates obtained from the EFM method compared well with the data obtained from the LP method. When Tafel slopes obtained from EFM with both activation and diffusion control models were used in the LP method, the corrosion rate was lower than the EFM corrosion rates, but still within experimental uncertainty limits.

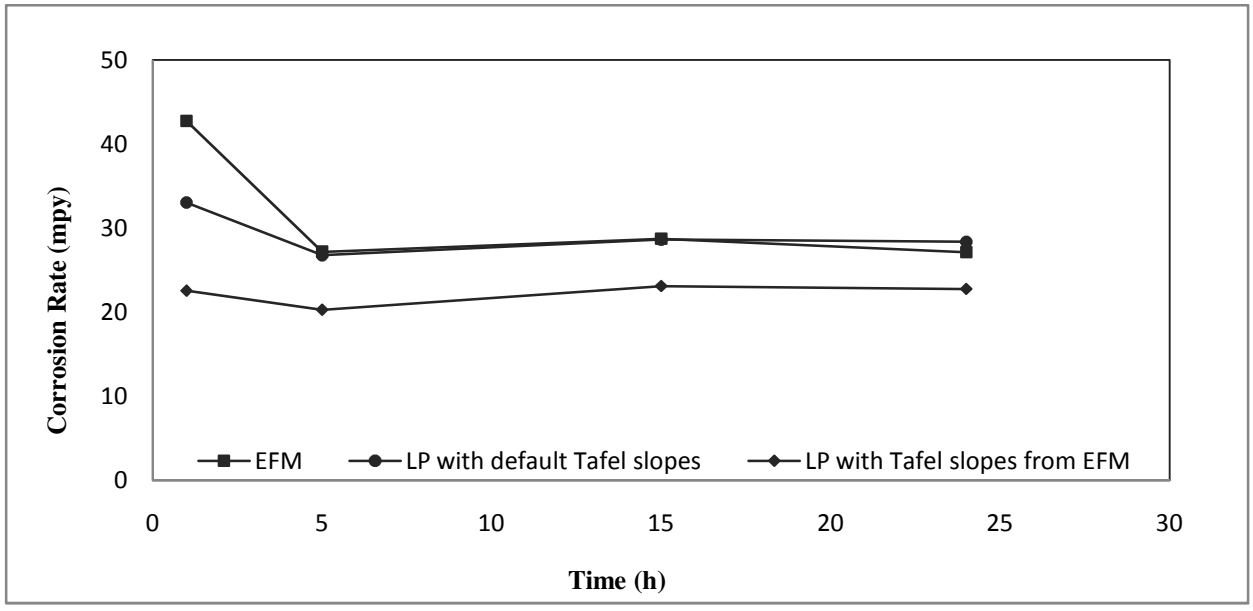

Figure 4.22. Variation of corrosion rate with exposure time for different electrochemical methods at 5 rpm, pH = 6.5 and at room temperature.

To clarify EFM results, the polarization resistance values obtained from EFM were compared with the values found using the EIS and LP methods and shown in Figure 4.23. The polarization resistance obtained from the EFM, LP and EIS methods followed the same trend and have reasonable agreement with each other. The kinetics of the electrochemical reaction varied significantly during the period of exposure. It can be seen from the Nyquist plot in Figure 4.24, that the diameter of the semicircles increased with the exposure time and this increasing trend can be attributed to the formation of iron carbonate films. Although the exposure time is not sufficient to form a dense film, the increasing semicircle diameter in the Nyquist plot gives an indication of the presence of iron carbonate films on the metal surface.

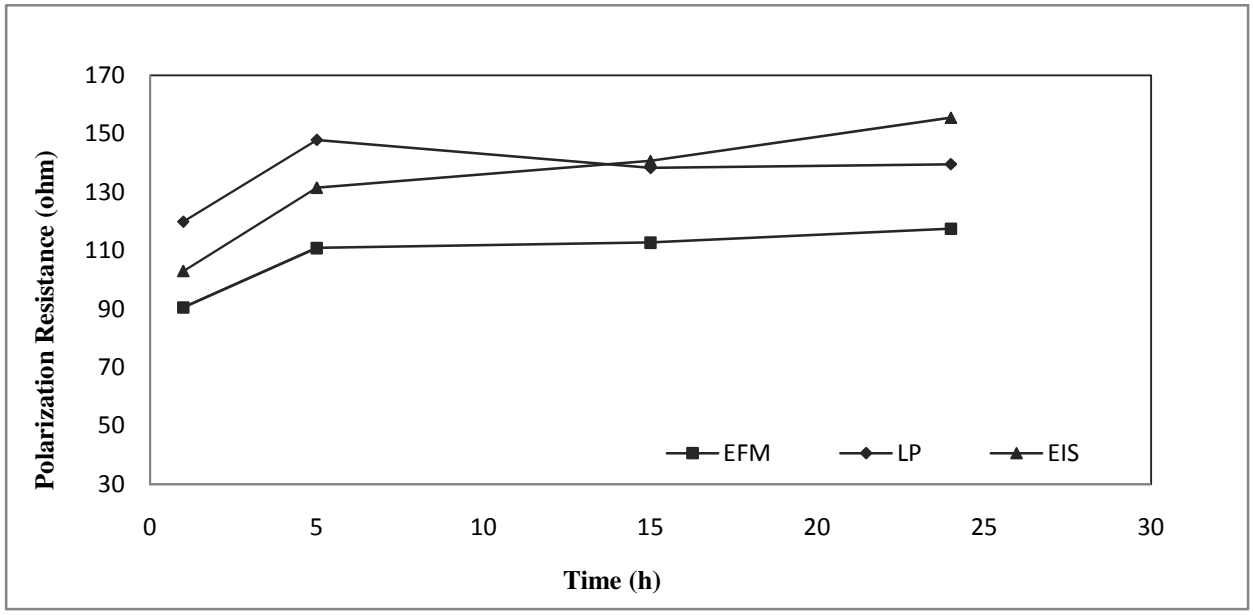

Figure 4.23. Comparison of polarization resistance values between EFM, EIS and LP method at 5 rpm in non-film forming condition.

According to present investigation it can be said that the concentration of Fe^{2+} and CO_3^{2-} ions attained supersaturation and exceeded solubility limit at a pH of 6.5 in a stagnant solution at room temperature. This condition initiated the formation of iron carbonate films on the surface

with a slight reduction of corrosion rate. However to form a compact and adherent scale, the exposure time has to be increased further. Similar results of Nyquist plots for the protective film formation from CO_2 corrosion were reported by Li *et al.*, under different environmental condition[3].

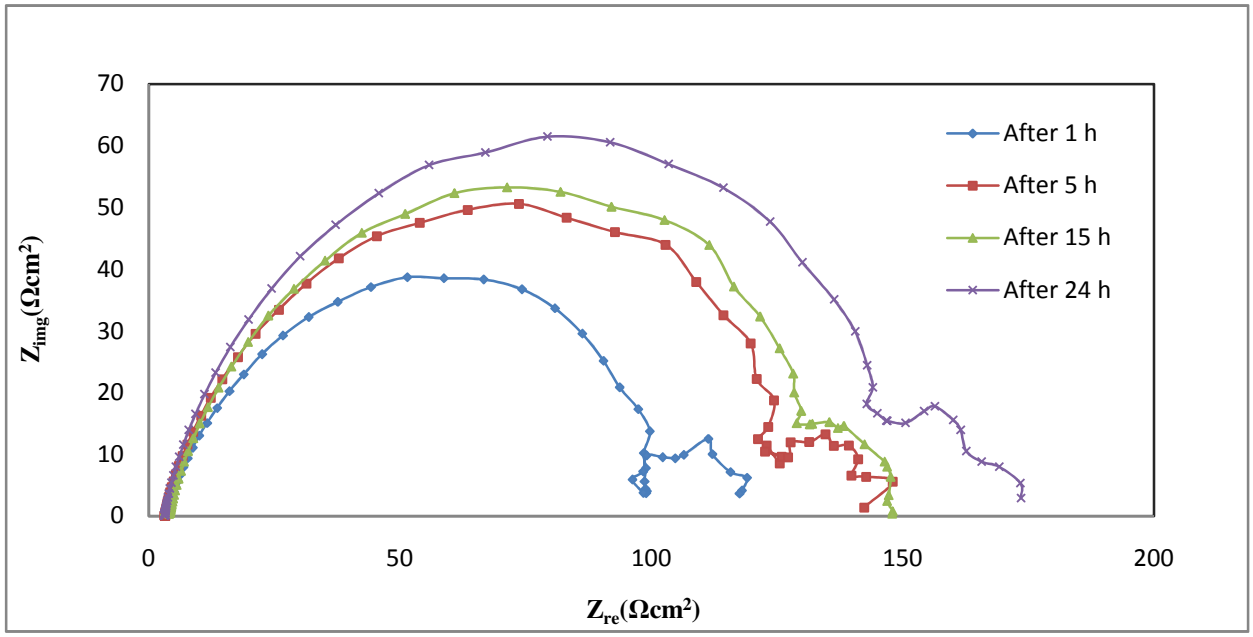

Figure 4.24. Nyquist plots of AISI 1018 carbon steel sample in CO_2 solution at various exposure times in film forming conditions at 5 rpm.

4.5.2. EFM measurements in the transition region and its comparison with LP and EIS methods

EFM was used to study the electrochemical properties of CO_2 corrosion in the transient region at a pH of 6.5 and at room temperature. For a RCE, the transition from laminar to turbulent flow occurs when the Reynolds number exceeds 200[56]. Therefore in this study, the RCE sample which had an outer diameter of 1.2 cm was rotated at 24 rpm corresponding to a Reynolds number of 202. The pH was maintained at 6.5 and the experiment was repeated for

various exposure times. EFM was used with a baseline frequency of 0.01 Hz, at which both activation and diffusion control model worked. This is because at a pH above 6, the limiting current for H_2CO_3 in the cathodic reaction had two different components, a flow-dependent diffusion controlled component and a flow-independent chemical reaction controlled component[19, 20]. As before, due to the constraint with EFM of using either activation control model or diffusion control model for analysis, an average of corrosion rate from both the model was taken and compared with the LP method.

The corrosion rate calculated from EFM at various exposure times was compared with LP method and shown in Figure 4.25. In the LP method the corrosion rate was calculated both by using default Tafel slopes (120 mV/decade) and by using Tafel slopes from EFM. The corrosion rate from the LP method, calculated using Tafel slopes from EFM, is in good agreement with the corrosion rates of EFM. It can be seen that the EFM and LP corrosion rate measurements agree within experimental uncertainty.

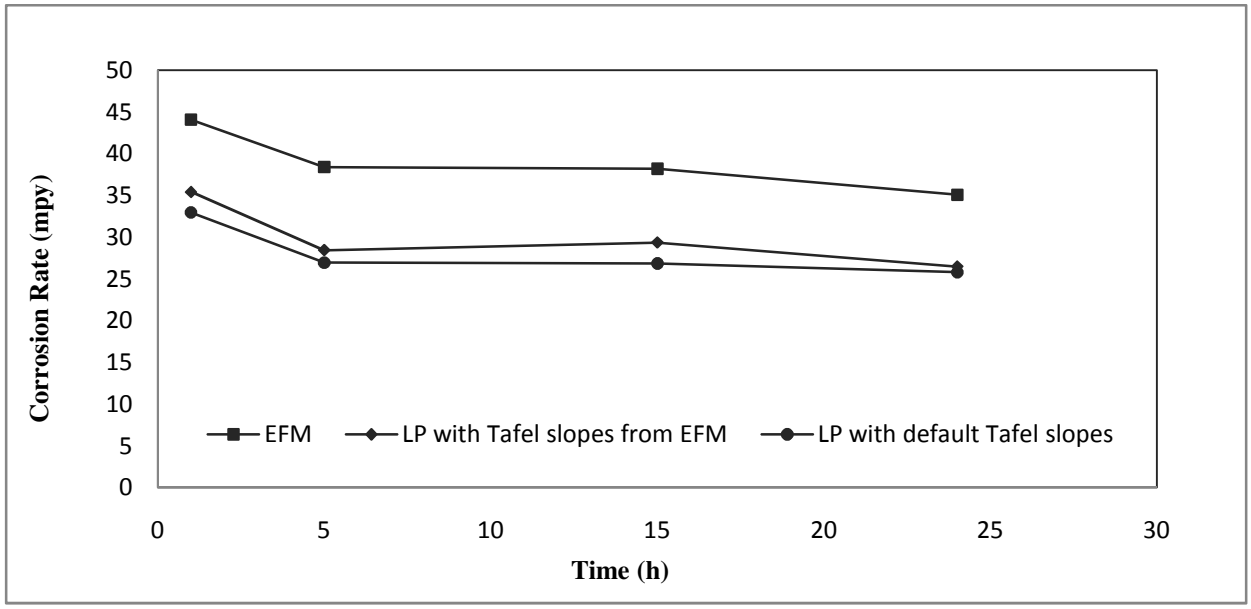

Figure 4.25. Variation of corrosion rates with exposure time for different electrochemical methods at 24 rpm and film forming conditions.

It was observed that the corrosion rate increased slightly compared to the stagnant flow condition at 5 rpm. The corrosion rate trend follows the same as in the stagnant flow situation. It is evident that the corrosion rate is flow dependent at this pH of 6.5. EIS was used to calculate polarization resistance value which was compared with the EFM and LP method and shown in Figure 4.26. The polarization resistance value calculated from EFM using the activation control model and diffusion control model had similar values. Therefore an average resistance value of both models was used to compare with EIS and LP methods. Although the polarization resistance value calculated from EFM is low compared with the value from the EIS and LP methods, the trend is similar in all three methods.

The polarization resistance value increased after 5 hours of exposure time and remained nearly constant thereafter until 24 hours of exposure time. The semicircle diameter in a Nyquist plot increased with exposure time which is similar to the situation observed in the stagnant flow regime. Although the precipitation of iron carbonate film started forming on the metal surface

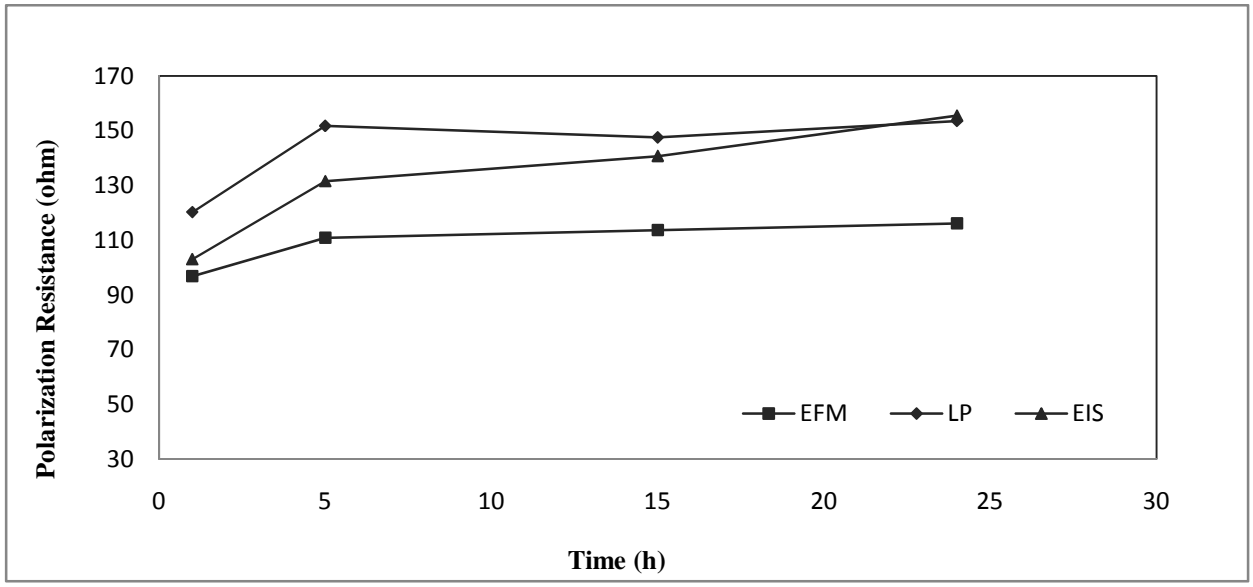

Figure 4.26. Comparison of polarization resistance values between EFM, EIS and LP method at 24 rpm and film forming conditions.

after 5 hours of exposure, the rate of precipitation was slow compared to the stagnant flow regime.

4.5.3. EFM measurements in the turbulent region and its comparison with LP and EIS methods

Oil and gas fields often encounter turbulent flow situations; therefore study of CO_2 corrosion in turbulent flow regimes is of primary interest. A RCE was used to study corrosion in a turbulent pipe flow situation, as the RCE has well-defined hydrodynamics and mass transfer enabling uniform current distribution. To analyze CO_2 corrosion under film forming conditions in a turbulent flow regime using EFM, the pH of the 3% (w/w) NaCl solution was increased to 6.5 at room temperature and the electrode was rotated at 100 rpm. The pH was increased and maintained at 6.5 using a saturated sodium bicarbonate solution. Rotation of the RCE at 100 rpm creates fully developed turbulence in the bulk of the fluid and corresponds to a Reynolds number of 844 and a surface velocity of 6.28 cm/sec.

To avoid the influence of an electrochemical double layer in the EFM results, a baseline frequency of 0.01 Hz was chosen. Similar to other flow regimes, EFM analyzed CO_2 corrosion system in turbulent region using both activation and diffusion models. At a pH value greater than 6, the availability of H^+ ions is scarce to the overall cathodic reaction and the higher cathodic current at a higher velocity comes from the accelerated H_2CO_3 reduction reaction[20].

The comparison of the corrosion rate calculated from various electrochemical methods is shown in Figure 4.27. It can be seen that the corrosion rate dropped after 5 hours of exposure similar to the situation seen in other flow regimes. This is because this pH initiates the

precipitation of iron carbonate films. At this pH only low levels of H^+ ions are available and even at the higher velocity they give little contribution to the cathodic reaction. A considerable amount of carbonic acid (H_2CO_3) is transported from bulk solution to the surface by diffusion in addition to the carbonic acid being formed by slow hydration. It has been proposed that there is a diffusion control component present at this pH of 6, in addition to the chemical reaction controlled component[19, 34]. Therefore the corrosion rate presented here via the EFM method is an average of the rates found by the activation and diffusion control models. It can be seen that the corrosion rate from EFM compares well with LP method and the comparison are within experimental uncertainty limits when the default Tafel slopes used in LPR method were replaced with Tafel slopes from EFM.

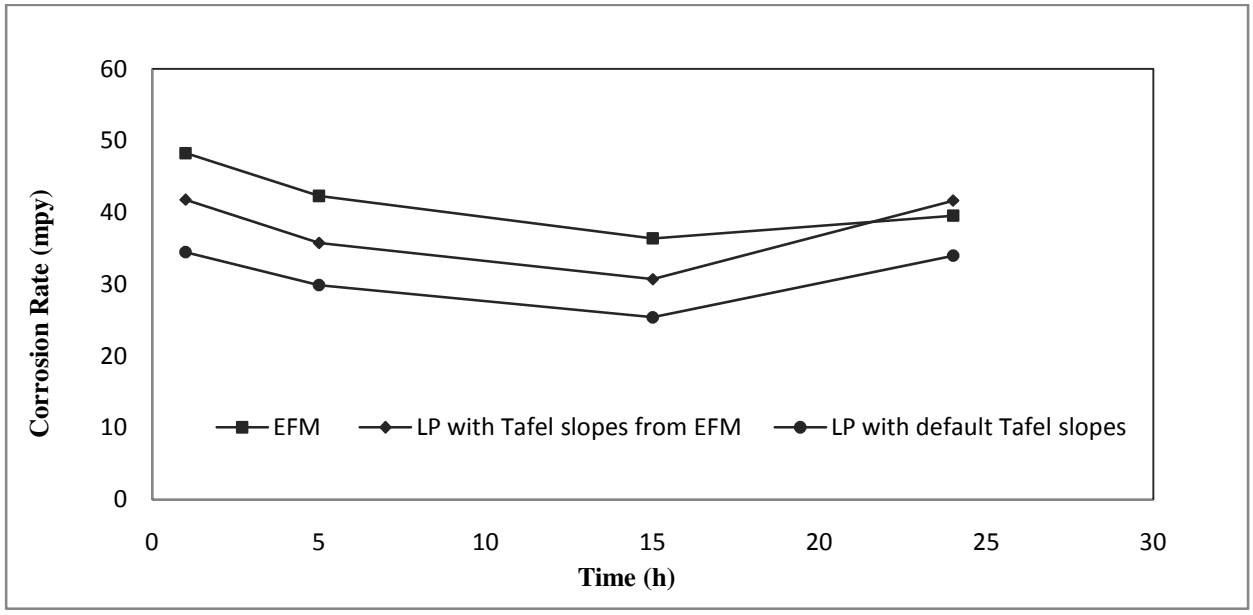

Figure 4.27. Variation of corrosion rates with exposure time for different electrochemical methods at 100 rpm and at film forming conditions.

The reduction of the corrosion rate with increasing exposure time supports the theory of iron carbonate initiation and film formation. SEM analysis was carried out on samples exposed

under film forming and non-film forming conditions. Surface morphology of the corroded samples reveals that iron carbonate film formation is more evident at a pH of 6.5 than pH 3.7 (Figure 4.28). This is also supported by the impedance spectrum from the EIS method which shows an increasing semicircle diameter with increasing exposure time at a pH of 6.5. The R_p values from the LP method are slightly higher than those found by EFM similar to other flow regimes.

The R_p value from the EIS method obtained by fitting the CPE model compared well with the EFM model within the implied experimental uncertainty limits (Figure 4.29). The R_p value obtained from both activation and diffusion control models in EFM are close to each other and compare well with the values found using other electrochemical methods (EIS and LP). In all three flow regimes the corrosion rate dropped during the first 5 hours of exposure, giving an indication of iron carbonate precipitation.

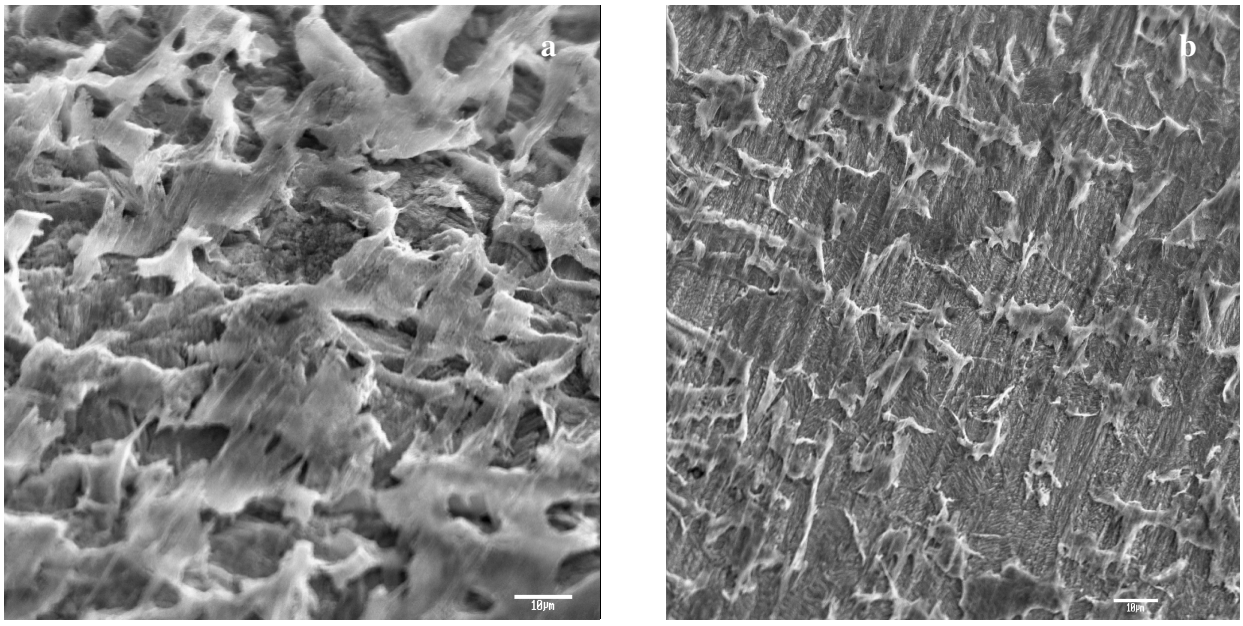

Figure 4.28. Surface morphology of AISI 1018 carbon steels exposed at film forming (a) and non-film forming conditions (b) at 100 rpm and room temperature.

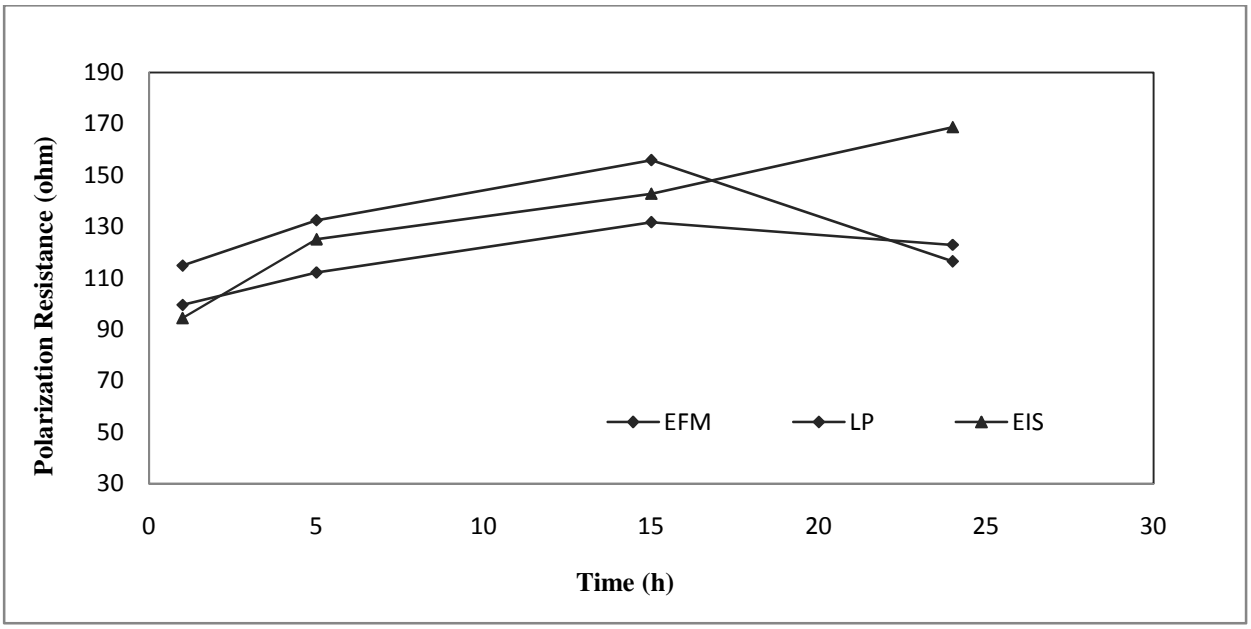

Figure 4.29. Comparison of polarization resistance values between EFM, EIS and LP method at 100 rpm and film forming conditions.

The corrosion rate from EFM are plotted for different flow regimes and shown in Figure 4.30. In all three flow regimes, the corrosion rate dropped during the first 5 hours of exposure, indicating iron carbonate precipitation. It can also be seen from Figure 4.30 that the results from the EFM method follow a trend that reflects the flow dependency of corrosion rate under film forming conditions. When the flow rate increases, the corrosion rate increases because of the rate of transport of chemical species to the metal surface and the protective iron carbonate film is either destroyed or prevented from forming. In this study the protective film formation is prevented at higher velocities and the rate of precipitation of iron carbonate drops with increasing surface velocity. This is in agreement with a mechanistic model developed by Nesic *et al.*,[30].

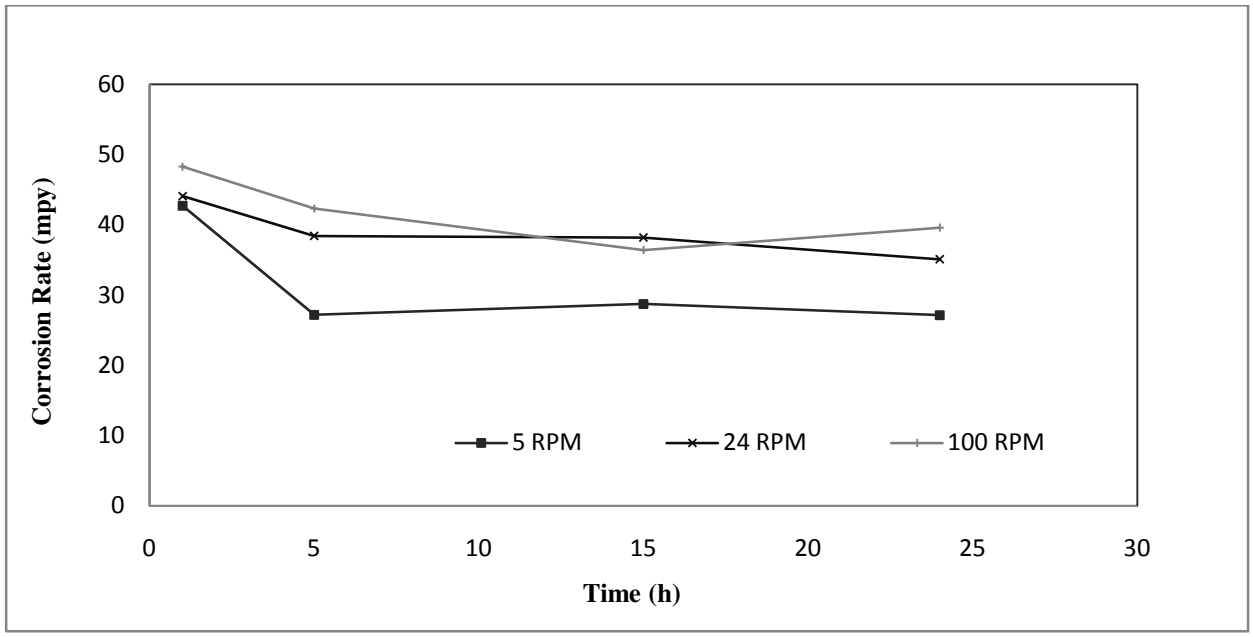

Figure 4.30. Effect of velocity on corrosion rate analyzed using EFM at a pH of 6.5, 1 atm CO_2 partial pressure and at room temperature.

4.6. Summary

EFM, a non-destructive electrochemical method which has never been used for analyzing CO_2 corrosion of carbon steel is used in this research work for the first time. Reproducibility studies on EFM and the corrosion rate date obtained for non-flim forming and film forming conditions are compared with other electrochemical methods and discussed in detail in this chapter. The conclusions that have been drawn from this research work and some recommendations for future work are mentioned in the following chapter.

5. CONCLUSIONS AND RECOMMENDATIONS

The principal purpose of this research was to determine whether EFM could be used to measure the CO_2 corrosion rate on AISI 1018 carbon steel. In this study the rotational speed of the electrode was varied from 5 to 100 rpm (Re 42 to 844) and two different pH values (3.7 and 6.5) were used. The range of exposure time was 1 hr to 24 hrs. From this study the following conclusions can be made:

1. EFM can be used as an effective tool to extract valuable information from CO_2 corrosion providing the complete reaction mechanism is known and a proper corrosion model and base frequency are used.

2. Exact matches between the corrosion rate measured using EFM and LP were not evident likely due to the corrosion measurement system's default Tafel slopes (120mV/decade) used in the LP calculation. EFM does not use the default Tafel slope but calculates Tafel slopes depending on the substrate and environment. However, the value of polarization resistance measured by EFM, EIS and LP were all similar and close to the experimental uncertainty boundaries.

3. The hydrodynamics of the electrolyte affects the corrosion rate of the substrate by changing the mass transfer of species. The corrosion rate is more sensitive to the flow at low pH (<4) than at high pH values (>6). EFM measurements shows this flow dependency at both film forming and non-film forming conditions and the results compare well with literature values of corrosion rate.

4. The three different cathodic reactions involved in CO_2 corrosion can either be under charge transfer control, chemical reaction control, mass transfer control, or a combination of these three control mechanisms. EFM indicates which control mechanism is predominant in different environmental conditions.

Recommendations for Future Research

The following recommendations are suggested for future research work to expand the knowledge of using EFM as a potential electrochemical method in monitoring CO_2 corrosion of carbon steel in oil fields. EFM has been used successfully on only few corrosion systems and this research has produced a basis for using EFM on CO_2 corrosion systems. Once this EFM technique is successfully validated for online monitoring of CO_2 corrosion at different environmental conditions observed in oil fields, it will be easier to mitigate CO_2 corrosion.

1. The preliminary work was carried out at room temperature and atmospheric pressure which is not realistic in oil fields. Experiments using the EFM technique at high temperature and high pressure simulating oil field conditions are suggested.

2. Experiments based on CO_2 corrosion at higher flow rates will assist in understanding the changing corrosion mechanism, giving more information about the mechanism of CO_2 corrosion.

3. Testing of corrosion inhibitors for CO_2 corrosion of carbon steel using EFM is recommended. This could assist in better prevention and control in industrial environments.

4. Developing a mixed control corrosion model and a measurement system based on the EFM technique will help in monitoring more complex corrosion systems.

REFERENCES

1. NACE Corrosion Costs and Preventive Strategies in the United States. http://events.nace.org/publicaffairs/images_cocorr/ccsupp.pdf (15 April 2009),

2. Li, D. G.; Feng, Y. R.; Bai, Z. Q.; Zheng, M. S., "Characteristics of CO_2 Corrosion Scale Formed on N80 Steel in Stratum Water with Saturated CO_2". *Applied Surface Science* **2007,** 253 (20), 8371-8376.

3. Li, T.; Yang, Y.; Gao, K.; Lu, M., "Mechanism of Protective Film Formation During CO_2 Corrosion of X65 Pipeline Steel". *Journal of University of Science and Technology Beijing, Mineral, Metallurgy, Material* **2008,** 15 (6), 702-706.

4. Lopez, D. A.; Simison, S. N.; de Sanchez, S. R., "Inhibitors Performance in CO_2 Corrosion: EIS Studies on the Interaction Between their Molecular Structure and Steel Microstructure". *Corrosion Science* **2005,** 47 (3), 735-755.

5. Nesic, S.; Postlethwaite, J.; Olsen, S., "An Electrochemical Model for Prediction of Corrosion of Mild Steel in Aqueous Carbon Dioxide Solutions". *Corrosion* **1996,** 52 (4), 280-294.

6. Sun, W.; Nesic, S., "Kinetics of Corrosion Layer Formation: Part 1-Iron Carbonate Layers in Carbon Dioxide Corrosion". *Corrosion* **2008,** 64 (4), 334-346.

7. Sun, W.; Nesic, S.; Papavinasam, S., "Kinetics of Corrosion Layer Formation. Part 2 - Iron Sulfide and Mixed Iron Sulfide/Carbonate Layers in Carbon Dioxide/Hydrogen Sulfide Corrosion". *Corrosion* **2008,** 64 (7), 586-599.

8. Wang, F.; Postlethwaite, J. "Modelling of Aqueous CO_2 Corrosion of Iron in Turbulent Pipe Flow", *CORROSION*/2001, paper no. 41 (Houston, TX: NACE, 2001).

9. Bilkova, K.; Gulbrandsen, E., "Kinetic and Mechanistic Study of CO_2 Corrosion Inhibition by Cetyl Trimethyl Ammonium Bromide". *Electrochemical Acta* **2008,** 53 (16), 5423-5433.

10. Dayalan, E.; de Moraes, F. D.; Shadley, J. R.; Shirazi, A.; Rybicki, E. F. "CO_2 Corrosion Prediction in Pipe Flow Under $FeCO_3$ Scale-Forming Conditions", *CORROSION*/1998, paper no. 51 (Houston, TX: NACE, 1998).

11. Chokshi, K.; Sun, W.; Nesic, S. "Iron Carbonate Scale Growth and the Effect of Inhibition in CO_2 Corrosion of Mild Steel", *CORROSION*/2005, (Houston, Texas: NACE, 2005).

12. Gao, K.; Yu, F.; Pang, X.; Zhang, G.; Qiao, L.; Chu, W.; Lu, M., "Mechanical Properties of CO_2 Corrosion Product Scales and Their Relationship to Corrosion Rates". *Corrosion Science* **2008,** 50 (10), 2796-2803.

13. Nafday, O. A.; Nesic, S. "Iron Carbonate Scale Formation and CO_2 Corrosion in the Presence of Acetic Acid", *CORROSION*/2005, (Houston, Texas: NACE International, 2005).

14. Ruzic, V.; Veidt, M.; Nesic, S., "Protective Iron Carbonate Films- Part 1: Mechanical Removal in Single-Phase Aqueous Flow". *Corrosion* **2006,** 62 (5), 419-432.

15. Nesic, S.; Lee, K. L. J., "A Mechanistic Model for Carbon Dioxide Corrosion of Mild Steel in the Presence of Protective Iron Carbonate Films - Part 3: Film Growth Model". *Corrosion* **2003,** 59 (7), 616-628.

16. Nordsveen, M.; Nesic, S.; Nyborg, R.; Stangeland, A., "A Mechanistic Model for Carbon Dioxide Corrosion of Mild Steel in the Presence of Protective Iron Carbonate Films - Part 1: Theory and Verification". *Corrosion* **2003,** 59 (5), 443-456.

17. Mora-Mendoza, J. L.; Turgoose, S., "Fe_3C Influence on the Corrosion Rate of Mild Steel in Aqueous CO_2 Systems under Turbulent Flow conditions". *Corrosion Science* **2002,** 44 (6), 1223-1246.

18. Ren, C.; Liu, D.; Bai, Z.; Li, T., "Corrosion Behaviour of Oil Tube Steel in Simulant Solution with Hydrogen Sulfide and Carbon Dioxide". *Materials Chemistry and Physics* **2005,** 93 (2-3), 305-309.

19. Nesic, S.; Pots, B. F. M.; Postlethwaite, J.; Thevenot, N., "Superposition of Diffusion and Chemical Reaction Controlled Limiting Currents - Application to CO_2 Corrosion". *Journal of Corrosion science and Engineering* **1995,** 1, 1-14.

20. Nesic, S.; Solvi, G. T.; Enerhaug, J., "Comparison of the Rotating Cylinder and Pipe Flow Tests for Flow-Sensitive Carbon Dioxide Corrosion". *Corrosion* **1995,** 51 (10), 773-787.

21. Bai, Z. Q.; Chen, C. F.; Lu, M. X.; Li, J. B., "Analysis of EIS Characteristics of CO_2 Corrosion of Well Tube Steels with Corrosion Scales". *Applied Surface Science* **2006,** 252 (20), 7578-7584.

22. Chen, C. F.; Lu, M. X.; Zhao, G. X.; Bai, Z. Q.; Yan, M. L.; Yang, Y. Q., "The EIS Analysis of Electrode Reactions of CO_2 Corrosion of N80 Steel". *Acta Metallurgica Sinica* **2002,** 38 (7), 770-774.

23. Chen, C. F.; Lu, M. X.; Zhao, G. X.; Bai, Z. Q.; Yan, M. L.; Yang, Y. Q., "The EIS Analysis of Cathodic Reactions During CO_2 Corrosion of N80 Steel". *Acta Metallurgica Sinica* **2003,** 39 (1), 94-98.

24. Wu, S. L.; Cui, Z. D.; He, F.; Bai, Z. Q.; Zhu, S. L.; Yang, X. J., "Characterization of the Surface Film Formed From Carbon Dioxide Corrosion on N80 Steel". *Materials Letters* **2004,** 58 (6), 1076-1081.

25. Wu, S. L.; Cui, Z. D.; Zhao, G. X.; Yan, M. L.; Zhu, S. L.; Yang, X. J., "EIS Study of the Surface Film on the Surface of Carbon Steel From Supercritical Carbon Dioxide Corrosion". *Applied Surface Science* **2004,** 228 (1-4), 17-25.

26. Zavala, G.; Hernandez, J., "Corrosion Inhibitors Performance for Mild Steel in CO_2 Containing Solutions". *Materials and Corrosion* **2007,** 58 (6), 427-437.

27. Abdel-Rehim, S. S.; Khaled, K. F.; Abd-Elshafi, N. S., "Electrochemical Frequency Modulation as a New Technique for Monitoring Corrosion Inhibition of Iron in Acid Media by New Thiourea Derivative". *Electrochemical Acta* **2006,** 51 (16), 3269-3277.

28. Han, L.; Song, S., "A Measurement System Based on Electrochemical Frequency Modulation Technique for Monitoring the Early Corrosion of Mild Steel in Seawater". *Corrosion Science* **2008,** 50 (6), 1551-1557.

29. Kus, E.; Mansfeld, F., "An Evaluation of the Electrochemical Frequency Modulation (EFM) Technique". *Corrosion Science* **2006,** 48 (4), 965-979.

30. Nesic, S.; Nordsveen, M.; Nyborg, R.; Stangeland, A., "A Mechanistic Model for Carbon Dioxide Corrosion of Mild Steel in the Presence of Protective Iron Carbonate Films - Part 2: A Numerical Experiment". *Corrosion* **2003,** 59 (6), 489-497.

31. Tebbal, S.; Hackerman, N., "Effect of the Liquid Film Thickness on the Carbon Dioxide Corrosion of Steel". *Corrosion* **1989,** 45 (7), 558-562.

32. Moiseeva, L. S.; Rashevskaya, N. S., "Effect of pH Value on Corrosion Behaviour of Steel in CO2-containing Aqueous Media". *Russian Journal of Applied Chemistry* **2002,** 75 (10), 1625-1633.

33. Nesic, S.; Nordsveen, M.; Nyborg, R.; Stangeland, A. "A Mechanistic Model for CO_2 Corrosion with Protective Iron Carbonate Films", *CORROSION*/2001, paper no. 01040 (Houston, Texas: NACE, 2001).

34. Wang, F. Modelling of Aqueous Carbon Dioxide Corrosion in Turbulent Pipe Flow. University of Saskatchewan, Saskatoon, 1999.

35. Ruzic, V.; Veidt, M.; Nesic, S., "Protective Iron Carbonate Films- Part 2: Chemical Removal by Dissolution in Single-Phase Aqueous Flow". *Corrosion* **2006,** 62 (7), 598-611.

36. Nesic, S.; Lee, K. L. J.; Ruzic, V. "A Mechanistic Model of Iron Carbonate Film Growth and the Effect on CO_2 Corrosion of Mild Steel", *CORROSION*/2002, (Houston, TX: NACE, 2002).

37. Hunnik Van, E. W. J.; Pots, B. F. M.; Hendriksen, E. L. J. A. "The Formation of Protective $FeCO_3$ Corrosion Product Layers in CO_2 Corrosion", *CORROSION*/1996, paper no. 6 (Houston, Texas: NACE, 1996).

38. Shoesmith, D. W.; Taylor, P.; Bailey, M. G.; Owen, D. G., "The Formation of Ferrous Monosulfide Polymorphs During the Corrosion of Iron by Aqueous Hydrogen Sulfide at 21°C.". *Journal of Electrochemical Society* **1980,** 127 (5), 1007-1015.

39. Silverman, D. C., "Rotating Cylinder Electrode for Velocity Sensitivity Testing". *Corrosion* **1984,** 40 (5), 220-226.

40. Schmitt, G.; Mueller, M.; Papenfuss, M. "Understanding Localized CO_2 Corrosion of Carbon Steel from Physical Properties of Iron Carbonate Scales", *CORROSION*/1999, paper no. 38 (Houston, TX: NACE, 1999).

41. Schmitt, G. "Fracture Mechanical Properties of CO_2 Corrosion Product Scales and Their Relation to Localized Corrosion", *CORROSION*/1996, paper no. 9 (Houston, TX: NACE, 1996).

42. Schmitt, G.; Bosch, C.; Pankoke, U. "Evaluation of Critical Flow Intensities for FILC in Sour Gas Production", *CORROSION*/1998, paper no. 46 (Houston, TX: NACE, 1998).

43. Nyborg, R. "Initiation and Growth of MESA Corrosion Attack During CO_2 Corrosion of Carbon Steel", *CORROSION*/1998, paper no. 48 (Houston, TX: NACE, 1998).

44. Lin, G. F.; Zheng, M. S.; Bai, Z. Q.; Zhao, G. X., "Effect of Temperature and Pressure on the Morphology of Carbon Dioxide Corrosion Scales". *Corrosion* **2006,** 62 (6), 501-507.

45. Bockris, J. O. M.; Reddy, A. K. N., *Modern Electrochemistry 1: Ionics*. Springer: 1998.

46. Romaniv, O. N.; Tsirul'nik, A. T.; Krys'kiv, A. S.; Ronchevich, I. C., "Electrochemical Methods in Corrosion Monitoring of Metals (Review)". *Materials Science* **1989,** 25 (1), 1-12.

47. Bard, A. J.; Faulkner, L. R., "Electrochemical Methods: Fundamentals and Applications," 2 ed.; John Wiley & Sons Inc.: 2001.

48. *Modern Aspects of Electrochemistry 32*. Springer: 1999.

49. Srinivasan, R.; Murphy, J. C., "Corrosion Rate Measurement under Cathodic Polarization by Faradaic Rectification". *Journal of Electrochemical Society* **1991,** 138 (10), 2960-2964.

50. Bosch, R. W.; Bogaerts, W. F., "Harmonic Analysis of Corroding Systems Considering Diffusion Phenomena". *Journal of Electrochemical Society* **1996,** 143 (12), 4033-4039.

51. Bosch, R. W.; Bogaerts, W. F., "Instantaneous Corrosion Rate Measurement with Small-Amplitude Potential Intermodulation Techniques". *Corrosion* **1996,** 52 (3), 204-212.

52. Bosch, R. W.; Hubrecht, J.; Bogaerts, W. F.; Syrett, B. C., "Electrochemical Frequency Modulation: A New Electrochemical Technique for Online Corrosion Monitoring". *Corrosion* **2001,** 57 (1), 60-70.

53. Bockris, J. O. M.; Reddy, A. K. N.; Gamboa-Adelco, M. E., *Modern Electrochemistry 2A: Fundamentals of Electrodics*. Springer: 2000.

54. PINE, "Mechanical Drawing for QC3 Cylinder Inserts," ACQCO12CY, Ed. Pine Research Instrumentation: Grove City, 1993; Vol. A.

55. Alloy Information Report for AISI 1018. http://www.steelforge.com/forgings/alloys/aisi1018report.html (24 June 2009),

56. Gabe, D. R., "The Rotating Cylinder Electrode". *Journal of Applied Electrochemistry* **1974,** 4, 91-108.

57. Gabrielli, C.; Keddam, M., "Review of Applications of Impedance and Noise Analysis to Uniform and Localized Corrosion". *Corrosion* **1992,** 48 (10), 794-811.

58. Nesic, S.; Nordsveen, M.; Maxwell, N.; Vrhovac, M., "Probabilistic Modelling of CO_2 Corrosion Laboratory Data using Neural Networks". *Corrosion Science* **2001,** 43 (7), 1373-1392.

APPENDIX A

Rotation Rate Calibration for MSR Style Rotators

The (modulated style rotator) MSR style rotators which holds the RCE assembly and maintains the hydrodynamic situation was calibrated before proceeding with experiments. The rotation rate for this style rotator has to be within ±1% of the setting on the control box. The rotating electrode assembly (shaft and tip) offered by PINE instruments specifically for use with MSR style rotators was used for all experiments and has a unique maximum rotation rate. The maximum rotation rate for this type of working electrode (RCE with MSR style rotator) is 2000 rpm; therefore the rotation rate was calibrated up to 2000 rpm. The calibration of MSR style rotator was performed using an optical tachometer (stroboscope).

The rotator was rotated at a fixed set speed starting from 5 rpm using settings on the control box and the actual rate was measured using stroboscope. After measuring the actual rotation rate, a graph was plotted between the set values on the control box against the actual value obtained using stroboscope. A straight line with a slope of 0.9944 was obtained and shown in Figure A.1. From the graph it can be said that the rotation rate of MSR style rotator was within the tolerance limit of ±1% setting on the control box. Therefore the rotation rates mentioned in the study are within the limits and represents different hydrodynamic conditions.

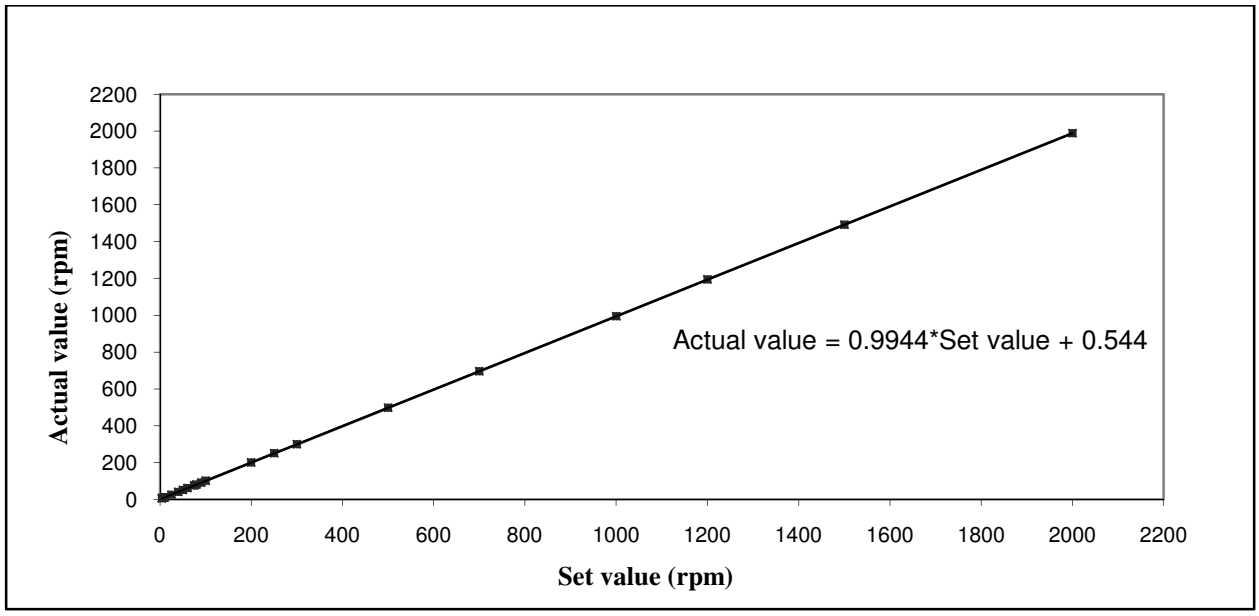

Figure A.0.1. Rotation rate calibration chart of MSR style rotators.

APPENDIX B

Mathematical Derivation for Activation Control System in EFM

The current-potential relationship for a system under activation control or kinetic control is given by Butler-Volmer equation[52]

$$i = i_{corr}\left[\exp\left\{\frac{2.303(E-E_{corr})}{b_a}\right\} - \exp\left\{-\frac{2.303(E-E_{corr})}{b_c}\right\}\right] \quad \text{(B.1)}$$

$$i = i_{corr}\left[\exp\left\{\frac{2.303(\eta)}{b_a}\right\} - \exp\left\{-\frac{2.303(\eta)}{b_c}\right\}\right] \quad \text{(B.2)}$$

Consider $\beta_a = b_a/2.303$ and $\beta_c = b_c/2.303$ which reduces the above equation to

$$i = i_{corr}\left[\exp\left(\frac{\eta}{\beta_a}\right) - \exp\left(-\frac{\eta}{\beta_c}\right)\right] \quad \text{(B.3)}$$

If an input distortion signal in the form of sine waves with two different frequencies ω_1 and ω_2 are applied to the system above,

$$\eta = U_0 \sin\omega_1 t + U_0 \sin\omega_2 t \quad \text{(B.4)}$$

Then the current-potential relation reduces to

$$i = i_{corr}\left[\exp\left(\frac{U_0 \sin\omega_1 t}{\beta_a}\right)\exp\left(\frac{U_0 \sin\omega_2 t}{\beta_a}\right) - \exp\left(-\frac{U_0 \sin\omega_1 t}{\beta_c}\right)\exp\left(-\frac{U_0 \sin\omega_2 t}{\beta_c}\right)\right] \quad \text{(B.5)}$$

The exponential terms in the above equation can be expanded in Taylor series which is given as

$$e^x = 1 + \frac{x}{1!} + \frac{x^2}{2!} + \frac{x^3}{3!} + \cdots, \ -\infty < x < \infty \quad \text{(B.6)}$$

Therefore the exponential term in the current-potential equation becomes

$$exp\left(\frac{U_0 \sin \omega_1 t}{\beta_a}\right) = 1 + \left(\frac{U_0 \sin \omega_1 t}{\beta_a}\right) + \frac{1}{2}\left(\frac{U_0 \sin \omega_1 t}{\beta_a}\right)^2 + \frac{1}{6}\left(\frac{U_0 \sin \omega_1 t}{\beta_a}\right)^3 + \cdots, \quad \text{(B.7)}$$

$$\exp\left(-\frac{U_0 \sin \omega_1 t}{\beta_c}\right) = 1 - \left(\frac{U_0 \sin \omega_1 t}{\beta_c}\right) + \frac{1}{2}\left(\frac{U_0 \sin \omega_1 t}{\beta_c}\right)^2 - \frac{1}{6}\left(\frac{U_0 \sin \omega_1 t}{\beta_c}\right)^3 + \cdots, \quad \text{(B.8)}$$

Similar relation was used for terms with ω_2 and neglecting the higher order terms (>3) in the Taylor series expansion, the Equation (B.5) becomes,

$$i = i_{corr}\left\{\left[1 + \left(\frac{U_0 \sin \omega_1 t}{\beta_a}\right) + \frac{1}{2}\left(\frac{U_0 \sin \omega_1 t}{\beta_a}\right)^2 + \frac{1}{6}\left(\frac{U_0 \sin \omega_1 t}{\beta_a}\right)^3\right]\left[1 + \left(\frac{U_0 \sin \omega_2 t}{\beta_a}\right) + \frac{1}{2}\left(\frac{U_0 \sin \omega_2 t}{\beta_a}\right)^2 + \frac{1}{6}\left(\frac{U_0 \sin \omega_2 t}{\beta_a}\right)^3\right] - \left[1 - \left(\frac{U_0 \sin \omega_1 t}{\beta_c}\right) + \frac{1}{2}\left(\frac{U_0 \sin \omega_1 t}{\beta_c}\right)^2 - \frac{1}{6}\left(\frac{U_0 \sin \omega_1 t}{\beta_c}\right)^3\right]\left[1 - \left(\frac{U_0 \sin \omega_2 t}{\beta_c}\right) + \frac{1}{2}\left(\frac{U_0 \sin \omega_2 t}{\beta_c}\right)^2 - \frac{1}{6}\left(\frac{U_0 \sin \omega_2 t}{\beta_c}\right)^3\right]\right\} \quad \text{(B.9)}$$

The terms inside Equation (B.9) were brought together and eliminating higher order terms and rearranging the terms gives

$$i = i_{corr}\left\{\left[1 + \frac{U_0}{\beta_a}\sin \omega_1 t + \frac{1}{2}\left(\frac{U_0}{\beta_a}\right)^2 \sin^2 \omega_1 t + \frac{1}{6}\left(\frac{U_0}{\beta_a}\right)^3 \sin^3 \omega_1 t + \frac{U_0}{\beta_a}\sin \omega_2 t + \frac{1}{2}\left(\frac{U_O}{\beta_a}\right)^2 \sin^2 \omega_2 t + \frac{1}{6}\left(\frac{U_0}{\beta_a}\right)^3 \sin^3 \omega_2 t + \left(\frac{U_0}{\beta_a}\right)^2 \sin \omega_1 t \sin \omega_2 t + \frac{1}{2}\left(\frac{U_0}{\beta_a}\right)^3 \sin^2 \omega_1 t \sin \omega_2 t + \frac{1}{2}\left(\frac{U_0}{\beta_a}\right)^3 \sin^2 \omega_2 t \sin \omega_1 t\right] - \left[1 - \frac{U_0}{\beta_c}\sin \omega_1 t + \frac{1}{2}\left(\frac{U_0}{\beta_c}\right)^2 \sin^2 \omega_1 t - \frac{1}{6}\left(\frac{U_0}{\beta_c}\right)^3 \sin^3 \omega_1 t - \frac{U_0}{\beta_c}\sin \omega_2 t + \frac{1}{2}\left(\frac{U_0}{\beta_c}\right)^2 \sin^2 \omega_2 t - \frac{1}{6}\left(\frac{U_0}{\beta_c}\right)^3 \sin^3 \omega_2 t + \left(\frac{U_0}{\beta_c}\right)^2 \sin \omega_1 t \sin \omega_2 t - \frac{1}{2}\left(\frac{U_0}{\beta_c}\right)^3 \sin^2 \omega_1 t \sin \omega_2 t - \frac{1}{2}\left(\frac{U_0}{\beta_c}\right)^3 \sin^2 \omega_2 t \sin \omega_1 t\right]\right\} \quad \text{(B.10)}$$

To further solve the equation the higher order (2^{nd} and 3^{rd}) in the above equation were solved using power-reducing/half angle trigonometric relations

$$\sin^2 x = \frac{1-\cos(2x)}{2} \tag{B.11}$$

$$\sin^3 x = \frac{3}{4}\sin x - \frac{1}{4}\sin 3x \tag{B.12}$$

$$\sin x \sin y = \frac{1}{2}[\cos(y-x) - \cos(x+y)] \tag{B.13}$$

$$\cos x \sin y = \frac{1}{2}[\sin(y-x) + \sin(x+y)] \tag{B.14}$$

Applying the above trigonometric relations in Equation (B.10), it becomes

$$\begin{aligned} i = i_{corr}\Bigg\{\Bigg[1 &+ \frac{U_0}{\beta_a}\sin\omega_1 t + \frac{U_0}{\beta_a}\sin\omega_2 t + \frac{1}{4}\left(\frac{U_0}{\beta_a}\right)^2 - \frac{1}{4}\left(\frac{U_0}{\beta_a}\right)^2\cos 2\omega_1 t + \frac{1}{4}\left(\frac{U_0}{\beta_a}\right)^2 - \\ &\frac{1}{4}\left(\frac{U_0}{\beta_a}\right)^2\cos 2\omega_2 t + \frac{1}{8}\left(\frac{U_0}{\beta_a}\right)^3\sin\omega_1 t - \frac{1}{24}\left(\frac{U_0}{\beta_a}\right)^3\sin 3\omega_1 t + \frac{1}{8}\left(\frac{U_0}{\beta_a}\right)^3\sin\omega_2 t - \\ &\frac{1}{24}\left(\frac{U_0}{\beta_a}\right)^3\sin 3\omega_2 t + \frac{1}{2}\left(\frac{U_0}{\beta_a}\right)^2\cos(\omega_2 t - \omega_1 t) - \frac{1}{2}\left(\frac{U_0}{\beta_a}\right)^2\cos(\omega_2 t + \omega_1 t) + \frac{1}{4}\left(\frac{U_0}{\beta_a}\right)^3\sin\omega_2 t + \\ &\frac{1}{8}\left(\frac{U_0}{\beta_a}\right)^3\sin(2\omega_1 t - \omega_2 t) - \frac{1}{8}\left(\frac{U_0}{\beta_a}\right)^3\sin(\omega_2 t + 2\omega_1 t) + \frac{1}{4}\left(\frac{U_0}{\beta_a}\right)^3\sin\omega_1 t + \frac{1}{8}\left(\frac{U_0}{\beta_a}\right)^3\sin(2\omega_2 t - \\ &\omega_1 t) - \frac{1}{8}\left(\frac{U_0}{\beta_a}\right)^3\sin(\omega_1 t + 2\omega_2 t)\Bigg] - \Bigg[1 - \frac{U_0}{\beta_c}\sin\omega_1 t - \frac{U_0}{\beta_c}\sin\omega_2 t + \frac{1}{4}\left(\frac{U_0}{\beta_c}\right)^2 - \\ &\frac{1}{4}\left(\frac{U_0}{\beta_c}\right)^2\cos 2\omega_1 t + \frac{1}{4}\left(\frac{U_0}{\beta_c}\right)^2 - \frac{1}{4}\left(\frac{U_0}{\beta_c}\right)^2\cos 2\omega_2 t - \frac{1}{8}\left(\frac{U_0}{\beta_c}\right)^3\sin\omega_1 t + \frac{1}{24}\left(\frac{U_0}{\beta_c}\right)^3\sin 3\omega_1 t - \\ &\frac{1}{8}\left(\frac{U_0}{\beta_c}\right)^3\sin\omega_2 t + \frac{1}{24}\left(\frac{U_0}{\beta_c}\right)^3\sin 3\omega_2 t + \frac{1}{2}\left(\frac{U_0}{\beta_c}\right)^2\cos(\omega_2 t - \omega_1 t) - \frac{1}{2}\left(\frac{U_0}{\beta_c}\right)^2\cos(\omega_2 t + \omega_1 t) - \\ &\frac{1}{4}\left(\frac{U_0}{\beta_c}\right)^3\sin\omega_2 t - \frac{1}{8}\left(\frac{U_0}{\beta_c}\right)^3\sin(2\omega_1 t - \omega_2 t) + \frac{1}{8}\left(\frac{U_0}{\beta_c}\right)^3\sin(\omega_2 t + 2\omega_1 t) - \frac{1}{4}\left(\frac{U_0}{\beta_c}\right)^3\sin\omega_1 t - \\ &\frac{1}{8}\left(\frac{U_0}{\beta_c}\right)^3\sin(2\omega_2 t - \omega_1 t) + \frac{1}{8}\left(\frac{U_0}{\beta_c}\right)^3\sin(\omega_1 t + 2\omega_2 t)\Bigg]\Bigg\} \end{aligned} \tag{B.15}$$

The terms with similar harmonic and intermodulation frequency components were combined together to derive the final expression for response current with harmonic and intermodulation components when disturbed by a distortion signal and it is given below

$$i = i_{fr} + i_{\omega_1}\sin\omega_1 t + i_{\omega_2}\sin\omega_2 t - i_{2\omega_1}\cos 2\omega_1 t - i_{2\omega_2}\cos 2\omega_2 t - i_{3\omega_1}\sin 3\omega_1 t - i_{3\omega_2}\sin 3\omega_2 t + i_{\omega_2\pm\omega_1}\cos(\omega_2 t - \omega_1 t) - i_{\omega_2\pm\omega_1}\cos(\omega_2 t + \omega_1 t) + i_{2\omega_2\pm\omega_1}\sin(2\omega_2 t - \omega_1 t) - i_{2\omega_2\pm\omega_1}\sin(2\omega_2 t + \omega_1 t) + i_{2\omega_1\pm\omega_2}\sin(2\omega_1 t - \omega_2 t) - i_{2\omega_1\pm\omega_2}\sin(2\omega_1 t + \omega_2 t) \quad \text{(B.16)}$$

where, i_{fr} is the Faradaic rectification current

$$i_{\omega_1} = i_{\omega_2} = i_{corr}\left(\frac{U_0}{\beta_a} + \frac{U_0}{\beta_c}\right) \quad \text{(B.17)}$$

$$i_{2\omega_1} = i_{2\omega_2} = \frac{1}{4} i_{corr}\left[\left(\frac{U_0}{\beta_a}\right)^2 - \left(\frac{U_0}{\beta_c}\right)^2\right] \quad \text{(B.18)}$$

$$i_{3\omega_1} = i_{3\omega_2} = \frac{1}{24} i_{corr}\left[\left(\frac{U_0}{\beta_a}\right)^3 + \left(\frac{U_0}{\beta_c}\right)^3\right] \quad \text{(B.19)}$$

$$i_{\omega_2\pm\omega_1} = \frac{1}{2} i_{corr}\left[\left(\frac{U_0}{\beta_a}\right)^2 - \left(\frac{U_0}{\beta_c}\right)^2\right] \quad \text{(B.20)}$$

$$i_{2\omega_2\pm\omega_1} = i_{2\omega_1\pm\omega_2} = \frac{1}{8} i_{corr}\left[\left(\frac{U_0}{\beta_a}\right)^3 + \left(\frac{U_0}{\beta_c}\right)^3\right] \quad \text{(B.21)}$$

Mathematical Derivation for Diffusion Control System in EFM

The mathematical part of EFM for corrosion systems, whose cathodic process under diffusion control is derived here[52]. Since the cathodic process is under diffusion control the cathodic Tafel coefficient (β_c) becomes infinite and the current-potential relation reduces to

$$i = i_{corr}\left[\exp\left(\frac{\eta}{\beta_a}\right) - 1\right] \quad \text{(B.22)}$$

A distortion signal is applied to the system in the form of sine waves with two different frequencies as given in Equation (B.4). Therefore the equation above changes to

$$i = i_{corr}\left[\exp\left(\frac{U_0 \sin\omega_1 t}{\beta_a}\right)\exp\left(\frac{U_0 \sin\omega_2 t}{\beta_a}\right) - 1\right] \quad \text{(B.23)}$$

The exponential terms above are expanded to third order using Taylor series expansion as given in Equations (B.6)-(B.8), therefore

$$i = i_{corr}\left\{\left[1 + \left(\frac{U_0 \sin\omega_1 t}{\beta_a}\right) + \frac{1}{2}\left(\frac{U_0 \sin\omega_1 t}{\beta_a}\right)^2 + \frac{1}{6}\left(\frac{U_0 \sin\omega_1 t}{\beta_a}\right)^3\right]\left[1 + \left(\frac{U_0 \sin\omega_2 t}{\beta_a}\right) + \frac{1}{2}\left(\frac{U_0 \sin\omega_2 t}{\beta_a}\right)^2 + \frac{1}{6}\left(\frac{U_0 \sin\omega_2 t}{\beta_a}\right)^3\right] - 1\right\} \quad \text{(B.24)}$$

$$i = i_{corr}\left\{\left[1 + \frac{U_0}{\beta_a}\sin\omega_1 t + \frac{1}{2}\left(\frac{U_0}{\beta_a}\right)^2 \sin^2\omega_1 t + \frac{1}{6}\left(\frac{U_0}{\beta_a}\right)^3 \sin^3\omega_1 t + \frac{U_0}{\beta_a}\sin\omega_2 t + \frac{1}{2}\left(\frac{U_O}{\beta_a}\right)^2 \sin^2\omega_2 t + \frac{1}{6}\left(\frac{U_0}{\beta_a}\right)^3 \sin^3\omega_2 t + \left(\frac{U_0}{\beta_a}\right)^2 \sin\omega_1 t \sin\omega_2 t + \frac{1}{2}\left(\frac{U_0}{\beta_a}\right)^3 \sin^2\omega_1 t \sin\omega_2 t + \frac{1}{2}\left(\frac{U_0}{\beta_a}\right)^3 \sin^2\omega_2 t \sin\omega_1 t\right] - 1\right\} \quad \text{(B.25)}$$

Applying power reducing/half angle trigonometric relations as given in Equations (B.11)-(B.14) to the above equation, the response current relation reduces to

$$i = i_{corr}\left\{\left[1 + \frac{U_0}{\beta_a}\sin\omega_1 t + \frac{U_0}{\beta_a}\sin\omega_2 t + \frac{1}{4}\left(\frac{U_0}{\beta_a}\right)^2 - \frac{1}{4}\left(\frac{U_0}{\beta_a}\right)^2 \cos 2\omega_1 t + \frac{1}{4}\left(\frac{U_0}{\beta_a}\right)^2 - \frac{1}{4}\left(\frac{U_0}{\beta_a}\right)^2 \cos 2\omega_2 t + \frac{1}{8}\left(\frac{U_0}{\beta_a}\right)^3 \sin\omega_1 t - \frac{1}{24}\left(\frac{U_0}{\beta_a}\right)^3 \sin 3\omega_1 t + \frac{1}{8}\left(\frac{U_0}{\beta_a}\right)^3 \sin\omega_2 t - \frac{1}{24}\left(\frac{U_0}{\beta_a}\right)^3 \sin 3\omega_2 t + \frac{1}{2}\left(\frac{U_0}{\beta_a}\right)^2 \cos(\omega_2 t - \omega_1 t) - \frac{1}{2}\left(\frac{U_0}{\beta_a}\right)^2 \cos(\omega_2 t + \omega_1 t) + \frac{1}{4}\left(\frac{U_0}{\beta_a}\right)^3 \sin\omega_2 t +$$

$$\frac{1}{8}\left(\frac{U_0}{\beta_a}\right)^3 \sin(2\omega_1 t - \omega_2 t) - \frac{1}{8}\left(\frac{U_0}{\beta_a}\right)^3 \sin(\omega_2 t + 2\omega_1 t) + \frac{1}{4}\left(\frac{U_0}{\beta_a}\right)^3 \sin \omega_1 t + \frac{1}{8}\left(\frac{U_0}{\beta_a}\right)^3 \sin(2\omega_2 t - \omega_1 t) - \frac{1}{8}\left(\frac{U_0}{\beta_a}\right)^3 \sin(\omega_1 t + 2\omega_2 t)\Big] - 1\Big\} \quad \text{(B.26)}$$

$$i = i_{fr} + i_{\omega_1} \sin \omega_1 t + i_{\omega_2} \sin \omega_2 t - i_{2\omega_1} \cos 2\omega_1 t - i_{2\omega_2} \cos 2\omega_2 t - i_{3\omega_1} \sin 3\omega_1 t - i_{3\omega_2} \sin 3\omega_2 t + i_{\omega_2 \pm \omega_1} \cos(\omega_2 t - \omega_1 t) - i_{\omega_2 \pm \omega_1} \cos(\omega_2 t + \omega_1 t) + i_{2\omega_2 \pm \omega_1} \sin(2\omega_2 t - \omega_1 t) - i_{2\omega_2 \pm \omega_1} \sin(2\omega_2 t + \omega_1 t) + i_{2\omega_1 \pm \omega_2} \sin(2\omega_1 t - \omega_2 t) - i_{2\omega_1 \pm \omega_2} \sin(2\omega_1 t + \omega_2 t)$$

where $i_{\omega_1} = i_{\omega_2} = i_{corr} \frac{U_0}{\beta_a}$ (B.27)

$$i_{2\omega_1} = i_{2\omega_2} = i_{corr} \frac{1}{4}\left(\frac{U_0}{\beta_a}\right)^2 \quad \text{(B.28)}$$

$$i_{3\omega_1} = i_{3\omega_2} = i_{corr} \frac{1}{24}\left(\frac{U_0}{\beta_a}\right)^3 \quad \text{(B.29)}$$

$$i_{\omega_2 \pm \omega_1} = i_{corr} \frac{1}{2}\left(\frac{U_0}{\beta_a}\right)^2 \quad \text{(B.30)}$$

$$i_{2\omega_2 \pm \omega_1} = i_{2\omega_1 \pm \omega_2} = i_{corr} \frac{1}{8}\left(\frac{U_0}{\beta_a}\right)^3 \quad \text{(B.31)}$$

Mathematical Derivation for Passivation Control System in EFM

This part derives the mathematical expression used for calculating corrosion current and Tafel coefficient for corrosion systems whose anodic process under passivation control[52]. With the anodic Tafel coefficient (β_a) value reaching infinite at these conditions, the current-potential relationship is given as

$$i = i_{corr}\left[1 - \exp\left(-\frac{\eta}{\beta_c}\right)\right] \quad \text{(B.32)}$$

Equation (B.4) is applied as input signal to distort the system under passivation control

$$i = i_{corr}\left\{1 - \left[\exp\left(-\frac{U_0 \sin\omega_1 t}{\beta_c}\right)\exp\left(-\frac{U_0 \sin\omega_2 t}{\beta_c}\right)\right]\right\} \quad \text{(B.33)}$$

Using Taylor series the exponential terms are expanded to third order as given in Equations (B.6)-(B.8), therefore

$$i = i_{corr}\left\{1 - \left[1 - \left(\frac{U_0 \sin\omega_1 t}{\beta_c}\right) + \frac{1}{2}\left(\frac{U_0 \sin\omega_1 t}{\beta_c}\right)^2 - \frac{1}{6}\left(\frac{U_0 \sin\omega_1 t}{\beta_c}\right)^3\right]\left[1 - \left(\frac{U_0 \sin\omega_2 t}{\beta_c}\right) + \frac{1}{2}\left(\frac{U_0 \sin\omega_2 t}{\beta_c}\right)^2 - \frac{1}{6}\left(\frac{U_0 \sin\omega_2 t}{\beta_c}\right)^3\right]\right\} \quad \text{(B.34)}$$

$$i = i_{corr}\left\{1 - \left[1 - \frac{U_0}{\beta_c}\sin\omega_1 t + \frac{1}{2}\left(\frac{U_0}{\beta_c}\right)^2 \sin^2\omega_1 t - \frac{1}{6}\left(\frac{U_0}{\beta_c}\right)^3 \sin^3\omega_1 t - \frac{U_0}{\beta_c}\sin\omega_2 t + \frac{1}{2}\left(\frac{U_0}{\beta_c}\right)^2 \sin^2\omega_2 t - \frac{1}{6}\left(\frac{U_0}{\beta_c}\right)^3 \sin^3\omega_2 t + \left(\frac{U_0}{\beta_c}\right)^2 \sin\omega_1 t \sin\omega_2 t - \frac{1}{2}\left(\frac{U_0}{\beta_c}\right)^3 \sin^2\omega_1 t \sin\omega_2 t - \frac{1}{2}\left(\frac{U_0}{\beta_c}\right)^3 \sin^2\omega_2 t \sin\omega_1 t\right]\right\} \quad \text{(B.35)}$$

Using power reducing/half angle trigonometric relations

$$i = i_{corr}\left\{1 - \left[1 - \frac{U_0}{\beta_c}\sin\omega_1 t - \frac{U_0}{\beta_c}\sin\omega_2 t + \frac{1}{4}\left(\frac{U_0}{\beta_c}\right)^2 - \frac{1}{4}\left(\frac{U_0}{\beta_c}\right)^2 \cos 2\omega_1 t + \frac{1}{4}\left(\frac{U_0}{\beta_c}\right)^2 - \frac{1}{4}\left(\frac{U_0}{\beta_c}\right)^2 \cos 2\omega_2 t - \frac{1}{8}\left(\frac{U_0}{\beta_c}\right)^3 \sin\omega_1 t + \frac{1}{24}\left(\frac{U_0}{\beta_c}\right)^3 \sin 3\omega_1 t - \frac{1}{8}\left(\frac{U_0}{\beta_c}\right)^3 \sin\omega_2 t + \frac{1}{24}\left(\frac{U_0}{\beta_c}\right)^3 \sin 3\omega_2 t + \frac{1}{2}\left(\frac{U_0}{\beta_c}\right)^2 \cos(\omega_2 t - \omega_1 t) - \frac{1}{2}\left(\frac{U_0}{\beta_c}\right)^2 \cos(\omega_2 t + \omega_1 t) - \frac{1}{4}\left(\frac{U_0}{\beta_c}\right)^3 \sin\omega_2 t - \frac{1}{8}\left(\frac{U_0}{\beta_c}\right)^3 \sin(2\omega_1 t - \omega_2 t) + \frac{1}{8}\left(\frac{U_0}{\beta_c}\right)^3 \sin(\omega_2 t + 2\omega_1 t) - \frac{1}{4}\left(\frac{U_0}{\beta_c}\right)^3 \sin\omega_1 t - \frac{1}{8}\left(\frac{U_0}{\beta_c}\right)^3 \sin(2\omega_2 t - \omega_1 t) + \frac{1}{8}\left(\frac{U_0}{\beta_c}\right)^3 \sin(\omega_1 t + 2\omega_2 t)\right]\right\} \quad \text{(B.36)}$$

$$i = i_{fr} + i_{\omega_1}\sin\omega_1 t + i_{\omega_2}\sin\omega_2 t + i_{2\omega_1}\cos 2\omega_1 t + i_{2\omega_2}\cos 2\omega_2 t - i_{3\omega_1}\sin 3\omega_1 t - i_{3\omega_2}\sin 3\omega_2 t - i_{\omega_2\pm\omega_1}\cos(\omega_2 t - \omega_1 t) + i_{\omega_2\pm\omega_1}\cos(\omega_2 t + \omega_1 t) + i_{2\omega_2\pm\omega_1}\sin(2\omega_2 t -$$

$$\omega_1 t) - i_{2\omega_2 \pm \omega_1} \sin(2\omega_2 t + \omega_1 t) + i_{2\omega_1 \pm \omega_2} \sin(2\omega_1 t - \omega_2 t) - i_{2\omega_1 \pm \omega_2} \sin(2\omega_1 t + \omega_2 t) \quad \text{(B.37)}$$

The harmonic and intermodulation current components of different corrosion models and the electrochemical properties derived from these components are summarized below in Table B.1.

Table B.1. Summary of response current components of activation, diffusion and passivation control models in EFM

Components	Activation Control	Diffusion Control	Passivation Control
$i_{\omega_1} = i_{\omega_2}$	$i_{corr}\left(\frac{U_0}{\beta_a} + \frac{U_0}{\beta_c}\right)$	$i_{corr}\frac{U_0}{\beta_a}$	$i_{corr}\frac{U_0}{\beta_c}$
$i_{2\omega_1} = i_{2\omega_2}$	$\frac{1}{4} i_{corr}\left[\left(\frac{U_0}{\beta_a}\right)^2 - \left(\frac{U_0}{\beta_c}\right)^2\right]$	$i_{corr}\frac{1}{4}\left(\frac{U_0}{\beta_a}\right)^2$	$i_{corr}\frac{1}{4}\left(\frac{U_0}{\beta_c}\right)^2$
$i_{3\omega_1} = i_{3\omega_2}$	$\frac{1}{24} i_{corr}\left[\left(\frac{U_0}{\beta_a}\right)^3 + \left(\frac{U_0}{\beta_c}\right)^3\right]$	$i_{corr}\frac{1}{24}\left(\frac{U_0}{\beta_a}\right)^3$	$i_{corr}\frac{1}{24}\left(\frac{U_0}{\beta_c}\right)^3$
$i_{\omega_2 \pm \omega_1}$	$\frac{1}{2} i_{corr}\left[\left(\frac{U_0}{\beta_a}\right)^2 - \left(\frac{U_0}{\beta_c}\right)^2\right]$	$i_{corr}\frac{1}{2}\left(\frac{U_0}{\beta_a}\right)^2$	$i_{corr}\frac{1}{2}\left(\frac{U_0}{\beta_c}\right)^2$
$i_{2\omega_2 \pm \omega_1} = i_{2\omega_1 \pm \omega_2}$	$\frac{1}{8} i_{corr}\left[\left(\frac{U_0}{\beta_a}\right)^3 + \left(\frac{U_0}{\beta_c}\right)^3\right]$	$i_{corr}\frac{1}{8}\left(\frac{U_0}{\beta_a}\right)^3$	$i_{corr}\frac{1}{8}\left(\frac{U_0}{\beta_c}\right)^3$
i_{corr}	$\frac{{i_{\omega_1,\omega_2}}^2}{2\sqrt{8 i_{\omega_1,\omega_2} i_{2\omega_2 \pm \omega_1} - 3{i_{2\omega_2 \pm \omega_1}}^2}}$	$\frac{{i_{\omega_1,\omega_2}}^2}{2 i_{\omega_2 \pm \omega_1}}$	$\frac{{i_{\omega_1,\omega_2}}^2}{2 i_{\omega_2 \pm \omega_1}}$
β_a	$\frac{i_{\omega_1,\omega_2} U_0}{i_{\omega_2 \pm \omega_1} + \sqrt{8 i_{\omega_1,\omega_2} i_{2\omega_2 \pm \omega_1} - 3{i_{\omega_2 \pm \omega_1}}^2}}$	$\frac{{i_{\omega_1,\omega_2}}^2}{2 i_{\omega_2 \pm \omega_1}} U_0$	∞
β_c	$\frac{i_{\omega_1,\omega_2} U_0}{-i_{\omega_2 \pm \omega_1} + \sqrt{8 i_{\omega_1,\omega_2} i_{2\omega_2 \pm \omega_1} - 3{i_{\omega_2 \pm \omega_1}}^2}}$	∞	$\frac{{i_{\omega_1,\omega_2}}^2}{2 i_{\omega_2 \pm \omega_1}} U_0$

APPENDIX C

Corrosion Rate Calculation by LP Method Using Tafel Slopes from EFM

The Tafel slopes obtained from EFM were used in the LPR method to recalculate the corrosion rate and compared with the EFM results. The corrosion rate calculation for both activation and diffusion control system are given below.

Activation Control System:

The corrosion rate calculation using the LPR method, for a system whose anodic and cathodic reactions were under kinetic control (activation control) was first derived by Stern and Geary in 1957[47]. The corrosion rate calculation depends greatly on the Tafel constants, so the Tafel constants must be known prior to the calculation. Usually the LP method assumes a default Tafel slopes of 120 mV/decade.

$$\text{Stern} - \text{Geary Equation}: \; R_p = \frac{b_a.b_c}{2.303(b_a+b_c)*i_{corr}} \tag{C.1}$$

$$\Longrightarrow i_{corr} = \frac{b_a.b_c}{2.303(b_a+b_c)*R_p} \tag{C.2}$$

The Tafel slopes obtained from EFM and the polarization resistance value calculated manually from the slope of the LPR curve were used in the above equation to calculate the corrosion current. From the corrosion current, the corrosion rate is calculated using Faraday's law given in Eqn C.3.

$$\text{Corrosion rate (mpy)} = \frac{M_w \mathrm{I}_{corr}}{zFA\rho} = 0.152 i_{corr} \tag{C.3}$$

where M_w is the molecular weight of iron (g/mol) = 55.847, I_{corr} is the corrosion current calculated from the experiments, z is the number of electrons transferred during the electrochemical reaction = 2, F is the Faraday constant (amp-sec/mol) = 96485, A is the area of the working electrode (cm^2) = 3.01 and ρ is the density of iron (g/cm^3) = 7.87.

Diffusion Control System:

The calculation of corrosion rate from LP method for a diffusion control system is similar to the calculations of activation control system.

$$\text{Diffusion control}: i_{corr} = \frac{b_a}{2.303 * R_p} \quad \text{(C.4)}$$

The calculation involves only the anodic Tafel constant since the cathodic Tafel slope is infinite for a system under diffusion control. Hence the corrosion rate for the system studied here is simply

$$\text{Corrosion rate (mpy)} = 0.152 i_{corr} \quad \text{(C.5)}$$